Louisiana Tech University
Louisiana Tech Digital Commons

Fall 2010

Halloysite clay nanotubes for controlled delivery of chemically active agents

Elshard Abdullayev

HALLOYSITE CLAY NANOTUBES FOR CONTROLLED DELIVERY

OF CHEMICALLY ACTIVE AGENTS

by

Elshad Abdullayev, M.S.

A Dissertation Presented in Partial Fulfillment
of the Requirements for the Degree
Doctor of Philosophy

COLLEGE OF ENGINEERING AND SCIENCE
LOUISIANA TECH UNIVERSITY

November 2010

UMI Number: 3438517

UMI®

Dissertation Publishing

ProQuest®

LOUISIANA TECH UNIVERSITY

THE GRADUATE SCHOOL
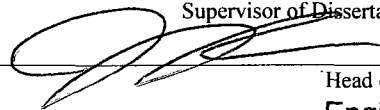
October 1st, 2010
_____
Date

We hereby recommend that the dissertation prepared under our supervision

by **Elshad Abdullayev**
_____

entitled _____

Halloysite Clay Nanotubes for Controlled Delivery of Chemically Active Agents

_____

_____

_____

be accepted in partial fulfillment of the requirements for the Degree of

Doctor of Philosophy in Engineering

_____
Supervisor of Dissertation Research

_____
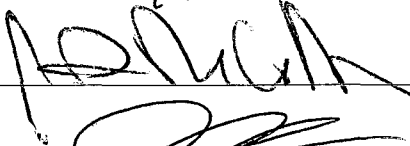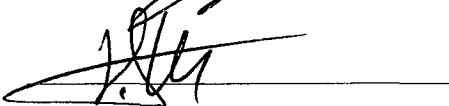Head of Department

Engineering
_____
Department

Recommendation concurred in:

_____

_____
Advisory Committee

_____

_____

Approved:
_____
Director of Graduate Studies

_____
Dean of the College

Approved:
_____
Dean of the Graduate School

ABSTRACT

In this work we explored the capabilities of halloysite nanotubes as capsules for encapsulation and controlled delivery of the chemically and biologically active substances. Halloysite is a two-layered aluminosilicate which has a predominantly hollow tubular structure in the submicron range and is chemically similar to kaolinite [1, 2].

In the first section of this work, we analyzed the structure of the halloysite nanotubes as well as its capability to encapsulate and deliver biologically and chemically active agents, similarities and differences between release characteristics of different agents and how these differences relate with their chemical structure. Models were used to describe the release characteristics of the active agents. Study of the interaction between loaded agents and halloysite nanotubes provides better understanding of the release characteristics of the loaded agents and how halloysite can be implemented for technological and medical applications.

The second part of the work deals with self-healing coatings produced on the basis of halloysite nanotubes loaded with corrosion inhibitors. Self-healing coatings are one of the effective methods to protect metals from corrosion and deterioration. The difference between self-healing coatings and the usual coatings is the ability of the first to recover after the formation of the damages due to external or internal stresses. High efficiency of the self-healing coatings produced by halloysite nanotubes were demonstrated on 110 Copper alloys and 2024 aluminum alloys. Controlled delivery of the corrosion inhibitors with additional encapsulation of the halloysite nanotubes by synthesizing stoppers at tube endings was also demonstrated. Additional encapsulation of the halloysite nanotubes may be necessary when
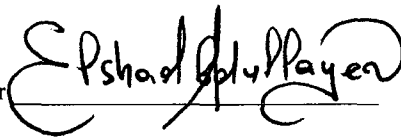
slow release of the loaded agents is required or rapid convection of the liquid in the surrounding environment takes place (since this may cause rapid release of the loaded agents without additional encapsulation).

The third part of this work deals with pharmaceutical applications of the halloysite nanotubes. Toxicity analysis was performed by using MCF-7 and HeLa cells since this is the main issue to be considered before using halloysite for any technological and medical applications. Halloysite nanotubes were readily taken up by the cells and cells survived for a reasonably long time after uptake indicating the biocompatible nature of the halloysite nanotubes. The possibility to encapsulate glycerol, a skin moisturizing agent, was also demonstrated for pharmaceutical applications. It was shown that halloysite has a huge capability for encapsulating a wide range of pharmaceuticals and effectively deliver over a long time range which may increase the quality of pharmaceutical products.

APPROVAL FOR SCHOLARLY DISSEMINATION

The author grants to the Prescott Memorial Library of Louisiana Tech University the right to reproduce, by appropriate methods, upon request, any or all portions of this Dissertation. It is understood that "proper request" consists of the agreement, on the part of the requesting party, that said reproduction is for his personal use and that subsequent reproduction will not occur without written approval of the author of this Dissertation. Further, any portions of the Dissertation used in books, papers, and other works must be appropriately referenced to this Dissertation.

Finally, the author of this Dissertation reserves the right to publish freely, in the literature, at any time, any or all portions of this Dissertation.

Author

Date   10/28/2010

DEDICATION

Dedicated to my friends Wajihuddin Mohammad, Ahmad Paintdakhi and Zohaib Ijaz Shaikh

TABLE OF CONTENTS

LIST OF TABLES

LIST OF FIGURES

ACKNOWLEDGMENTS

CHAPTER 1

INTRODUCTION

The study of nanotubular templates is one of the emerging fields of nanotechnology. Carbon nanotubes gained big interest among scientists due to their superior mechanical and electrical properties derived from their nanotubular structure. Boron nitride nanotubes are also attracting scientists due to thermal and mechanical properties and nanotubular geometry. These nanotubes are expected to find applications in nanodevices, sensors and functional composite materials.

The major disadvantage of synthetic nanotubes is their lesser availability and cost effectiveness. Any kind of manufacturing process requires hundreds of tons of these materials to be available for manufacturing products. So far no method exists to produce synthetic nanotubes in the level of kilograms with sufficient quality. It is perhaps for this reason that naturally occurring nanomaterials started to gain more interest in recent years.

Halloysite is a naturally occurring clay nanotube with dimensions of 50-100 nm in diameter and 0.5-3 micron in length [3]. These minerals are formed from kaolinite over millions of years due to the action of weathering and hydrothermal processes [4]. Layers are rolled into nanotubes due to the strain caused by lattice mismatch between adjacent silicone dioxide and aluminum oxide sheets [1-4]. It is mined from natural deposits in USA, New Zealand, Korea, China, Turkey and available up to fifty thousand tons per year [2, 6]. The Dragon mine in Utah contains halloysite deposits up to 90% in purity which makes these nanotubes readily available for nanotechnology applications [6]. Even though halloysite

nanotubes do not have the superior electrical and mechanical properties that carbon nanotubes have, they contain all the superior properties that emerge from nanotubular geometry.

Historically, halloysite has been extensively utilized as a raw material for the ceramics industry, especially for the manufacture of porcelain and bone china [2, 7]. Having nanotubular structure, halloysite particles can potentially be applied in several fields of nanotechnology. These multilayer tubes are commonly used for plastic composites in controlled release applications [3, 5], and may be coated with metal by electroless plating to make conductive fillers [12]. Due to their porous structure and high catalytic activity, halloysite particles can be used in remediation of acid mine drainage, petroleum conversion in refining industries, as well as in the separation of liquids and gaseous mixtures [2].

1.1. Templates for Encapsulating Active Agents

Several template designs were introduced by scientists for encapsulation and controlled delivery of the active agents. They can be analyzed in three categories. The first category includes nanoparticles that can absorb active agents on their surfaces and effectively deliver them when needed. This kind of templates includes ceramic particles of different origin produced by sol gel processing or ball milling [8, 9]. Active agents can be absorbed on the surface of these particles and desorbed upon external signal. Shchukin, *et al.* demonstrated silica nanoparticles coated with polyelectrolytes by using layer by layer nanoassembly to produce capsules that can release corrosion inhibitors upon the change of pH of the external environment [10]. The major disadvantage of these kinds of particles is their low loading capability.

The second type of template includes nanocapsules that can entrap active agents within themselves and rupture upon external influence to release active agents. Polyelectrolyte

nanocapsules produced by using layer by layer deposition of polyelectrolytes on spherical cores and then core dissolution [8, 10], or spherical alginate particles [11], liposomes and polymer capsules [13] that can entrap active agents within themselves are examples of this kind of templates. Even though these capsules have high loading capability, they cannot hold active agents for a long time [8]. Because of the three dimensional mechanism of diffusion and the presence of many holes on the capsule surface, agents easily leak from the capsules reducing the overall release time.

The third type of template for the encapsulation of active agents includes nanotubes that can entrap active agents within their pores. Examples include carbon nanotubes [14], boron nitride nanotubes [15] and halloysite [5]. Nanotubes provide a compromise between higher loading capability and high retention of loaded agents within the tube lumen [14, 15]. Their loading capability is lower than spherical nanocapsules but higher than nanospheres but their retention time for the active agents is higher than both the nanocapsules and nanospheres [8]. In addition, nanotubes provide controllable delivery of the active agents by synthesizing artificial stoppers at tube endings [16].

None of the abovementioned synthetic templates gained much interest in the industry, mainly due to their limited availability and toxicity related issues. On the other hand, halloysite nanotubes, a naturally available product, were inadvertently forgotten by the researchers. In this work, we studied the possibility of the usage of the halloysite for encapsulation and controlled delivery of some chemically and biologically active agents, such as corrosion inhibitors, pharmaceuticals, antiseptics and drugs. This study sheds light on some of the application areas of halloysite nanotubes in anticorrosion metal coatings, pharmaceutical and medical industries.

1.2. <u>Research Goals</u>

In this work, naturally available halloysite nanotubes were analyzed as potential capsules for encapsulating chemically and biologically active agents for technological and biomedical applications. Agents that were studied included corrosion inhibitors, pharmaceuticals, drugs and antiseptic agents. The work was developed according to the following schematic on a step by step basis:

1) Analysis of the structure of the halloysite nanotubes and the nature of the interaction between loaded agents and halloysite

2) Preparation of the halloysite nanotubes loaded with corrosion inhibitors and testing them for self-healing anticorrosion metal coatings

3) Possibility to provide controllable delivery of the corrosion inhibitors from loaded tubules.

4) Biocompatibility test on halloysite nanotubes

5) Study of glycerol loaded halloysite nanotubes for pharmaceutical applications

1.3. <u>Dissertation Overview</u>

This dissertation contains seven individual chapters. Chapter 2 contains some background information on hallloysite structure, release characteristics of chemically and biologically active agents and major application areas to which halloysite nanotubes can be applied. It also gives a comparison between the release characteristics of the loaded agents, depending on their chemical natures, which is useful in predicting the release characteristics of a great variety of the active agents. Moreover, processes that take place upon loading the halloysite nanotubes with active agents are explained in detail.

Chapters 3 and 4 describe self-healing coatings produced by inhibitor loaded halloysite nanotubes and industrial paint. Benzotriazole, 2-mercaptobenzothiazole and

2-mercaptobenzimidazole were used as corrosion inhibitors and anticorrosion efficiency was checked on 110 copper and 2024 aluminum alloys. Some techniques that were used for prediction of corrosion process are analyzed in detail.

Chapter 5 contains a profound analysis on benzotriazole release behavior from halloysite nanotubes and some details of its further encapsulation by synthesizing artificial stoppers at halloysite tube endings. Controllable release of benzotriazole with a desirable release rate was achieved through artificial caps in the tube endings. Some interesting facts related to the interaction between the halloysite surface and the end caps were also discussed.

In Chapter 6 a biocompatibility study was performed on halloysite nanotubes by using HeLa and MCF-7 cell lines. Biocompatibility is the main requirement for the usage of any material for medical and technological applications.

Chapter 7 is focused on pharmaceutical applications of the halloysite nanotubes. Glycerol, a model moisturizing agent, was encapsulated in halloysite nanotubes that were obtained from two different deposits; New Zealand and Utah, USA. Results indicate that halloysite based encapsulation of pharmaceuticals can significantly increase the quality of pharmaceutic products

CHAPTER 2

BACKGROUND AND THEORY

In this chapter the literature review regarding the structure and properties of the halloysite nanotubes will be discussed. Capability of halloysite nanotubes to encapsulate active agents such as drugs, pharmaceuticals, antiseptics and corrosion inhibitors was discussed. The major application areas of the halloysite nanotubes were also presented. Some sections of this chapter were published in a paper written by the author of this thesis as "Halloysite Clay Nanotubes; Structural Study and Technological Applications", in *Processes of Petrochem. & Oil Refining*, vol.10 (3-4), 2009, p. 260 – 273.

2.1. Halloysite Structural Characterization

Halloysite occurs in nature as a hydrated mineral that has the ideal chemical formula of $Al_2Si_2O_5(OH)_4.nH_2O$, which is similar to kaolinite except for the presence of an additional water monolayer between the adjacent layers. When n=2 the mineral is called halloysite – (10 Å) due to its layer periodicity of 10 Å. Heating halloysite – (10 Å) can easily and irreversibly dehydrate to form halloysite – (7 Å) [1-5]. Dehydrated halloysite has a formula of $Al_2Si_2O_5(OH)_4$ with interlayer spacing of about 7.2 Å [2].

A relationship between hydrated and dehydrated forms of the halloysite was an issue of long debates among many scientists. Some scientists were considering them as different minerals [17] due to the irreversibility of the halloysite-(10 Å) to halloysite-(7 Å) transformations and lack of intermediate states between them, while others were attempting

to classify them as different hydrated levels of the same mineral [17, 18]. Churchman, *et al.* [19], by analyzing the dehydration process of the hydrated halloysite with X-Ray Diffraction, concluded that the dehydration process includes many intermediate stages with different values of n ranging from 0 to 2 and dehydrated halloysite is the last product of the dehydration process. However, all of the halloysites with intermediate levels of hydration contained a combination of 7.2 Å and 10 Å interlayer spacing.

Pure halloysite is a white mineral and can easily be processed to obtain fine powder (Figure 2.1 a) and b)). However, in many cases the mineral is colored to many different colors ranging from yellowish to brown and sometimes greenish depending on the deposit. The reason for these colors are trace amounts of other metal ions such as Fe^{+3}, Cr^{+3}, Ti^{+4}[2] that substitute Al^{+3} or Si^{+4} in the halloysite mineral. Keller, *et al.*, determined 11 different ions from the aqueous extracts of the halloysite samples obtained from the Dragon mine in Utah, USA [20].

a)   b)
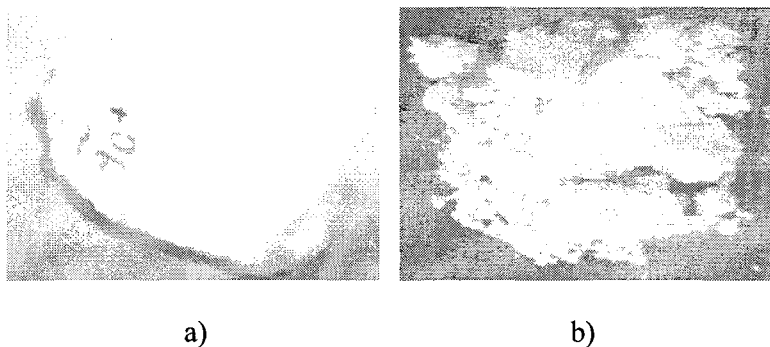
Figure 2.1 Halloysite mineral obtained from Dragon mine, Utah, USA [30].

Iron oxide is the most common impurity that is observed in halloysite minerals (up to 3 wt %). This high amount of iron oxide may be due to the presence of associated iron oxides in the mineral as well as due to the isomorphous substitution of Fe^{+3} for Al^{+3} in the

octahedral alumina sheet [22]. According to Joussein, *et al.*, Fe^{+3} has never been reported to substitute for Si^{+4} in the tetrahedral sheet of halloysite (Figure 2.2) [2].
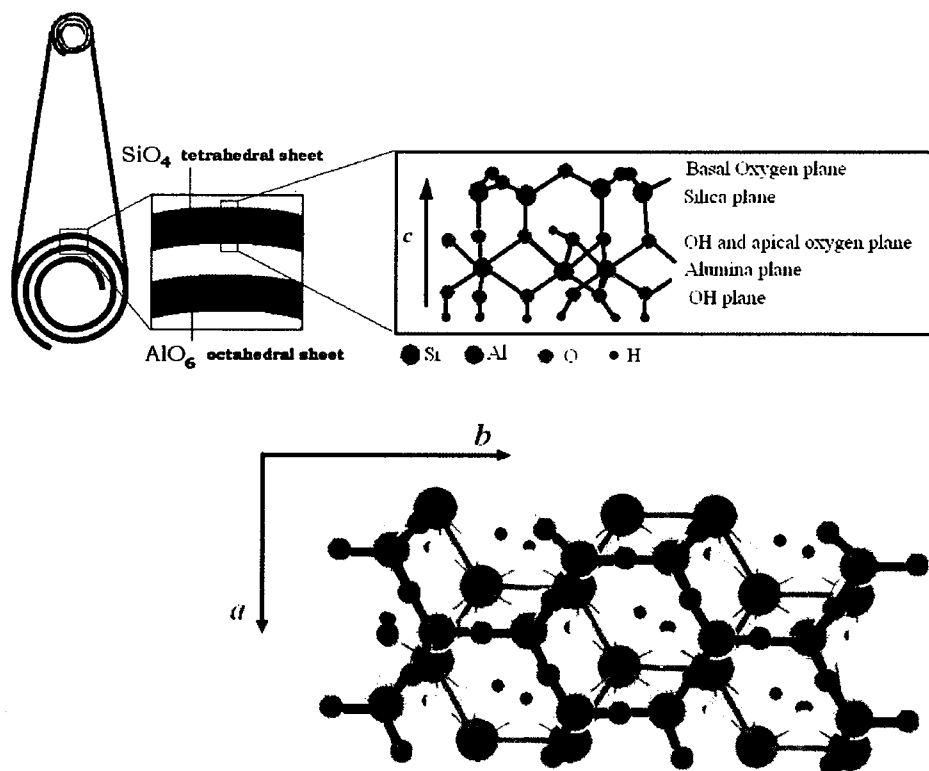
Figure 2.2 Representation of halloysite structure; tubular morphology, side view and top view of the halloysite layer. a, b, c are crystalline directions [31].

The halloysite purification process from the raw mineral is described in [12]. Briefly, a crude mineral is ground up and screened through 125 μm size sieves and suspended in water. For 100 grams of the initial crude mineral, approximately 2 L of water is used. Particles that do not precipitate in 5 minutes are collected from the supernatant and redispersed in water containing 0.5 M EDTA (ethylenediaminetetraacetate) and the suspension was shaken for 24 hrs. Fine particles of halloysites were collected from supernatant by centrifugation of the suspension.

A halloysite layer is composed of sheets of aluminum and silicon oxides. The thickness of the layers in the hydrated mineral is about 10.3 Å and reduces to 7.2 Å in the dehydrated mineral [1- 3]. These layers are rolled into tubes in the halloysite mineral due to the action of weathering and hydrothermal processes [2, 4, 6]. The outside diameters of the tubes vary from 50 to 200 nm, with an average value of ~70 nm [1]. The diameters of the internal lumen range from 10 to 50 nm and average 20 nm [1]. The lengths of the tubules cover a range of 0.5 to 2.0 µm [1-3].

Halloysite has monoclinic crystal structure and dimensions of the unit cells are as follows [23]:

$$a = 5.14Å, b = 8.9Å, c = 20.7Å, \beta = 99.7° \quad \text{for} \quad \text{halloysite (10Å)}$$

$$a = 5.14Å, b = 8.9Å, c = 14.6Å, \beta = 101.9° \text{ for} \quad \text{halloysite (7Å)}$$

Where, a direction coincides with the tube axis and c direction is always normal to the tube axis [1, 24]. This data indicates that only c and angle β change during the dehydration process. Preservation of the lateral dimensions of the halloysite layers and the changing of the interlayer spacing and β angle strongly suggest that the dehydration process is taking place by the partial unrolling of the halloysite tubules as shown in Figure 2.3. Complete unrolling is blocked by strong interlayer hydrogen bonds [1]. The overall diameter of the tubes increases by 10 - 15 % during this process, as was experimentally observed by some authors [2, 23].
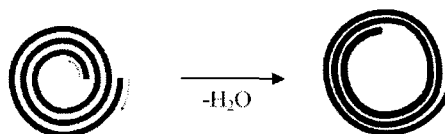
Figure 2.3 Dehydration of the halloysite-(10Å).

In Figure 2.4, X-ray powder diffraction spectra of halloysite samples are presented. A Cu-Kα radiation source was used for obtaining the spectrum (λ=0.15415 nm). A broad peak

corresponding to the 7.3 ± 0.1Å interlayer distance is clearly visible, which corresponds to first

order basal reflection. This peak is broader than the analogous peak for stacked kaolinite sheets

even though both of them have similar multilayer structure. This is due to the fact that the

rolled multilayer structure of halloysite has lesser crystallinity than the stacked kaolinite

multilayer and halloysite has smaller particle dimensions. Also, this peak was slightly shifted

by about 0.1Å. In kaolinite, this peak corresponds to a 7.2Å spacing [25]. In hydrated

halloysite this peak is shifted to 10.3Å. The high intensity peak at 4.5Å spacing is indicative for

the tubular halloysite structure. The peak at 3.6Å is approximately half of the 7.3Å and

corresponds to the second order basal reflection [26].
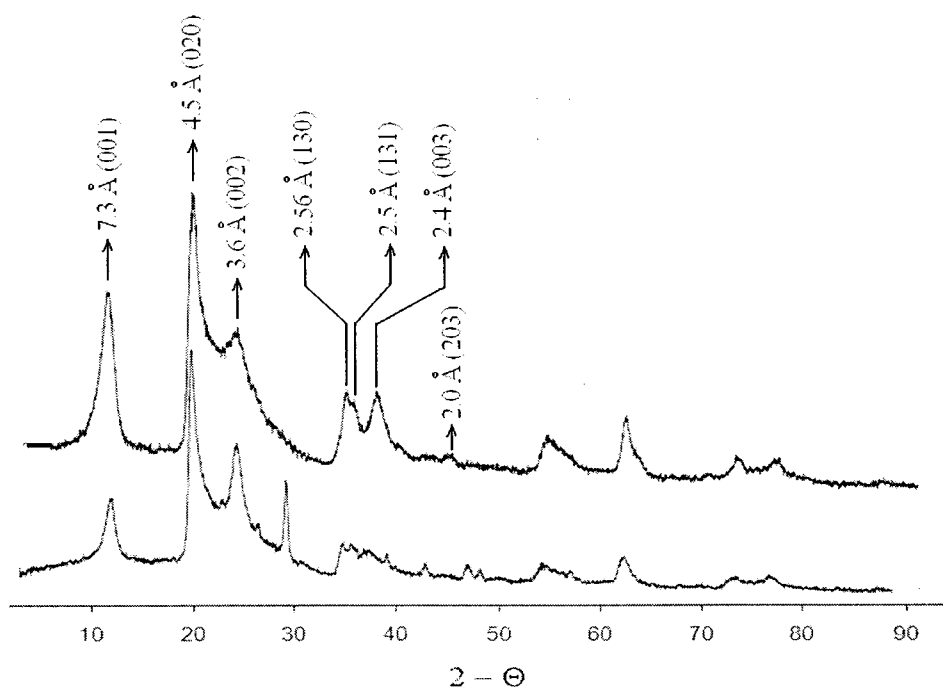
Figure 2.4 XRD pattern of the two halloysite samples from Dragon mine, Utah, USA.

Scanning Electron Microscope images of the halloysite samples from different deposits

clearly indicate that they have a completely rolled tubular structure with hollow cylindrical

geometry. Figure 2.5a shows the rolled structure of the halloysite at the tube ending. The

empty tubular lumen of the halloysite nanotube is clearly visible in the transmission electron

microscopy (TEM) images of the tubes as described in Figure 2.5b. This geometry of the

halloysite nanotubes makes them a very interesting material for many nanotechnology

applications, such as nanocontainers for encapsulation and fillers for plastics. Figures 2.5c

and 2.5d show that broken pieces of the tubes are also present in some deposits.

a)   b)   c)   d)
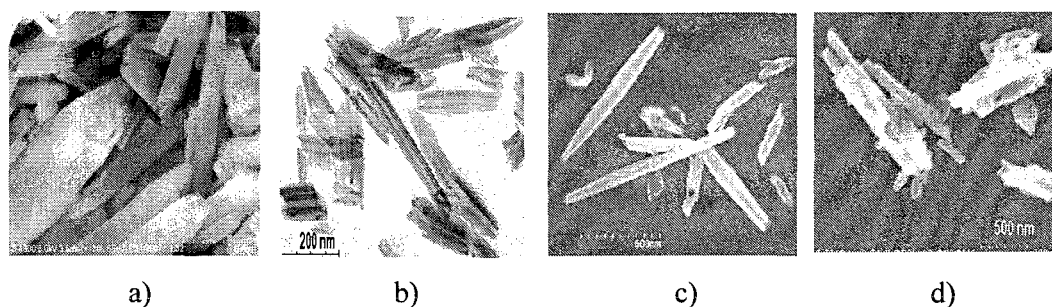
Figure 2.5 Scanning and Transmission Electron Microscopy images of halloysite samples; (a,b) from Dragon mine, Utah (Applied Minerals, Inc) and (c, d) from New Zealand (China Clays, Inc and Imerys Corp).

In halloysite nanotubes, the silica layer is relevant to the outer surface of tube, while the

alumina layer is relevant to the inner lumen surface [2]. The different chemical structure of the

opposite sides of the halloysite layer gives halloysite nanotubes unique properties which do

not exist in other nanotubes. One of the specialties of halloysite is the different surface

chemical properties at the inner and outer sides of the tubes [27].

Aluminum and silicon oxides have different dielectric and ionization properties, which is

evident from the observations of the electrical zeta-potentials of these oxide nanocolloids in

water. The first one (alumina) has a positive charge up to the pH value of the solution 8.5

while the other one (silica) is negative above the solution pH of 1.5 (Figure 2.6). The ability

to have different charges at inner and outer parts of the halloysite nanotubes allows for the

selective loading of negatively charged molecules inside the nanotubes by means of

electrostatic interaction [28]. These tubes can also be selectively modified at external or

internal sides by using silanes [29] and polyunsaturated fatty acids that can benefit many applications. One of the possible applications of such nanotubes may include inorganic micelles with hydrophobic inner surfaces for water treatment.
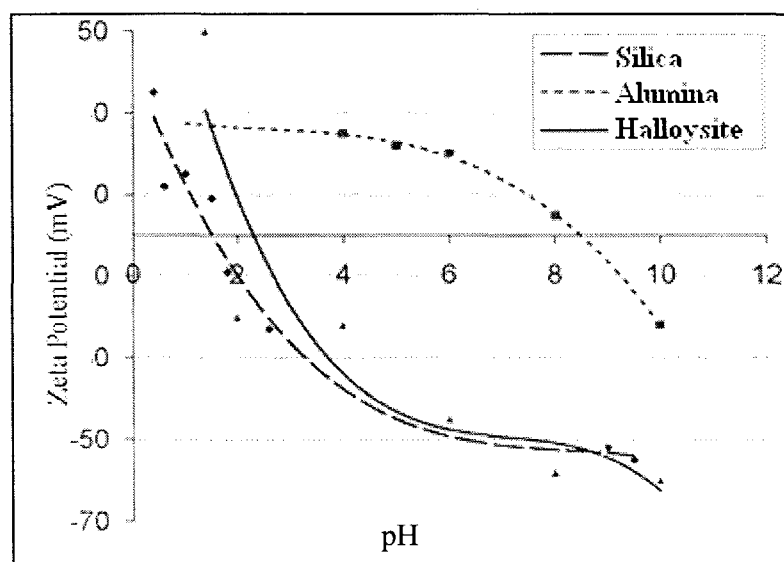
Figure 2.6 Comparison of ξ-potential curves for halloysite nanotubes and silica (blue) and alumina (red) particles [27].

In Figure 2.7, pore volume histograms from two halloysite samples are described. Histograms were observed for the nitrogen absorption isotherm on halloysite. Halloysite nanotubes in both of the samples have pores up to 30 nm in width. Most of the pores have less than 10 nm width in the first sample; however, the relative quantity of larger pores is increased in the second sample. This might be associated with the substitution of Al^{+3} with larger Fe^{+3} ions causing halloysite layers to lose their curvature. Besides hollow cylindrical tubes, halloysite also has incompletely rolled tubes and broken pieces, which are observed by SEM.

a)   b)
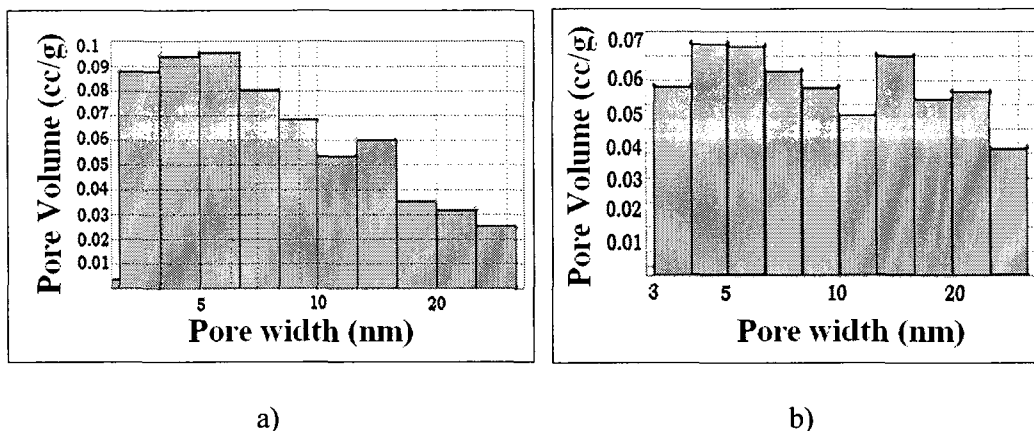
Figure 2.7 Pore volume histogram of the two halloysite samples from Dragon mine, Utah, USA. Histogram obtained from nitrogen absorption isotherm. Sample (b) has Fe+3 ion impurities [57].

2.2. Explanations of the Halloysite Layer Rolling

The reason for the formation of the rolled nanotubular structure is still considered to be a debatable issue. Two facts are clearly established that there is a dimensional misfit between alumina and silica layers in both a and b directions (for silica a = 5.02Å, b = 9.164Å, and for alumina a = 5.066Å, b = 8.655Å) and halloysite layer rolling in the b direction is preferred over the a direction [1, 24]. Therefore, some scientists concluded that lattice mismatch between adjacent silica and alumina layers is responsible for the halloysite layer rolling, and the fact that the mismatch in b direction is more than in a direction explains the preferential rolling in the b direction [1, 2, 24]. This hypothesis was rejected by other scientists [32] due to the possibility of an alternative way for the correction of the dimensional misfit in the silica layer, which takes place due to the rotation of adjacent silica tetrahedrons from hexagonal to ditrigonal geometry, as shown in Figure 2.8. This rotation is the main mechanism in the stabilization of dimensional misfit in kaolinite layers [32]. However, Singh provided a theoretical calculation on the basis of the increase of the electrostatic repulsion between adjacent silica ions due to tetrahedral rotations and concluded that curling of the halloysite layer to form tubes is more energetically preferable than hexagonal to ditrigonal

transformation [24]. This calculation was further proven experimentally by exfoliation of the kaolinite layers with potassium acetate. It was shown that individual kaolinite layers tend to roll into tubes. Moreover curling occurs either in a or b directions [33]. Bates theoretically calculated the diameter of the tubular structure based on the assumption that dimensional misfit alone is responsible for the halloysite layer rolling and discovered that the minimal internal diameter is about 25 nm, if the axis of the tube is parallel to the a axis direction and 57 nm, if it is parallel to the b direction. He concluded that the diameter of the halloysite tubes have to lie between these two values depending on the direction of the roll [1]. However, tubules with diameters lying outside the range of these values were already presented by many scientists [2, 3, 5, 22] and this fact suggests that the dimensional misfit cannot be the only reason for the rolling of the halloysite layers.
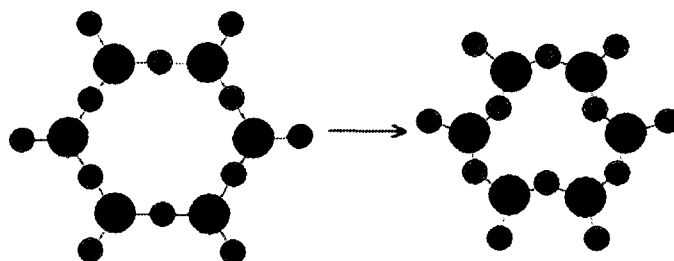
Figure 2.8 Transformation of hexagonal tetrahedral sheet to ditrigonal tetrahedral sheet in silica plane.

Another mechanism was proposed due to the electrostatic attraction of the hydroxide functional groups in the OH plane, which leads to the contraction of the OH bonds causing the halloysite layer to curl [32]. However, this mechanism does not explain why the halloysite layer is preferentially rolled into tubes instead of random curling from all the edges.

A third explanation for the halloysite layer rolling was provided by the role of the ionic substitutions in the halloysite layers. Tari, *et al.*, [4] claim that the substitution of the Si(IV)

with larger size Al(III) ions in the tetrahedral silica plane might be responsible for the rolling of the individual halloysite layers into halloysite nanotubes. According to their hypothesis, interlayer hydrogen bonding in the kaolinite mineral weakens due to the hydration process, which causes to the exfoliation of the multilayer kaolinite stack and the substitution of the silicon with aluminum ions expands the size of the silica plane causing sheets to roll into tubes [4]. The high content of aluminum in the halloysite samples analyzed by them shows the evidence that indeed the substitution of silicon atoms might take place. In this case, one should expect on increase of the tetrahedral aluminum ions in the halloysite nanotubes, which was not observed for the Georgia halloysite samples, as was reported by Newman, *et al.* [34].

One more curling mechanism was proposed by Kirkman on the basis of crystal dislocations theory, which states that continuous crystalline dislocations are responsible for the halloysite layer curling [35]. In Figure 2.9a, a crystal is bent due to plastic deformation and dislocations are randomly distributed. Figure 2.9b contains the same number of dislocations; however, dislocations are located at the boundaries causing the formation of the edges. It was proposed that plastically bent and polygonized forms of the dislocations correspond to the hydrated and dehydrated states of the halloysite. Indeed, polygonized morphology was observed for some dehydrated halloysite particles [36]. Relatively high cation exchange capacity (CEC) of the halloysite compared to kaolinite also supports this argument [2, 22].

a)   b)
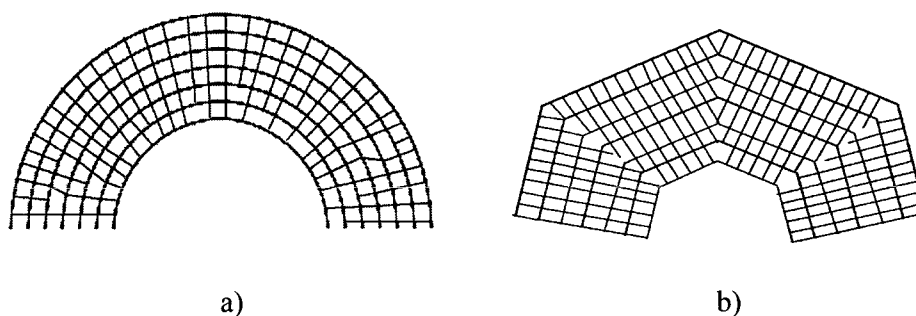
Figure 2.9 Plastically bent (a) and polygonized (b) crystals with continuous dislocations.

From all above discussion one can conclude that it is very hard to point out a single effect that can explain halloysite layer rolling. The highly variable nature of the halloysite nanotubes at different deposits also significantly complicates the analysis. Probably all of the above mentioned effects are responsible for the halloysite layer rolling to some extent leading to halloysite nanotubes with big variations in particle shapes and sizes.

Another factor affecting halloysite morphology that should be acknowledged is the impurities present in the halloysite. It was already mentioned that halloysite nanotubes may have lots of different impurities, mainly transition metal ions. All these impurities generate defects in the halloysite structure and cause the formation of lathes and uncompletely rolled tubules [2]. Substitution of the Al(III) ions with larger Fe(III) ions in octahedral sheets cause halloysite tubes in some deposits to unroll. On the other hand some scientists reported spherical halloysite samples with high iron content [2, 22]. Soma, *et al.* observed a double decrease in aluminum content with the increase of the iron content in some halloysite samples, which suggests that two aluminum ions were substituted with a single iron ion causing the increase of the vacancies and negative charge in the overall halloysite layer [22]. This might explain the high CEC of the tubular halloysites with high iron content.

2.3. <u>Comparison of Halloysite and Imogolite</u>

Imogolite is another mineral with a rolled layer structure with the alteration of silica tetrahedral and alumina octahedral units in the unit layer. Both of these minerals are thought to be formed from amorphous allophane in volcanic ash [37]. Comparison of the structures of these minerals might be very interesting for revealing some facts about the halloysite structure. In Table 2.1, some of the parameters of the halloysite and imogolite are described. Imogolite has one more alumina octahedron in its unit cell, as compared to halloysite [1, 38]. Therefore, in an imogolite layer both external and internal surfaces contain alumina octahedral sheets. The

positive surface charge of the imogolite gives strong evidence that in halloysite the internal alumina octahedrons are also positively charged, since both of these alumina octahedral sheets are chemically identical. Halloysite nanotubes are multiple walled and tubes are rolled like spirals, while imogolite is a single walled concentric tube [5, 38]. Therefore, external and internal diameters of the imogolite are much smaller than halloysite. On the contrary, layer thickness of the imogolite is bigger than halloysite [38]. The single walled structure of imogolite provides very large Specific Surface Area (SSA) compared to halloysite. The larger observed SSA of the halloysite compared to the theoretical value indicates that interlayer spacing between multilayer halloysite walls is partially available for nitrogen adsorption. One would expect imogolite to have a larger Cation Exchange Capability (CEC) than halloysite due to its larger SSA, which is not the case. CEC of these minerals are comparable with each other [2, 42]. This is probably due to the higher density of the vacancies in the rolled halloysite layers compared to imogolite. Vacancies increase the charge density of the halloysite layer and consecutively the Cation Exchange Capacity (CEC).

Table 2.1 Some structural parameters of halloysite and imogolite [2-5, 37-42].

	Halloysite	Imogolite
Morphology	mostly tubular, sometimes spherical or platy [1 - 5]	tubular thread-like units [37]
Ideal unit formula	$Al_2Si_2O_5(OH)_4$ [1-5]	$Al_4Si_2O_6(OH)_8$ [38]
Dimensions	10-50 nm inner diameter, 50-200 nm external diameter, 0.5-2 micron length [1-3]	1-7 nm inner diameter, 2-10 nm external diameter, 1-5 micron length [38 - 40]
Layer thickness	7.2Å [2]	8.4 Å [38]
Tube exterior chemistry	Silica tetrahedrons [2, 3]	Alumina octahedrons [38, 39]
Tube interior chemistry	Alumina octahedrons [2, 3]	Silica tetrahedrons / Alumina octahedrons [38, 39]
Surface charge	Negative [3, 4]	Positive [39]
Density	2.55 g/cm^3 [3]	2.65 g/cm^3 [40]
Specific Surface Area	Theoretical[a]: 20.4 m^2/g	Theoretical[a]: 530 m^2/g
	Observed[b]: 110-150 m^2/g [1-5]	Observed[b]: 200-400 m^2/g [41]
Cation Exchange Capacity	2 – 68 cmol+/kg [2]	23 – 57 cmol+/kg [42]

[a] Theoretical value of SSA was calculated for halloysite with 15 nm inner diameter and 50 nm external diameter, and for imogolite with 1 nm inner diameter and 2 nm external diameter.
[b] Value vased on Nitrogen adsorption BET measurements

2.4. Halloysite Nanotubes as Capsules for Encapsulation of Active Agents

Halloysite nanotubes can be loaded with a broad variety of substances from organic and inorganic molecules to drugs, polymers and proteins [3, 5, 43-46]. It can interact with molecules in a number of ways including, adsorption on the external and internal walls of the tubes [26, 47, 48], intercalation [2, 49-53] and loading of the substances into the internal lumen accompanied by crystallization of the loaded samples inside the pores [43-46, 54].

Partially or completely hydrated halloysite tubules are shown to intercalate a large variety of inorganic and organic substances into its interlayer spacing, which causes its interlayer spacing to expand [2]. Carr, *et al.*, reviewed intercalation behavior of more than 50 salts into halloysite interlayer spacing [50] and they concluded that most of the potassium and ammonium salts readily intercalate into halloysite interlayer spacing, while lithium and sodium salts are intercalating only in the forms of acetates. They related the intercalation behavior of the cations to their influence on the entropy of the interlayer water [50]. Besides, halloysite was shown to intercalate organic substances, such as ethylene glycol, glycerine, formamide, and dimethyl sulfoxide [2, 52, 53]. In all of the cases strong interaction between substance and halloysite layers is required. Frost, *et al.*, summarized the substances that can be intercalated into halloysite layers in three categories [51]. The first group includes compounds that form strong hydrogen bonds with the silicon tetrahedral sheets, such as urea, hydrazine, acetamide, etc. Substances have to contain either NH_2 or OH functional groups for the formation of the hydrogen bonds. The second group is the substances that can interact with the silica layer with strong dipole interactions. Molecules with high dipole moments, such as dimethyl sulfoxide, can be included in this group. The third group are the organic salts (mainly acetates or propionates) of the alkali metals, such as potassium or sodium that can interact with the alumina layer through their anions [51].

The intercalation phenomenon is strongly associated with the presence of the interlayer water between halloysite layers, since completely dehydrated halloysite does not show any intercalation in many cases even though some authors reported partial intercalation for samples from certain deposits in New Zealand [52, 55]. This is probably due to the presence of small traces of water in the interlayer spacing of these samples which did not influence interlayer distance. Indeed, complete removal of the interlayer water requires a high temperature treatment (up to ~ 300° C) [2]. Tubules that underwent high temperature

treatment do not show intercalation behaviour due to the strong interlayer hydrogen bonds existing between halloysite layers [52]. Intercalation of the dehydrated halloysite would take place similar to the process shown in Figure 2.3, except in the opposite direction. It is obvious that such a process, i.e. sliding of the halloysite layers relative to each other, is accompanied by the breaking of the interlayer hydrogen bonds and requires large amounts of energy. Intercalation behaviour of the halloysite samples can be very useful for the treatment of water from impurities, since halloysite can absorb large amounts of the substance due to its high surface area. However, in terms of applications for sustained release, this mechanism of loading is not very impressive since intercalated substances are easily lost upon washing with water. Besides, small space between layers is not available for most of the high molecular weight substances such as proteins, polyelectrolytes and drugs.

The empty lumen of the halloysite nanotubes provides very effective capsules for loading with active agents. The general procedure for the halloysite loading is as follows. First, halloysite is mixed as a dry powder with a saturated solution of the compound to be loaded. The solvent has to be non-viscous and in which the active agent has high solubility and halloysite forms a stable colloid. Water, acetone and ethanol are the most commonly used solvents [3, 5, 10, 16, 56]. Once halloysite is added to the solution, the suspension is sonicated for 20 min in order to disperse the halloysite. Then a beaker containing the suspension is transferred to a vacuum jar, which is then evacuated using a mechanical vacuum pump. The suspension should be kept under vacuum for approximately 30 min and then removed to atmospheric pressure. Slight fizzing of the solution under vacuum indicates air bubbles being removed from the tubule lumen under vacuum. Once the vacuum is broken, the solution containing the active agent enters into the pores and partial crystallization of the loaded substance takes place inside the pores. After this procedure, tubules are washed with water in order to remove loosely attached substance from the external walls [5, 16].

The processes taking place during the loading procedure is briefly described in Figure 2.10. Evaporation of the solvent under vacuum elevates the concentration of the loading substance in the bulk solution which increases the concentration gradient between the tubule lumen and external solution. The concentration gradient plays a major role in tube loading therefore; fast drying solvents with low viscosities, such as acetone or ethanol, are preferable for organic substances. On the other hand, a high dielectric constant of the solvent is desirable since it provides ionization of the hydroxyl groups at the external and internal walls of the halloysite tubes, which stabilizes halloysite in the suspension and enhances the loading of the negatively charged molecules by means of electrostatic force (inner lumen of the halloysite has positive charge at pH of the solution below 8.5) [16]. Therefore, water with high dielectric constant of 80.1 at room temperature is most commonly used for loading inorganic substances [54]. In addition, water can be preferred in some cases due to toxicity issues related with other solvents or in order to preserve the activity of the loaded agents (such as enzymes).
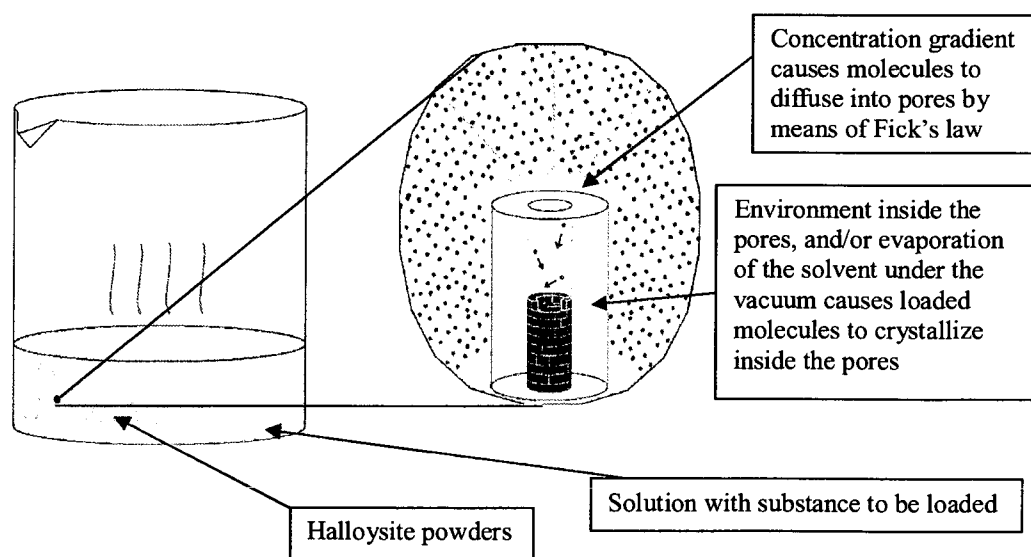
Figure 2.10 Processes taking place during the loading process.

In Figure 2.11, TEM images of halloysite nanotubes loaded with some inorganic substances are described. Silver was loaded into halloysite by using silver acetate solution in water by following the general procedure described above. Then, loaded tubules were washed with fresh water, dried at 100 °C and further heated at 300 °C in order to decompose the silver acetate into silver. As seen from the images Figure 2.11a and Figure 2.11b the tubule lumen is filled with silver, indicating the high efficiency of the loading. Figure 2.11b is the expanded image of the selected area in Figure 2.11a. The clear crystalline structure of the silver is visible from the image.

Figure 2.11c shows halloysite nanotubes loaded with sodium tetrachloropalladate, a catalyst that is used for the metallization of the halloysite. Earlier, Price, *et al.,* successfully demonstrated the deposition of the metallic iron and copper onto halloysite external and internal walls by using this catalyst. Halloysite nanotube loaded with potassium permanganate is shown in Fig. 2.11d. Potassium permanganate is deposited both on the external surface and the inner lumen. Exterior substances are washed away much easier during the exposure of the tubes to water.

Figures 2.11e and 2.11f describe halloysite nanotubes loaded with calcium carbonate. Calcium carbonate was deposited inside the tubes by means of the interaction between calcium ions from the external solution and carbonate ions produced by urease enzyme. The urease that was preliminarily loaded inside the tubes absorbs urea from the external bulk solution and releases carbonate ions into the pores of the tubes. Upon exposure of the tubes to a solution containing Ca^{+2} ions, calcium carbonate starts to precipitate inside the pores. The TEM image clearly indicates the efficient loading of the tubes and the SEM image shows calcium carbonate precipitate at the tube openings. Presence of calcium carbonate inside the tubes was further verified by X-ray diffraction analysis and calcium carbonate was observed to be in its vaterite modification rather than more stable calcite [36].
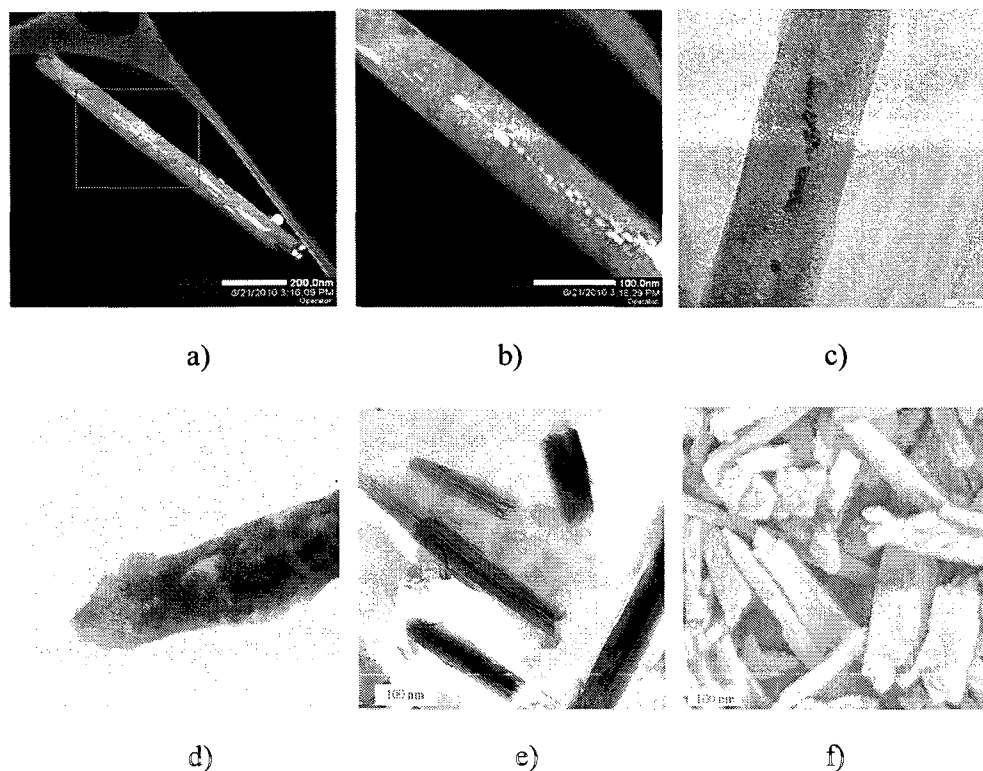
Figure 2.11 Images of the halloysite samples loaded with silver (a, b), sodium tetrachloropalladate - Na_2PdCl_4 (c), potassium permanganate-$KMnO_4$ (d) and calcium carbonate (e, f), *National Institute of Materials Sciences, Tsukuba, Japan* [36, 57].

2.5. Release Characteristics of Active Agents

2.5.1. Inorganic substances

Halloysite nanotubes provide long time sustained release for the loaded salts and effectively encapsulate them from the influence of the external environment. Complete release of the inorganic compounds from halloysite nanotubes is achieved within 1-2 hrs, which is faster than organic compounds (will be described further). This is related to several factors namely; faster diffusivity of the inorganic ions in water, higher solubility of the inorganic salts than organic substances and weaker interaction of the inorganic ions with the walls of the halloysite nanotubes, which is limited to electrostatic force. In the case of organic substances, interaction is more complex and may include a number of forces including hydrogen bond, electrostatic and Van der Waals interactions.

In Figure 2.12, release profiles of four inorganic substances; ammonium molybdate

$((NH_4)_6Mo_7O_{24})$, potassium permanganate $(KMnO_4)$, sodium silicate (Na_2SiO_3) and sodium

chromate (Na_2CrO_4) is described. Substances were loaded into halloysite nanotubes by using

their saturated solution in water.A release experiment was conducted in water and

supernatants were collected at certain time intervals in order to determine the concentration

of ions leaked from the tubules. Fresh water was added instead of taken supernatants.

Concentrations of the ions were determined by UV-Vis spectrophotometry at a wavelength of

210 nm for molybdate ions, 530 nm for permanganate ions, 370 nm for chromate ions and

190 nm for silicate ions. Partial decomposition of potassium permanganate to water insoluble

manganese dioxide was observed during the release experiment.
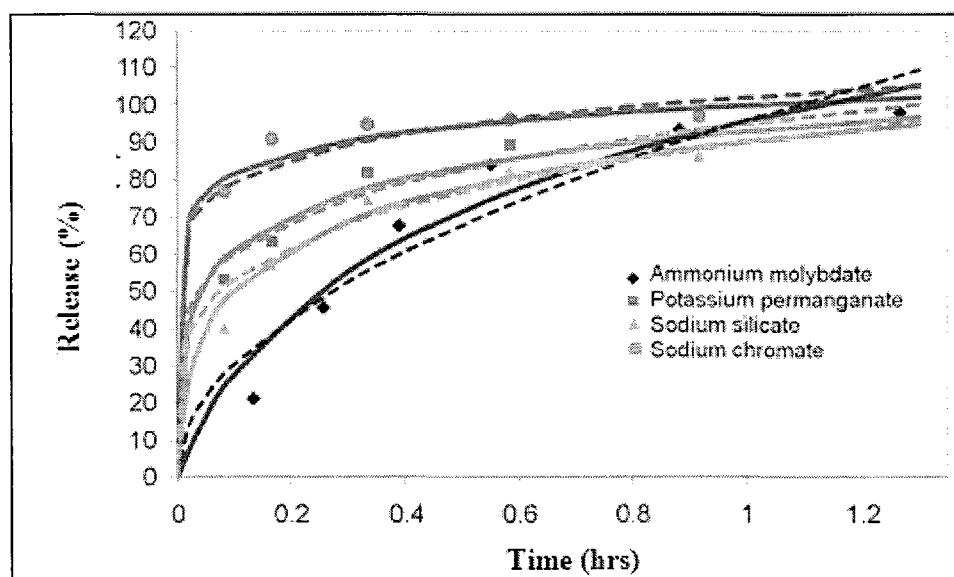
Figure 2.12 Release of 4 inorganic salts; ammonium molybdate $((NH_4)_6Mo_7O_{24})$, potassium permanganate $(KMnO_4)$, sodium silicate (Na_2SiO_3) and sodium chromate (Na_2CrO_4) from halloysite nanotubes. Curves were fit with power function $(R_t = K*t^n$, dashed lines) and logarithmic function $(R_t = A*ln(t+b)+C$, solid lines) [57].

Release profiles were fit with both power and logarithmic functions. $R_t = K*t^n$ function

was used to describe power function profile, where R_t is the amount of released inorganic

substance at time t and K and n are experimental constants determined from the best fit. On the other hand, $R_t = A*ln(t+b)+C$ function was used for the logarithmic profile, where, A, b and C are experimental constants determined from the best fit. As is seen from the curves, both of the profiles are very much close to each other. The power function profile is the basis of the Peppas-Sahlin model in which K is related to the diffusion speed of the leaking substance and n is related to the diffusion mechanism and geometry of the capsules. When n = 0.5, diffusion is Fickian, and when n = 1.0, zero diffusion follows zero order kinetics. Further, we will use the power function to describe release profiles.

Table 2.2 describes the empirical parameters of the exponential and logarithmic functions determined from the best fit. As one can observe, the K value in the power model is very close in all of the cases being in the range of the 90-105. However, the n value of the molybdate ions is significantly different than the other salts. This might be related to the higher interaction of the molybdate ions with the halloysite tubule interior due to its higher negative charge (-6 for molybdate, -1 for permanganate and -2 for others). Higher charge of the ions increases electrostatic interaction with the positively charged tubule inner walls, which significantly alters its release profile. Significant difference is also evident in the values of A on the logarithmic profile between ammonium molybdate and other salts.

Table 2.2 Constants of the exponential and logarithmic functions determined from the best fit of the release of the inorganic substances [57].

Salts		$(NH_4)_6Mo_7O_{24}$	$KMnO_4$	Na_2CrO_4	Na_2SiO_3
Exponential model	K	96.0	95.0	102.0	90.0
	n	0.50	0.20	0.11	0.23
Logarithmic Model	A	40.0	14.0	8.0	18.0
	b	0.10	$1.3*10^{-3}$	$3.7*10^{-6}$	$6.8*10^{-3}$
	C	92.0	93.0	100.0	90.0

2.5.2. Organic substances

Organic substances include a wide range of chemicals, such as organic corrosion inhibitors, antifouling agents, drugs, antiseptics, enzymes and proteins [5, 16, 43]. Due to the wider range of the organic substances, we will analyze them in three categories; (a) low molecular weight substances (Mw < 200 g/mole), (b) medium molecular weight substances (Mw in the range of 200 – 1000 g/mole) and (c) high molecular weight substances (Mw more than 1000 g/mole).

2.5.2.1. Low molecular weight substances. Low molecular weight organic compounds include organic corrosion inhibitors, insecticides, some pharmaceuticals, such as glycerol and ascorbic acid.

In Figure 2.13, release profiles of 4 different corrosion inhibitors; benzotriazole, 8-hydroxyquinoline, 2-mercaptobenzothiazole and 2-mercaptobenzimidazole are shown. Curves were fit with the power function in all of the cases. Loading efficiency of the inhibitors were ~ 6 wt% for benzotriazole and 10-30 wt% for the rest of the corrosion inhibitors. Higher loading efficiency of the other corrosion inhibitors may be ascribed to their lower solubilities in water compared to benzotriazole. More benzotriazole is washed away from the tubes in the washing stage due to its higher
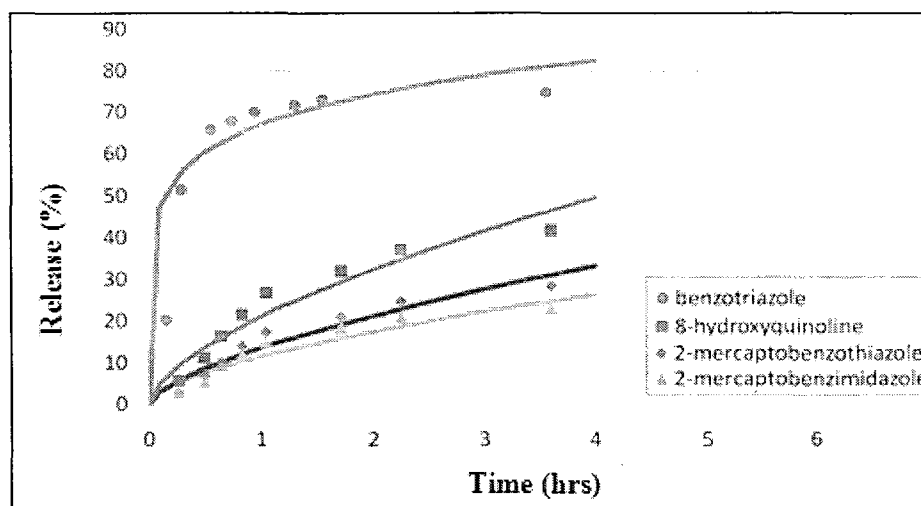
Figure 2.13 Release profiles of three different organic corrosion inhibitors; benzotriazole, 8-hydroxyquinoline, 2-mercaptobenzothiazole and 2-mercaptobenzimidazole from halloysite nanotubes in water [57].

A power function was found to fit fairly well with most of the release profiles that were described so far. However, this function fails to describe long time release profiles with a reasonable match. A power function with constant values of K and n describes only certain section of the release profile reasonably well. In Figure 2.13, release profiles of the corrosion inhibitors were described only within 4 hours. A different set of values for K and n are required to describe different sections of the release profile in most of the cases. This finding leads us to conclude that the values of K and n changes with time during the release experiment and a simple relationship with constants K and n is not sufficient in most of the cases, i.e. both K and n are functions of time. In the simple case we can use polynomial functions to determine the functional dependence between values of K and n, and time.

In Figure 2.14, the release profile of the benzotriazole from halloysite nanotube is shown. The data was fit to a power function with variable values of K and n which have polynomial dependence with respect to time. For simplicity, we used 1st order and 2nd order polynomials to describe the dependence of K and n with time. Higher order polynomials

significantly complicate the analysis. A curve with constant values of K and n (0th order) was also plotted for comparison. 1st and 2nd order polynomial dependence makes the model fit the experimental data fairly well, much better than the original power function with constant K and n. Table 2.3 describes the functions that were used to fit release data with the power function model.

Table 2.3 Polynomial functions used for determination of the values of K(t) and n(t) at time t for benzotriazole release profile [57].

Order of polynomials	0th order	1st order	2nd order
K	53.37	0.47t + 63.0	$- 0.017t^2 + 3.1t + 58.0$
n	0.163	$- 0.0017t + 0.10$	$0.00019t^2 - 0.0138t + 0.105$
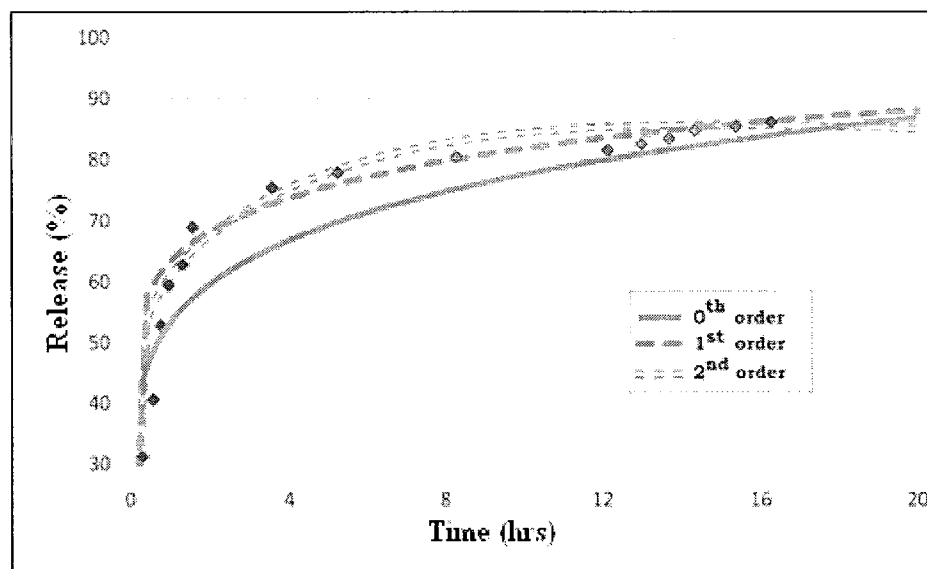
Figure 2.14 Release profile of benzotriazole from halloysite nanotube. Data was fit with the power model $R_t = K(t)*t^{n(t)}$ [57].

Halloysite nanotubes can be used for encapsulation of pharmaceuticals to provide a long time effect to cosmetic creams. A patent exists regarding the usage of halloysite nanotubes

for cosmetic agents [74]. In Figure 2.15, the release profile of glycerin, a skin humectant, is shown. The concentration of the glycerin was measured by using the discoloration of the potassium dichromate solution which was proportional to the concentration of the glycerin. The release profile was fit to the power function where values of K and n were 12.5 and 0.547. Halloysite stores most of the glycerin at the initial stage. Only 30% of the glycerin was released within 10 hours. Loading efficiency of the glycerin was 20.0 wt% [58].
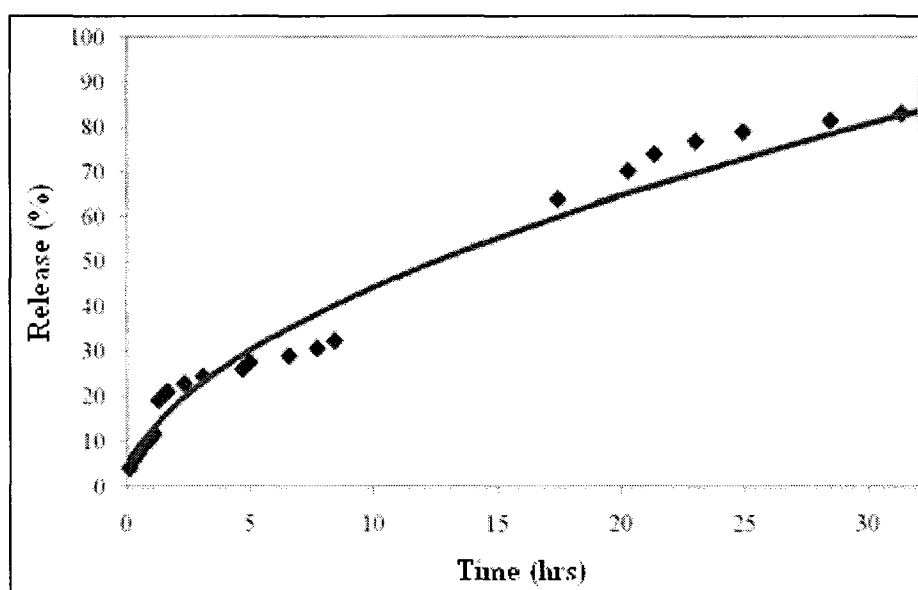
Figure 2.15 Glycerine release profiles from halloysite sample obtained from Dragon mine in Utah [58].

2.5.2.2. Medium molecular weight substances. Medium molecular weight substances include most of the drugs, antiseptics and some pharmaceuticals. In Figure 2.16, the chemical formulas of three hydrophobic drugs; furosemide, nifedipine and dexamethasone are shown. All of these drugs have low solubility in water [28].
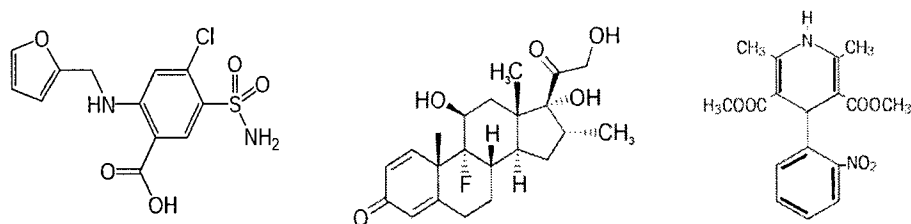
Figure 2.16: Chemical formulas of furosemide (MW 330.8), dexamethasone (MW 392.5), nifedipine (MW 346.3) [28].

In Figure 2.17, the release profiles of the drugs entrapped in halloysite nanotubes are shown. Release profiles from the naked drug crystals are also shown for comparison. Complete dissolution of furosemide, dexamethasone and nifedipine crystals took place in 15, 30 and 40 minutes, respectively. However, encapsulation with halloysite reduced the drug release rate by more than 5 times. Only 70% of dexamethasone was released within 4.0 hrs. In the case of furosemide and nifedipine, the release rate was even lower, being 50% and 40% [43].
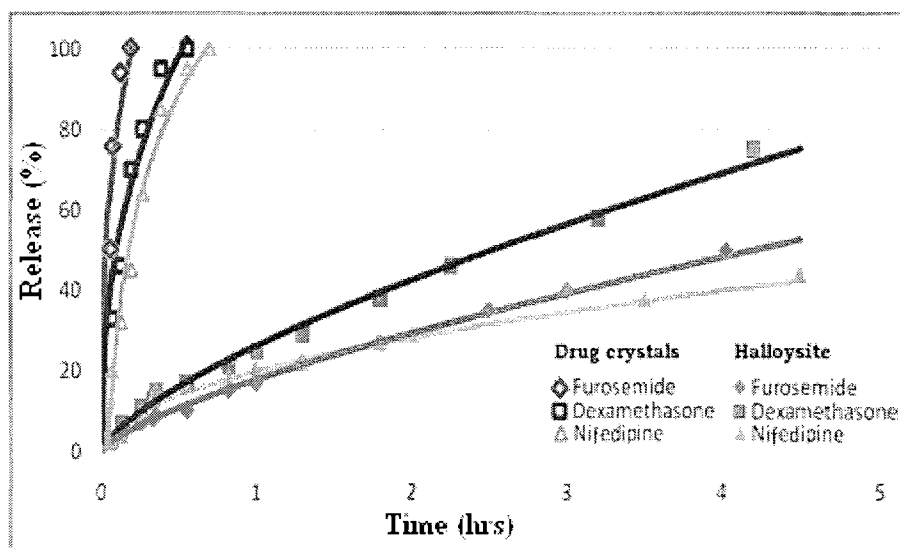
Figure 2.17 Release of three hydrophobic drugs from halloysite nanotubes (filled markers) and dissolution from naked drug crystals (empty markers) in water. Drugs were loaded into halloysite by using 50% ethanol-water solution [28, 43].

Table 2.4 describes the parameters of the Peppas-Sahlin model for the described release curves. Values of K decreased 5 – 6 times for dexamethasone and nifedipine, which indicates the reduced diffusion rate of the drugs in the halloysite lumen. In the case of furosemide, a 10 fold reduction of K was observed. Probably, furosemide has stronger interaction with halloysite nanotubes compared to dexamethasone and nifepidine. The release mechanism of the furosemide and dexamethasone seems to be identical, both of the drugs fit to the model with an identical exponential constant of 0.70 which is approaching zero order kinetics. Nifedipine follows Fickian mechanism with n being equal to 0.5. Drug release profiles from naked crystals are also very close to the Fickian profile [43].

Table 2.4 Constants of the Peppas-Sahlin model for drug release determined from the best fit of the release profiles [28, 43].

Drugs	Release from drug crystals		Release from halloysite	
	K	n	K	n
Furosemide	176	0.34	17.8	0.71
Dexamethasone	130	0.40	26.2	0.70
Nifepidine	120	0.45	20.0	0.50

The acidity of the solution was observed to have a significant effect on drug loading and release properties. Figure 2.18a describes dexamethasone release profiles from halloysite nanotubes loaded from water of different acidity. Low values of pH increases the loading efficiency, i.e. 5.5 wt% loading was observed for pH = 1.4 while loading was only 2.0 wt% at pH of 9.4. Higher loading efficiency of the drug can be related to a number of reasons; higher solubility of the drug at low pH and increased positive charge of the halloysite inner lumen. The type of solvent used also has a significant effect on the loading efficiency of the drugs. Ethanol – water mixture provides better loading efficiency than just pure water, which is

related to the higher solubility of the drugs in ethanol (Figure 2.18b). In all of the cases

higher loading efficiency leads to faster release [43].
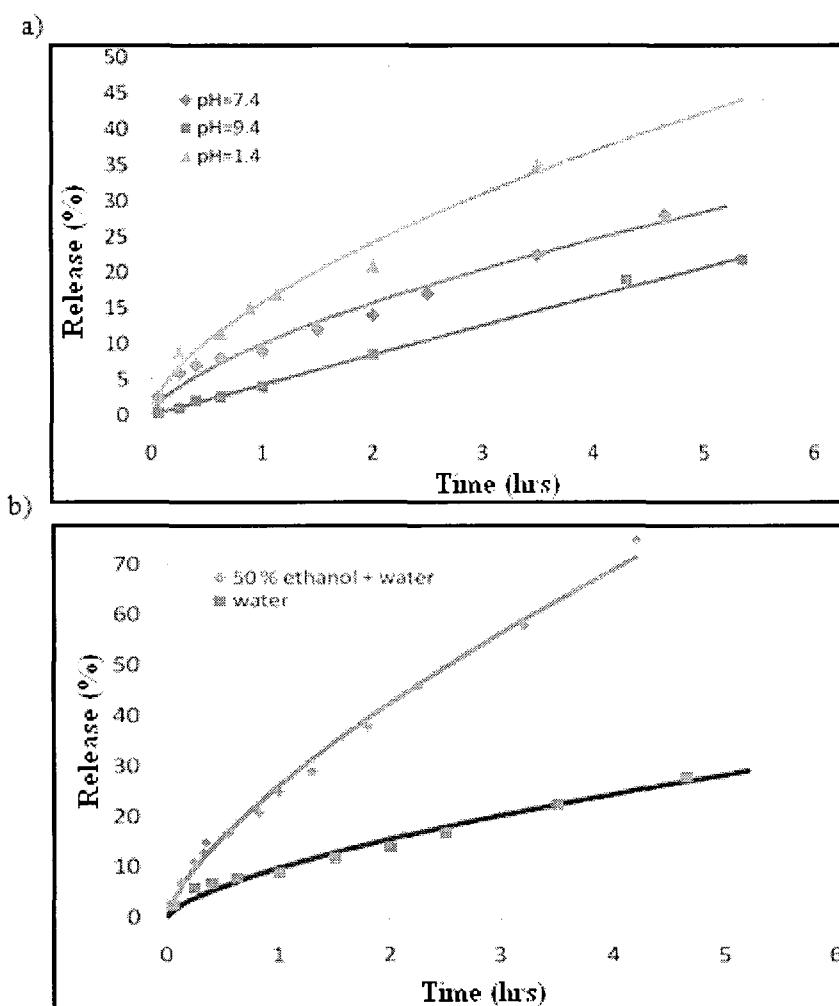
Figure 2.18 Release of Dexamethasone that was loaded into halloysite at different conditions (a) in water with three different pH values of the solution; 1.4, 7.4 and 9.4, (b) in water and 50% ethanol-water mixture [43].

There seems to be some connection between loading efficiency and the release rate of

the loaded drugs. Higher loading leads to higher values of K and lower values of n. In the

current case, the value of K reduces from 15 to 4 while increasing the pH of the solution from

1.4 to 9.4. The values of n increases from 0.6 to 1.0 indicating that the release mechanism is

approaching from Fickian diffusion to zero order kinetics with increasing pH [28, 43].

While using ethanol-water mixture instead of water to load dexamethasone, exponential constant n remained almost constant 0.65 ± 0.05, however, values of K increased from 10.0 to 26.2 by addition of 50% ethanol. This result indicates that the release profile is affected mainly due to the diffusion of the molecule from the pores of the halloysite rather than the change in the release mechanism (Fickian or zero order kinetics) while using ethanol-water mixture for loading drugs [43].

2.5.2.3. High molecular weight substances.

High molecular weight substances include enzymes, proteins, and polyelectrolytes with molecular weight above 2000 g /mole. Release rates of high molecular weight substances are very slow, complete release lasting more than 500 hrs in many cases. This is due to their lower diffusion rate in water as well as stronger adsorption to the halloysite surface. High molecular weight substances have more OH, NH_2, or other functional groups that can interact with the halloysite surface OH groups through hydrogen bonding or Van de Waals interaction, which makes their release very slow.

In Figure 2.19, the release profile of insulin from halloysite nanotubes is shown. Insulin is a globular protein with diameter of about 2 nm and isoelectric point at pH=5.9. Seventy percent release was observed within 140 hours. For comparison, it takes about 5 hours for low molecular weight substances and 10 hours for medium weight substances to achieve such an amount of release. Data fits with Peppas-Sahlin model reasonably well with the parameters of 3.8 and 0.6 for K and n, respectively. Reduction in the release rate was primarily due to the reduced diffusion rate of the polymers and the release mechanism is very close to the Fickian profile. This interesting phenomenon was observed while conducting the release of insulin in the presence of tiny amounts of positively charged polyelectrolyte, polyethyleneimine. The release rate increased more than 50 times by adding 0.1% of polyethyleneimine. It is believed that polyethyleneimine adsorbs to the halloysite lumen and interacts with insulin, which has negative charge at neutral pH of the solution, by forming

interpolyelectrolyte complexes. The interpolyelectrolyte complex has significantly less interaction with the halloysite surface than pure insulin due to the neutralization of its charge by polyethyleneimine. The release profile of the insulin fits to the Peppas-Sahlin model with the values of K and n being 38.0 and 0.6 respectively. Value of the K increased 10 fold. This might indicate that the insulin-polyethyleneimine complex has 10 fold less interaction with halloysite compared to pure insulin.
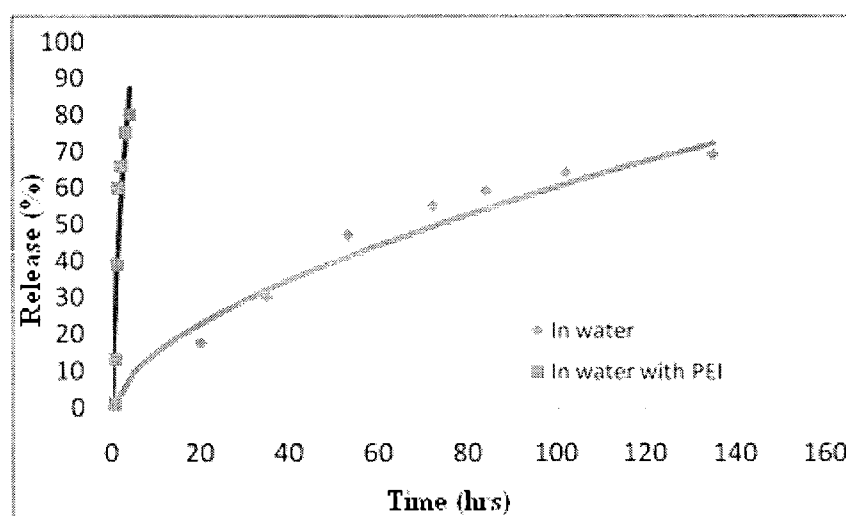
Figure 2.19 Insulin release at two different conditions; fresh water and water containing 0.1% cationic polyelectrolyte, polyethylenimine (PEI) in neutral pH [43].

2.6. Application Areas of Halloysite Nanotubes

Having high surface area, elongated tubular shape with a lumen which can serve as a nanocontainer, and being environmentally friendly, halloysite mineral can be extensively used in the industry, mainly in ceramic materials [59, 60]. It belongs to the clay minerals family and can substitute for kaolinite, montmorillionite bentonite, etc., as additives in composites. Particularly in paper production, modification of wood fibers by halloysite nanotubes has proven to increase the brightness and porosity of the paper sheets [43, 59]. In the ceramic industry, halloysite is mainly used in the tableware market as an addition to bone

china and porcelain products [60]. Halloysite also has several current and potential applications in the field of nanotechnology. Companies in the United States of America, United Kingdom and China (such as Applied Minerals Inc., NanoDynamics, Imerys) are producing halloysite materials [61]. Applications of the halloysite nanotubes in nanotechnology can be in the following major areas:

1) Additives in polymer composites [63-73]

2) Controlled release of biologically active compounds for medical and pharmaceutical applications [3, 5, 28, 43-46]

3) Nanocontainers to embed corrosion inhibitors into metal coatings for increased corrosion protection [10, 16, 56, 62]

4) Synthesis of nanoengineered electroactive composites for applications in the electronic industry [2, 12, 86-88]

5) Catalysts for hydrocarbon conversion for the petroleum industry [89-93]

2.6.1. Polymer nanocomposites

Polymer nanocomposites are one of the emerging and expanding fields in plastic technology offering a broad spectrum of useful material properties, such as increased tensile strength and flame retardancy, reduced weight, and lower cost [63-69]. Due to these useful properties polymer nanocomposites find application in automotive components, construction materials, packaging materials, in drug delivery, sensor applications and medical devices [63, 64].

Platy clay minerals are one of the most commonly used materials in plastic nanocomposites due to their high availability in nature [63]. However, one of the drawbacks of the platy clay minerals is their incompatibility with hydrophobic polymers. They require a long, time consuming exfoliation process to break down the multilayered structure in order to obtain fine dispersion in polymers. This process often involves modification of the clay

minerals with surfactants or organosilanes to obtain hydrophobic surface for better dispersion in the polymer matrix [63, 64].

Halloysite nanotubes offers great promise in polymer composite applications, since these materials do not require long processing, due to the absence of the stacked platy sheets (contrary to the platy clays, such as kaolinite) [64]. Halloysite mineral is more disordered as compared to platy minerals, which makes its dispersion simpler [2, 64]. Many different halloysite-polymer composites were produced by Guo, *et al.* (such as rubber [65], polyamide [66], epoxy resin [67], polypropylene [68 – 70]). Mechanical properties were reported to improve remarkably in many of the cases. Du, *et al.* showed that incorporation of 5 % halloysite in polypropylene increased the flexural modulus of the composite by 35% while tensile strength was improved by 6.1% [68]. An addition of halloysite into polar polymers such as polyamide and polybutylene terephtalate, also showed significant improvement in the tensile properties of the composite as compared to the pure polymer [66]. The reason for the improvement in polymer composite tensile properties is believed to be the high aspect ratio of the halloysite tubes. On the other hand, adjustment of the polymer-halloysite interaction with surface modification, such as silanization of the tubes, results in even more significant improvement in polymer composite mechanical properties, as compared to neat halloysite [68].

Halloysite polymer composites also show increased flame retardancy. Improved resistance towards thermal decomposition was attributed to encapsulation of decomposition products by the halloysite empty lumen and barrier properties of the tubes in the polymer matrix [69, 70].

There are three most common ways to prepare halloysite-polymer nanocomposites: One of the ways is to disperse fine halloysite nanoparticles in monomer and conduct *in situ* polymerization. In this method, molecules of the monomer interact with the halloysite surface

and form a uniform suspension. Sonication might be required to obtain fine dispersions. Then an initiator is added to the system to start polymerization. Polymerization can be initiated by light or heat. An advantage of this process is that it does not require a solvent and can be applied to insoluble polymers. This kind of polymerization often leads to low molecular weight products. Uniformity of the composite depends on the diffusion rate of the monomers into the spacing between nanoparticles [63].

Another method is solution casting or exfoliation, which involves the dispersion of halloysite and polymer in the solvent to obtain a uniform matrix. Sonication might be required in many cases to obtain uniform dispersion. Then the solvent is evaporated to obtain halloysite-polymer composites. This method is preferred for water soluble polymers, such as polyvinyl alcohol [63, 71].

The third method involves the addition of halloysite directly into the polymer in a molten state and blending to obtain a uniform distribution of the halloysite nanotubes in the polymer matrix. The advantage of this method is its simplicity and environmental friendliness. However, slow penetration of polymer molecules into clay matrix usually results in poorly distributed nanoparticles inside the composite which leads to clay aggregates. Halloysite nanotubes were shown to form uniformly distributed composites using the melt blending method for polyamides and polybutadiene terephtalate [63, 66].

Another prospective application of halloysite nanotubes is the paint industry. Current paint products contain a lot of based on nanoparticles, such as titanium dioxide (rutile), silica, clay, mica, latex, etc. Some of these nanoparticles are added to improve the properties of the paint while others are added just for the reduction of the product price [72, 73]. Halloysite nanotubes offer great promise for the paint industry because these particles are readily miscible with a large variety of coatings and significantly improve their mechanical properties.

In Figure 2.20a, stress-strain relationship of oil based blue paint and halloysite paint composite is shown. Addition of 10% of the halloysite significantly improved the tensile strength of the paint. On the other hand, halloysite paint composite also shows much better performance towards rapid deformation, as compared to pure paint, which is demonstrated in Figure 2.20b and 2.20c. A 0.2 kg metal bar was dropped onto the painted iron plates (on the basis of A366 alloy) from the height of 1 m in order to subject the plates to the rapid deformation. The thickness of the metal plate was 1 mm in both cases. As is indicated in the picture, metal coated with pure paint has a lot of cracks in it due to rapid deformation of the plate, while the same paint containing 10% halloysite did not show any evidence of cracking. In addition to the improvement of mechanical properties, halloysite nanotubes can effectively be used to incorporate corrosion inhibitors into metal coatings. This property of the halloysite nanotubes will be discussed in the next section [30].
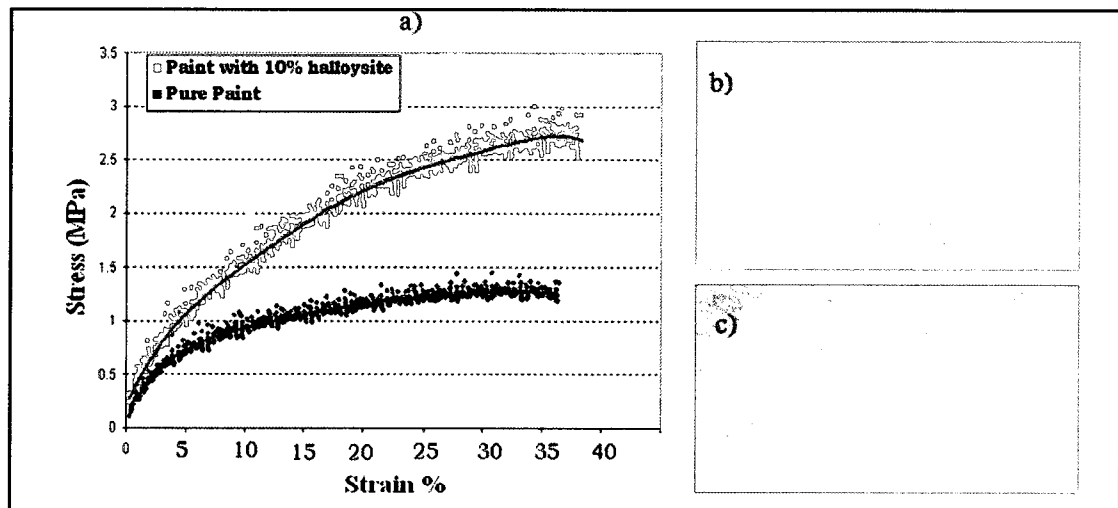
Figure 2.20 Mechanical properties of pure paint and halloysite paint nanocomposite. a) Stress-strain relationship, and images of the b) pure paint and c) 10% halloysite-paint composite after weight drop test. Paint was prepared on the basis of ECS 34 powder, blue (manufactured by True Test Co.) [30].

2.6.2. Controlled release of biologically active agents

There is an increasing demand for the usage of nanometer scale containers for different technological [8, 10, 16] and biomedical applications [3, 5, 28, 43-46]. Ideally, such containers would retain chemical agents for a long time and release them on demand due to an external influence or signal, thus providing self-healing. Cylindrical nanotubes have gained substantial interest due to their high loading capacity. A hollow tubular structure makes halloysite very interesting in terms of controlled release applications due to their higher availability and cost effectiveness [5]. A lot of biologically active substances including biocides [5, 74], antifouling agents [5] and drugs [3, 5, 28, 43-46] were effectively encapsulated by using halloysite nanotubes.

Controllable and sustained drug delivery is very highly prized in medicine due to the fact that slow release of medicines into the organism provides a long term healing effect without drug overdose [28, 74]. It was shown that encapsulation of drugs by halloysite significantly slows the drug dissolution rate in the surrounding liquid media [28, 43]. Sustained release during days and weeks is highly desirable when continuous supply of the drug is necessary.

Even though halloysite is biocompatible it cannot be injected into the body since it is not biodegradable. Therefore, medical applications of the halloysite is confined to over skin applications, artificial bone cements and dental applications which do not lead to the accumulation of the clay particles in the body [75, 76]. One of the possible medical applications of halloysite nanotubes includes porous scaffolds for healing wounds or cuts. Halloysite nanotubes can be mixed with biocompatible polymers such as polycaprolactame (PCL) and porous scaffolds can be produced from it by a procedure called electrospinning. Electrospinning involves the migration of the jet of charged liquid under high electric field. Figure 2.21a describes the experimental setup for the electrospinning process. The substance to be electrosprayed is contained inside the syringe. Pressure drives the liquid out of the

needle and a high potential (5-50 kV) that is applied between the needle and metal screen drives the jet towards the screen. A fibrous scaffold was produced from PCL by using the electrospinning process, as described in Figure 2.21b. When halloysite is added, ball shaped aggregates of the halloysite forms in the scaffold (Figure 2.21c). The diameters of the balls range from 5 to 20 microns depending on the concentration and the dispersion state of the halloysite in the initial PCL solution. These balls provide an opportunity to entrap antiseptic agents such as iodine, brilliant green, chlorhexidine, etc. to provide antiseptic coatings for over-skin medical applications [75].
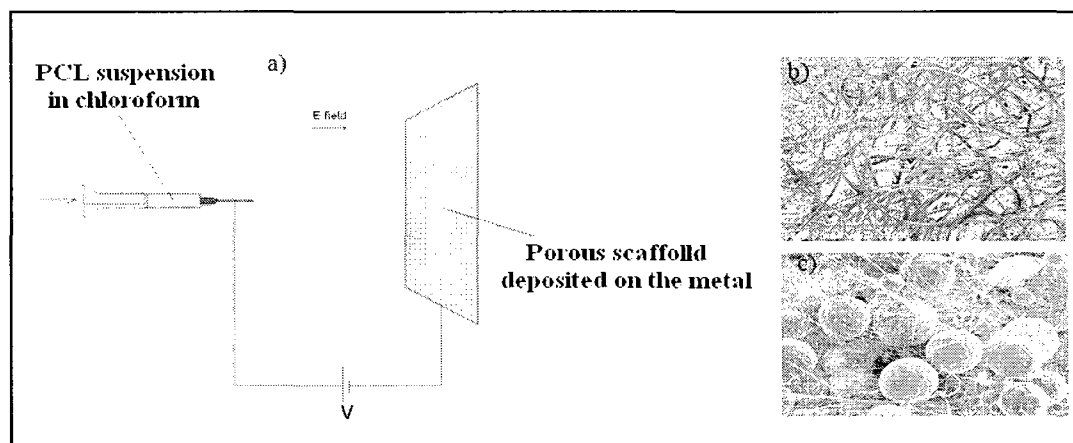
Figure 2.21 Preparation procedure of the polycaprolactame (PCL) scaffold by electrospinning (a), SEM image of the PCL scaffold (b), and PCL-halloysite composite (c) [75].

Another prospective medical application of the halloysite nanotubes includes the production of artificial bone cements. Figure 2.22 shows SEM images of polymethylmetacrilate (PMMA) bone cement samples containing halloysite nanotubes. Strong adhesion between halloysite and PMMA is clearly evident. Addition of 5% halloysite into PMMA significantly increases its tensile strength, which is very crucial to avoid failures in the cement. Halloysite nanotubes can also encapsulate some active agents, such as antibiotics and bone growth hormones. Encapsulation with halloysite avoids the interaction

between loaded agents and other bone cement components and provides a long time release which is necessary for long time effect [76].
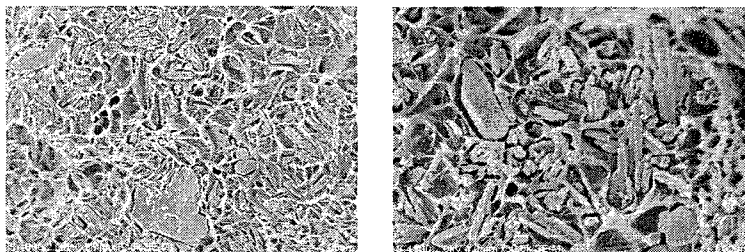
Figure 2.22 SEM images of the artificial bone cement based on halloysite-PMMA composite [76].

2.6.3. Nanocontainers for corrosion inhibitors

One of the fields of technology that benefits from the unique tubular structure of the halloysite is the paint and coatings industry. Halloysite empty lumens can be loaded with corrosion inhibitors to achieve sustained slow release. Being compatible with polymer paints, loaded halloysite tubes are readily miscible with metal coatings. Earlier it was mentioned that the addition of 10% halloysite into paints significantly improves their tensile properties. In addition to all these benefits, due to its empty lumen, halloysite nanotubes can be utilized to entrap corrosion inhibitors, which may improve anticorrosive metal coatings [16, 77].

A corrosion resistance study on painted copper strips (Figure 2.23) revealed the increased corrosion inhibition performance of the coatings on the basis of the paint-halloysite composites. Strips were exposed to a highly corrosive solution containing 24 g/L of NaCl, 3.8 g/L of $CaCl_2$, and 2 g/L of Na_2SO_4 for 10 days. As seen from the image, the strip coated with ordinary paint is completely covered with rust while the strip coated with halloysite-paint composite shows no evidence of rust [30]. The reason for the increased corrosion resistance of this coating is the slow release of the corrosion inhibitor entrapped in

the hollow lumen of the tubes. The corrosion inhibitor is slowly released to the corrosive media, once the paint is damaged, facilitating the healing of the damage [30, 77].

a)   b)
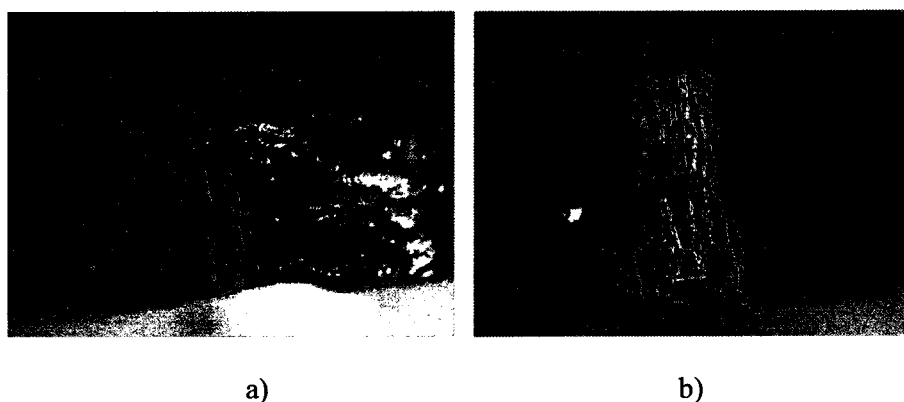
Figure 2.23 Copper strips coated with pure paint (a) and paint-halloysite composite (b) [30].

Halloysite nanotubes also significantly improved the anticorrosive performance of the sol-gel coatings. Shchukin, *et al.* showed that tubules loaded with various organic corrosion inhibitors, such as benzotriazole and 8-hydroxyquinoline significantly improves the anticorrosion property of the coatings for 2024 Aluminum alloy [5, 8, 10, 16, 77]. In Figure 2.24, localized corrosion current densities on coated and artificially scratched metal strips are shown. Corrosion current densities were measured by using the Scanning Vibrating Electrode Technique, a method that uses a vibrating PtIr electrode to detect corrosion current densities at certain locations on the metal surface [78]. The activity of the anodic corrosion current at the scratch of the pure sol-gel film was very high and rapidly increased over several hours, which indicates a fast pitting corrosion process. However, in the case of modified sol-gel coating with halloysite nanotubes corrosion process was significantly reduced. No corrosion current was detected over 24 hours and this clearly indicates that incorporation of inhibitor loaded halloysite tubes into sol-gel coating significantly reduced the rate of corrosion process [5, 16].

a)   b)
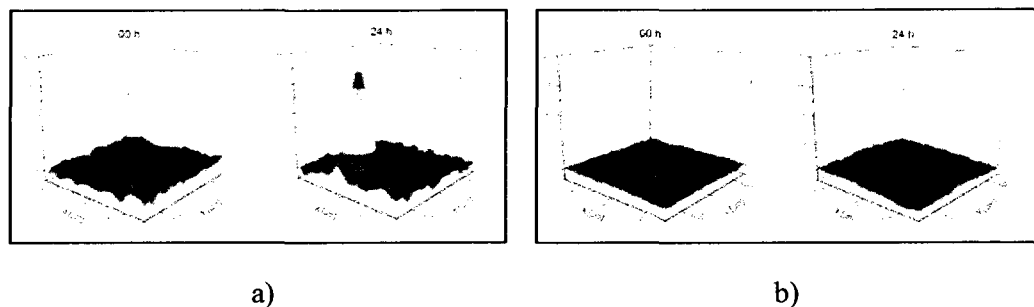
Figure 2.24 Corrosion current densities from metal strips made from 2024 Al alloy. Strips were coated with usual sol-gel coating (a), and with sol-gel containing halloysite (b), *Max Plank Institute of Colloids and Interfaces, Golm, Germany* [5].

2.6.4. Electroactive nanocomposites

Metallic nanoparticles and nanowires have gained big interest in the industry, particularly in the electronic industry, due to their unique physiochemical properties resulted from quantum confinement effects [79, 80]. They can be used in the design logical arrays in quantum computers as well as other electronic devices that are benefited from quantum mechanical effects [79]. Different template structures were utilized for synthesizing magnetic nanoparticles, such as carbon nanotubes [81], porous alumina templates [82], lipozomes [83] and DNA [84]. Halloysite nanotubes are attractive due to their availability and cost effectiveness. They have a very high aspect ratio and can be utilized to synthesize 1-D array of metallic nanoparticles [2, 5, 12].

One of the most promising ways to synthesize metal-halloysite nanocomposites is the electroless plating method, which involves chemical reduction of metal ions on a halloysite tubular template [12, 86-88]. The use of a halloysite template for the synthesis of nanoparticles arrays from magnetic nickel nanoparticles was first demonstrated by Baral, *et al.* They were able to synthesize magnetic needles on the basis of halloysite nanotubes by using Niposit468 Nickel plating bath. Plating was conducted by using Pd nanoparticles as a catalyst for Ni reduction [12]. Later on Fu, *et al.* also successfully demonstrated Nickel plated halloysite tubules by reducing Ni^{+2} salt with dimethylamine borane complex in water solution [86].

In Figure 2.25, linear arrays of different nanoparticles on halloysite template are demonstrated. Gold nanoparticles (Fig. 2.25a) are formed by simple reduction of $AuCl_3$ by acidic citric acid solution in water. Another simple method to deposit metal nanoparticles is sputtering (Fig. 2.25b). High equipment cost is the main disadvantage of the sputtering method. On the other hand deposition of nanoparticles on tubular templates by using electrostatic Layer by Layer nanoassembly of the polyelectrolytes offers a simple and versatile method for deposition of metallic, semiconductive and insulating nanoparticles on 1-D and 2-D arrays. Figure 2.25c and 2.25d clearly demonstrates the one dimensional array of insulating silica and magnetic Fe_3O_4 nanoparticles deposited by Layer by Layer nanoassembly using polyacrylic acid and polyethylenimine as polyelectrolytes. Comprehensive information about Layer by Layer nanoassembly can be found in ref. [85].
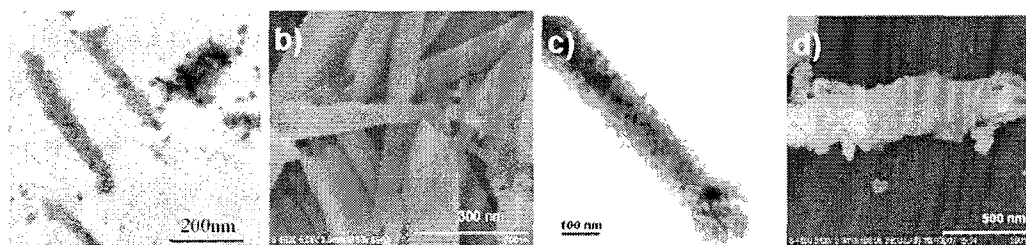
Figure 2.25 Nanoparticle arrays on tubular halloysite template; gold nanoparticles (a, b), silica nanoparticles (c) and magnetite (Fe_3O_4) nanoparticles (d) [30].

All the analysis and results clearly indicate that the tubular structure of the halloysite particles are very impressive in terms of the synthesizing of 1-D nanoparticle arrays. Besides electronic applications, these nanocomposite materials can be used to improve the quality of polymer composites and ceramic products. A patent application exists regarding the usage of copper plated halloysite tubes for producing radio frequency shielding coatings [87].

2.6.5. Hydrocarbon conversion catalysis

Alumosilicates are extensively used in hydrocarbon conversion process since the development of the early petroleum industry. Several United States patents exist for the utilization of halloysite for hydrocarbon isomerization and cracking [91-93]. Halloysite belongs to the kaolinite family of the clay minerals with high Al/Si ratio compared to other alumosilicates. It is due to the acidic sites provided by aluminum oxide that cracking of the hydrocarbons occur. These acidic sites promote the heterolytic breakage of the chemical bonds that usually form unstable carbocations that undergo chain rearrangements and C-C scission through beta elimination or hydride transfer. All of these processes generate highly reactive radicals and ions that further speeds up the cracking process [94].

The early works on the usage of halloysite nanotubes as hydrocarbon processing catalysts dates back to the 1950s. W. Offutt and A. Whitaker from Gulf R&D Co. developed a hydrocarbon conversion catalyst based on magnesium oxide supported halloysite catalyst. Their catalyst showed lesser coke formation compared to montmorillonite clay, another active hydrocarbon cracking catalyst of that time [91]. Another advantage of the halloysite is its higher performance towards the cracking of the high sulfur content hydrocarbons [91, 92]. Since that time, halloysite based hydrocarbon catalysts drew the attention of researchers. D. Santilli of Chevron Co. patented a catalyst for hydrotreatment and hydrometalation of asphaltene containing hydrocabonaceous feedstocks (crude petroleum, shale oil, tapped crudes, etc.) based on halloysite doped with binder metal oxides, particularly with Al, Mg, Si, Ti, B and Zr oxides [92]. Oxides of other transition metals, such as Cr, V, Fe, Mo were also added in addition to binder oxides to improve the performance of the catalyst. They showed that the halloysite nanotubes with pore size ranging from 20 to 70 nm are especially good for the deasphalting property of the hydrocarbons. In Figure 2.26, results of the process of deasphalting of toluene solution in the presence of several catalysts prepared from halloysite

are shown. Deasphalting takes place faster in the presence of pure halloysite and 5% alumina doped halloysite indicating the higher adsorptivities of the porous catalysts. Conversion of the adsorbed hydrocarbons, such as hydrocracking and desulfurization, takes place in the presence of transition metal oxides doped into halloysite [92].
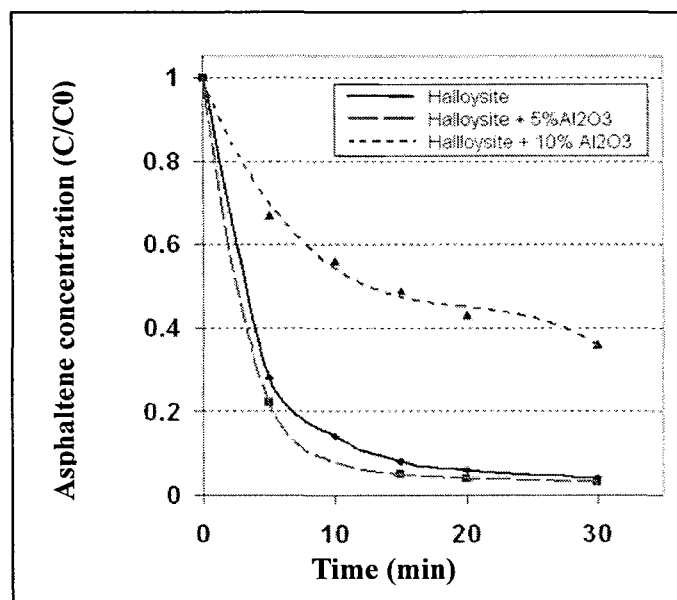
Figure 2.26 Reduction of asphaltene concentration in toluene solution by various catalysts on the basis of halloysite [30, 92].

Besides natural halloysites, synthetic halloysites were also utilized for hydrocarbon cracking process. Robson, et al. successfully demonstrated that synthetic halloysites with Mg and Ni impurities have higher cumene cracking efficiency than the natural halloysite nanotubes. Higher efficiency of the synthetic halloysite was attributed to the presence of iron impurities in natural halloysite samples that acts as a poison in the cracking process [93].

2.7. <u>Conclusion</u>

The structure and main applications of the halloysite nanotubes are described. Halloysite nanotubes, having tubular shape with a high aspect ratio and 50-100 nanometers in diameter, offer great promise for commercial applications, including nanoscale additives in polymers, nanocontainers for chemical storage and controlled release (anticorrosion and antimolding protection, dentistry, cosmetics), catalysts for hydrocarbon cracking, and many others. The unique geometry of nanotubes enables them to be used for storing, delivering and controlling the release of various chemicals and materials. Unlike other types of nanotubes, halloysites are readily available in nature in thousands of tons and does not require complicated synthesis or fabrication as a template. There is no doubt that further investigation of halloysite physical-chemical properties will benefit the current industry, particularly polymer and petroleum industries.

CHAPTER 3

HALLOYSITE CLAY NANOTUBES AS "GREEN" NANOCONTAINERS FOR ANTICORROSION METAL COATINGS

3.1. Introduction

Metals are widely used in the current world and corrosion of the metals is a serious technical problem. An extensive variety of corrosion protection methods, such as cathodic protection, protective coatings and corrosion inhibitors were introduced by scientists. Protective coatings are one of the cost effective methods to protect metals from corrosion. However, the efficiency of the coatings may not be sufficient in very aggressive environments, such as sea water. Therefore, additional improvements in the performance of the coatings is required in many cases. A possible improvement is the addition of corrosion inhibitors into the coatings. Many different types of the corrosion inhibitors were explored, such as chromates, phosphates, molybdates, lanthanides, etc. [8, 16, 95-97]. The main disadvantage of the inorganic inhibitors is their toxicity. For example, chromates are proven to cause several diseases, such as DNA damage and cancer [10, 95]. Therefore, the introduction of environmentally friendly corrosion inhibitors is one of the main tasks for scientists. Organic corrosion inhibitors are potential competitors for inorganic corrosion inhibitors. Nitrogen containing corrosion inhibitors based on the triazole functional group are one of the most effective corrosion inhibitors, which are widely used for protection of a large variety of metals [8, 10, 16, 30, 98-100].

48

Direct addition of inhibitors into the paint is not effective since it is easily washed away with water, and leaves empty holes in the paint after washing out, which further exposes the metal underneath to the corrosive environment and enhances the corrosion process. On the other hand, the introduction of inhibitors into paint with some kind of encapsulation seems to be the best solution to the problem. A lot of different capsule designs were introduced by researches, such as polyelectrolyte and polymer microcapsules, sol-gel nanoparticles and nanotubes [8, 10, 16, 77, 101, 102].

Another way for the improvement of the anticorrosive performance of the metal coatings is based on the idea of self-repairing coatings. In this case, microcapsules containing monomers, having similar nature to the polymer paint, and curing agent are embedded into the coatings. Such capsules rupture upon scratch formation releasing their content into the damaged area and providing self-healing of the damage by polymerization of the monomers [8, 103, 104].

In this work, we suggest utilizing naturally available halloysite clay nanotubes as containers for the loading, storage and controlled release of the corrosion inhibitors, as well as improving the anticorrosion properties of the metallic coatings by the addition of loaded nanotubes into the paint. Halloysite is a "green" material [27, 105] and can easily be mixed with a great variety of metal coatings [66]. Three corrosion inhibitors; benzotriazole, 2-mercaptobenzothiazole and 2-mercaptobenzimidzole were used as corrosion inhibitors. Additional improvement of the paint qualities were achieved by loading the main components of the paint into halloysite nanotubes and mixing them with the paint for healing the damaged coating.

3.2. Materials and Methods

3.2.1. Chemicals

Halloysite samples were obtained from Atlas Mining Co. (currently Applied Minerals Inc.) and Imerys Corp. Benzotriazole was purchased from Sigma-Aldrich, USA. $CuSO_4*5H_2O$ was purchased from Fluka Chemika, Switzerland as a dry powder. Ammonia solution was purchased from Fluka as a saturated solution (28 % by weight) in water. Sodium diethyldithiocarbamate trihydrate was received from Sigma as dry powder. Acrylic and polyurethane paints were purchased from Krylon and Minwax Co. respectively.

3.2.2. Instrumentation

Halloysite samples were characterized by Scanning Electron Microscope (Hitachi S 4800 FE-SEM) to observe nanotube external surface morphologies. The elemental composition of the halloysite samples was determined by using SEM EDX elemental analysis. Electrons were accelerated at 5-15 kV for imaging purposes and at 25 kV for EDX elemental analysis. Halloysite samples were coated with 1.6 nm thick platinum by Cressington Sputter coater (208HR) before each SEM experiment in order to reduce charging effect. Samples were coated at 80 mA current for 1 minute. The internal hollow lumen of the halloysite was analyzed by using a Transmission Electron Microscope (TEM, Zeiss EM 912) at 120 kV electron accelerating voltage.

UV-Vis spectrophotometer (Agilent 8453) was used to determine the concentrations of corrosion inhibitors and Cu (II) concentrations during release experiments. Solutions were calibrated relative to pure DI water before each experiment. Benzotriazole concentration was measured by the intensity of the peak at 265 nm wavelength in the UV spectrum. Copper (II) concentration was measured by the peak of $[Cu(NH_3)_4]^{+2}$ complex ion at 650 nm or with sodium diethyldithiocarbamate at 450 nm (for concentration below 10 ppm). A light

Microscope (Olympus, Japan) with video camera (Sony SSC DC 80) was used to observe corrosion spots on the scratched metal surface. The image was magnified by 10 – 15 times.

3.2.3. Nanotube loading procedure

To entrap desired substances into halloysite nanotubes, a saturated solution of the loading agent in acetone was mixed with halloysite as a dry powder. A beaker containing halloysite suspension was transferred to a vacuum jar, which was then evacuated using a vacuum pump. Slight fizzing of the suspension indicates that air is being removed from the core of the halloysite tubules and replaced with benzotriazole solution. Suspension was kept under vacuum for 3-5 hours, and then was cycled back to atmospheric pressure. This process was repeated three times in order to increase loading efficiency. Finally, halloysite nanotubes were separated from solution by centrifugation and washed with water.

3.2.4. Corrosion inhibitor release kinetics

All release experiments were performed in water, pH 6-7 at room temperature. Suspension of halloysite nanotubes was constantly stirred with a magnetic stirrer during the release process in order to establish equilibrium conditions and to increase the release rate. Concentrations of corrosion inhibitors were determined with UV spectrophotometry. For scaling release curves, at the end of each release experiment, a complete release was determined with 1 hour sonication of the halloysite samples.

3.2.5. Corrosion resistance testing

Inhibition efficiency of the original corrosion inhibitors were tested by immersing 2 mm x 5 mm size copper strips into 30 g/L NaCl solution in water containing 0.1 M of corrosion inhibitor. A solution without any inhibitor was used as a blank. The corrosion process was evaluated by measuring the concentration of copper ions in the corrosive media.

Corrosion process was studied visually by optical microscope. Four strips were coated with acrylic latex paint; three of them containing 10 wt% halloysite loaded with

benzotriazole, 2-mercaptobenzimidazole and 2-mercaptobenzothiazole and one without halloysite. Backsides of the strips were coated with transparent polyurethane paint for visual observation of the corrosion process underneath the paint. In order to test anticorrosive performances of these coatings, strips were kept in 30 g/L NaCl solution for 6 month. The corrosion process was evaluated based on the concentration of Cu (II) ions in the corrosive environment by UV-Vis spectroscopy. Halloysite was added to the liquid paint as a powder and dispersed by means of simple mechanical mixing in all of the cases.

3.2.6. Corrosion inhibitor adsorption kinetics

Three metal wafers of 7.0 mm x 3.3 mm x 0.1mm dimensions from 110 copper alloy were exposed to the 30 ml 0.25 mM solutions of benzotriazole, 2-mercaptobenzothiazole and 2-mercaptobenzimidazole in DI water. Fractions of solution were collected within selected time intervals and analyzed by UV-Vis spectroscopy for corrosion inhibitor content. A similar procedure was applied for the solutions of corrosion inhibitors in salt water solution, containing 30 g/L NaCl. 30 ml 1.35 mM solutions of corrosion inhibitors were used in this case.

3.2.7. Self-repairing epoxy coating

Two separate solutions containing Epoxy resin and curing agent (on the basis of polymercaptan amines) in 50% acetone was prepared. Then halloysite was added into these solutions with the concentration of 5.0 wt%. A vacuum cycle was applied in order to load these agents into the tube. After that these two solutions were mixed and applied to the A366 iron alloy. Once the coating was completely dried (two days), it was artificially scratched with a knife blade followed by waiting two more days. Then, the damage on the coating was checked by applying 0.25 M copper sulfate solution on the scratched surface. A similar procedure was applied for pure epoxy coating without halloysite.

3.2.8. Epoxy resin release kinetics

Loaded halloysites were washed with acetone two times and split into two parts. One of the samples was dispersed in 0.5 ml water, the other one in 0.5 ml 2,2,4-trimethylpentane. Release was conducted under continuous stirring and supernatant was collected by centrifugation (5000 rpm, 1 min) in selected time intervals. A new portion of solvent was added after the removal of supernatant in each case. Release was stopped after 8 hours and complete loading of epoxy resin was determined by sonication of the halloysite for 1.5 hours. The amount of epoxy resin released after this was considered to be 90%. Epoxy concentration was determined by UV-Vis spectrometer from the signal at 226 nm wavelength in water and pentane.

3.3. Results and Discussion

3.3.1. Halloysite clay nanotube characterization

In Figure 3.1 TEM and SEM images of the halloysite nanotubes are shown. The halloysite layer, which has 7.2 Å thickness is structurally similar to the kaolinite layer [1-5]. Empty tubular lumens of the tubes are clearly visible in the TEM image. The outside diameter of the tubes is about 50 nm and the inner diameter is ~ 20 nm. The lengths of the tubules cover the range of 0.5 to 3.0 μm. Elemental composition of the halloysite sample is as follows (atomic %): Al, 17.1; Si, 16.7; O, 63.3; Fe, 0.5; Ca, 1.6. Brunauer-Emmett-Teller (BET) surface area of the halloysite was 120 m^2/g.

a)   b)
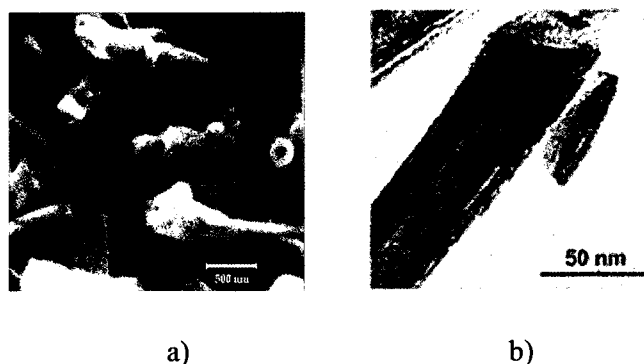
Figure 3.1 SEM (a) and TEM (b) images of halloysite nanotubes.

The hollow tubular structure of the halloysite nanotubes makes it very attractive for use as nanocontainers for encapsulating corrosion inhibitors and other active agents for active and passive corrosion protection. These tubes were utilized for producing self-healing coatings. The self-healing effect is demonstrated in Figure 3.2. First, halloysite nanotubes, loaded with desired substances for the self-healing effect, are added to the liquid paint and applied to the metal surface. Loaded substances stay in the halloysite lumen as long as no crack occurs in the paint. Once paint is cracked, loaded agents leak into the corrosive environment and stop the corrosion process, either by healing the coating or by inhibiting the corrosion process. Both of these approaches were analyzed in the current work. First, we demonstrate self-healing process by using corrosion inhibitors.

Loaded
and
sealed
halloysite tubes

Metal Panel coated   Crack on the coating   Self healing effect by
with halloysite-paint   leaking of the protective
composite coating   agents from halloysite
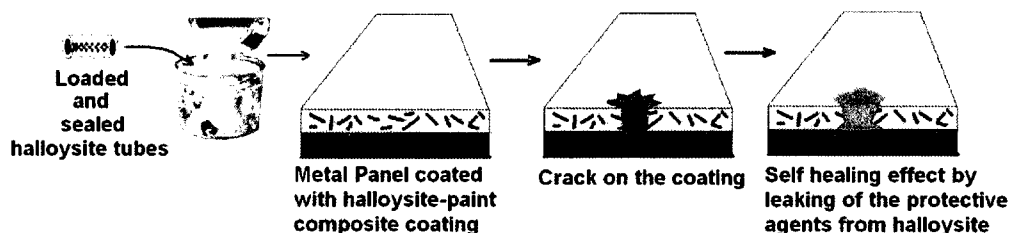
Figure 3.2 Schematic demontration of the self-healing effect.

3.3.2. Inhibitors for corrosion protection

Benzotriazole, 2-mercaptobenzothiazole and 2-mercaptobenzimidazole were used as corrosion inhibitor for the protection of the metals (Figure 3.3).

a)   b)   c)
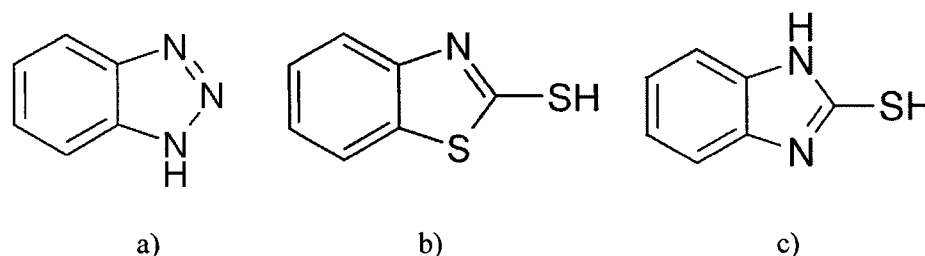
Figure 3.3 Chemical structures of benzotriazole (a), 2-mercaptobenzothiazole (b) and 2-mercaptobenzimidazole (c).

These inhibitors form two dimensional thin films with metal ions on the metal surface, which insulates the metal from the corrosive environment and protects it from corrosion. Corrosion inhibition efficiency of these inhibitors was evaluated on copper strips in corrosive media containing 30 g/L NaCl. Concentrations of the inhibitors were 0.1 M. The corrosion process was evaluated by measuring the concentration of the copper ions in the corrosive media (Figure 3.4). Concentration of the copper ions is constantly increasing in the absence of corrosion inhibitor, while the corrosion process was significantly suppressed in the presence of corrosion inhibitors.

Corrosion inhibition efficiency of the corrosion inhibitors were calculated by the formula:

$$I.E.(\%) = \frac{v_{uninhibited} - v_{inhibited}}{v_{uninhibited}} * 100 = \frac{[Me^{+n}]_{uninhibited} - [Me^{+n}]_{inhibited}}{[Me^{+n}]_{uninhibited}} * 100 \qquad (3.1)$$

where, v is the corrosion reaction rate and $[Me^{+n}]$ is the concentration of the metal ions in the corrosive environment due to the corrosion process (in this case the metal is copper). Corrosion inhibition efficiencies of the benzotriazole, 2-mercaptobenzothiazole and 2-mercaptobenzimidazole were 95.0, 99.6 and 99.7 %, respectively.
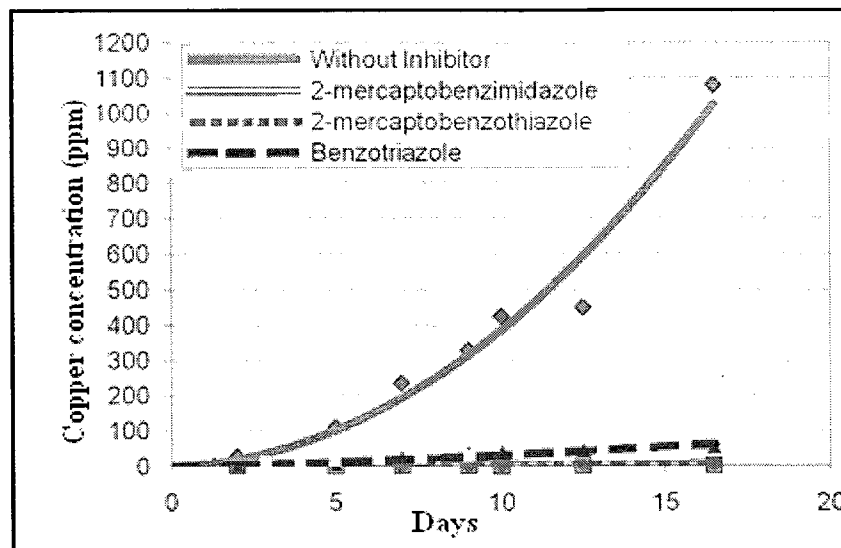
Figure 3.4 Copper concentration change during corrosion test performed by dipping copper strips in salty water with 30 g/L NaCl and 0.009 M corrosion inhibitor.

The process of corrosion inhibition by the above mentioned corrosion inhibitors is based on the formation of a 2-D thin film based on the Copper-Inhibitor complex that covers the entire metal surface and insulates it from the corrosive environment [99]. Once the surface of the metal is completely covered with the isolating film, the reaction between the inhibitor and copper stops. The kinetics of this process follows second order reaction kinetics, i.e. the reaction rate depends on both the inhibitor concentration and the concentration of the unreacted copper atoms at the surface of the metal.

$$Cu^{+2} + Inh \longrightarrow [Cu(Inh)]_n$$
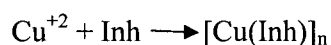
The rate of the reaction can be calculated by the following differential equation:

$$Rate = -\frac{d[Inh]}{dt} = k * [Cu] * [Inh].$$

(3.2)

If we assume that only a monolayer of the corrosion inhibitor deposits on the copper surface and the insulating film covers the metal surface uniformly, then the following equation is obtained.

$$a(t) = \frac{a_0 a_\infty}{a_0 + (a_0 - a_\infty) * \exp(-a_\infty kt / (a_0 - a_\infty))},$$ (3.3)

where, a_0 and a_∞ are the initial and final concentrations of the benzotriazole, $a(t)$ is the concentration of the benzotriazole at time t and k is the reaction rate constant. Derivation of this equation is given in *Appendix A*.

In Figure 3.5a the kinetics of the corrosion inhibitor interaction with copper wafers is shown. As one can see from the images, theoretical calculations fit with the experimental data points reasonably well. Reaction rate constants were determined from the best fit of the model to the experimental points and the values of k were equal to 0.13, 0.65 and 0.015 for benzotriazole, 2-mercaptobenzothiazole and 2-mercaptobenzimidazole, respectively. Initial concentrations of the corrosion inhibitors were 0.25 mM in all of the cases and final concentrations of the unreacted corrosion inhibitors were 0.21, 0.02 and 0.17, mM for 2-mercaptobenzimidazole, 2-mercaptobenzothiazole and benzotriazole, respectively. As one can see, more 2-mercaptobenzothiazole is consumed for the corrosion protection of the copper compared to benzotriazole and 2-mercaptobenzimidazole which makes it less efficient in terms of corrosion protection.

a)

b)
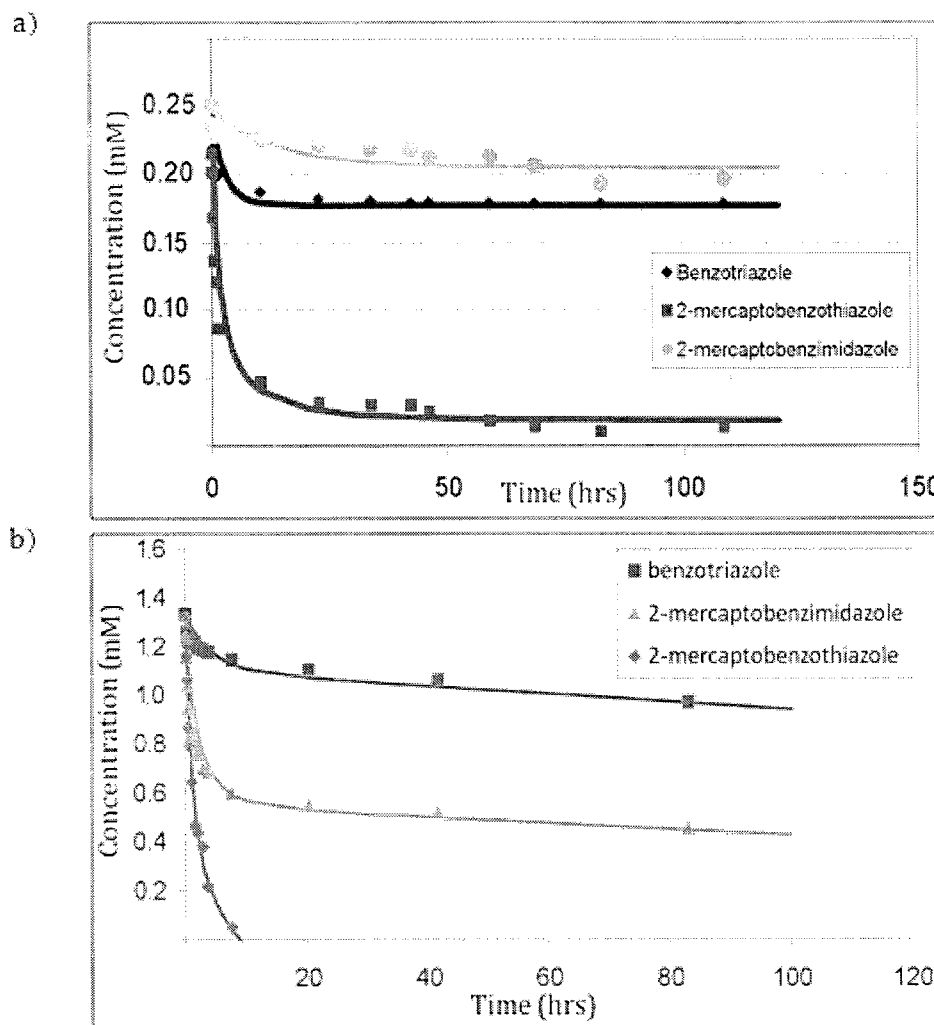
Figure 3.5 Adsorption of three different corrosion inhibitors; 2-mercaptobenzothiazole, 2-mercaptobenzimidazole and benzotriazole, on copper metal surface in fresh water (a) and salty water (b) with 30.0 g/L NaCl.

In the case of chlorine containing salt water, consumption of the corrosion inhibitor is still going on even after complete coverage of the copper surface. Experimental data indicates that two processes are going on in parallel; interaction of corrosion inhibitor with metal atoms at the surface to form an isolating thin film, and deterioration of this insulating film by chlorine ions from the environment which requires a new portion of inhibitor to heal it.

$$Cu^{+2} + Inh \xrightarrow{k_1} [Cu(Inh)]_n$$

$$[Cu(Inh)]_n + Cl^- \xrightarrow{k_2} [Cu(Inh)]_{n(loose)}$$
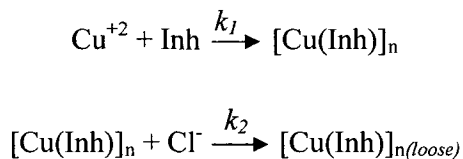
The speed of the second reaction is very low; however, deterioration of the insulating thin film requires additional corrosion inhibitor to heal the damage. The $-k_2t$ term was added to the reaction rate equation in the case of salt water to consider the consumption of the corrosion inhibitor from the environment due to the damage to the isolating film by chlorine ions. We get the following reaction rate equation for the case of chlorine containing corrosive environment:

$$a(t) = \frac{a_0 a_\infty}{a_0 + (a_0 - a_\infty) * \exp(-a_\infty k_1 t /(a_0 - a_\infty))} - k_2 t , \qquad (3.4)$$

where, k_1 is the constant for the formation of the isolating film on the metal surface and k_2 is the constant of the reaction for the damage to the isolating film by chlorine ions. Constants for the formation of the insulating films k_1, were 0.045, 1.0 and 0.3, while reaction rate constants for the damage to the insulating layers, k_2 were $1.6*10^{-6}$, $1.5*10^{-5}$ and $1.2*10^{-6}$ for benzotriazole, 2-mercaptobenzothiazole and 2-mercaptobenzimidazole, respectively. As one can see from the curves in Figure 3.5b, more corrosion inhibitor is required in chlorine containing corrosive environment to protect metals from the corrosion process. Consumption of the 2-mercaptobenzothiazole was highest among all the inhibitors and consumption of the benzotriazole was the least.

3.3.3. Loading halloysite with self-healing agents

Processes taking place during the loading procedure are described in detail in the previous chapter. Briefly, the halloysite was mixed as a dry powder with a saturated solution of the inhibitors in acetone (80 mg/mL). Then, a beaker containing the suspension was transferred to a vacuum jar, which was then evacuated using a mechanical vacuum pump.

The suspension was kept under vacuum for approximately 20 min, and then removed to atmospheric pressure. This process was repeated 3 times in order to increase loading efficiency. In addition, halloysite particles were kept in the solution overnight, which is believed to further increase loading efficiency. Finally, halloysite nanotubes were separated from solution by centrifugation and washed with water.

Acetone was considered to be the optimal solvent to load corrosion inhibitors into halloysite nanotubes even though water wets halloysite better than acetone. The higher stability of halloysite colloid in water compared to acetone is the clear indication for that. Halloysite is easily dispersed in water and its colloidal solution stays stable for a few hours while it almost does not form any colloid with acetone, which is due to the fast aggregation of halloysite particles in acetone. The reasons for the higher loading of benzotriazole into halloysite by using acetone as a solvent are numerous. Possible reasons are listed as follows:

1) Higher solubility of corrosion inhibitors in acetone: Almost all of the organic corrosion inhibitors readily form highly concentrated solutions with acetone, up to 15 – 20% by weight while their solubility in water hardly increases more than 0.5 % by weight.

2) Acetone has lower viscosity compared to water. At nanoconfined volumes, viscous forces can play a significant role in the diffusion of substances. The lower viscosity of acetone is definitely its advantage over water, which makes diffusion of corrosion inhibitors in acetone faster than in water.

3) Acetone evaporates faster than water. Under applied vacuum (during the loading procedure) fast evaporation of acetone gradually increases the concentration of inhibitors in the solvent.

Evaporation of the solvent under vacuum elevates the concentration of the loading substance in the bulk solution which increases the concentration gradient between tubule

lumen and the external solution. The concentration gradient plays a major role in loading the tubes therefore; fast drying solvents with low viscosities, such as acetone or ethanol, are preferable for organic substances. Acetone was chosen as the solvent in the current study to load halloysite with corrosion inhibitors.

In Figure 3.6, XRD spectrums of the halloysite samples loaded with corrosion inhibitors are described. Basal reflection of the halloysite nanotubes (7.2 Å) remained unchanged after the loading process indicating that corrosion inhibitors were loaded mainly due to precipitation inside the pores. No peaks of benzotriazole and 2-mercaptobenzothiazole were observed in the XRD spectra showing that the loaded corrosion inhibitors are mainly in amorphous form. On the other hand basal reflection of 2-mercaptobenzimidazole at 22.5°, corresponding to a 4.0 nm interplanar distance is, clearly visible from the XRD spectrum (Figure 3.6c).

2θ-angle
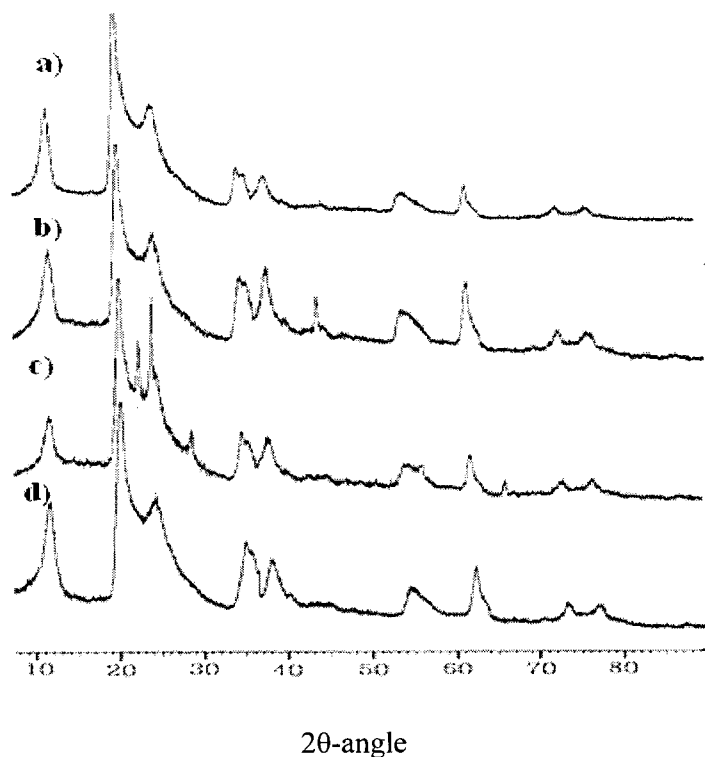
Figure 3.6 X-Ray Powder Diffraction Spectrums of the halloysite loaded with benzotriazole (a), 2-mercaptobenzothiazole (b), 2-mercaptobenzimidazole (c) and empty halloysite nanotubes (d). Cu-Kα radiation source was used.

3.3.4. Analysis of corrosion inhibitor release characteristics

In Figure 3.7 release profiles of three different corrosion inhibitors; benzotriazole, 2-mercaptobenzothiazole and 2-mercaptobenzothiazole from halloysite are shown. Release rates of benzotriazole and 2-mercaptobenzothiazole are close to each other with more than 80% being within 40 hours while the release rate of 2-mercaptobenzimidazole is a bit slower (only 50% in 50 hrs).

The Peppas model [106] was the best model describing the release profile for the corrosion inhibitors from the halloysite samples ($M_t/M_\alpha = kt^n$, where M_t is the amount of substance released at time t, M_α is the amount loaded inside the tubes, n is the exponential constant related to the release mechanism, and k is a constant). Values for k are 64.0, 60.0

and 12.5 for benzotriazole, 2-mercaptobenzothiazole and 2-mercaptobenzimidazole, respectively, while the values of n are 0.10, 0.08 and 0.37. Lower value of k and higher value of n for 2-mercaptobenzothiazole is associated with smaller initial burst for this substance. Probably a significant amount of this inhibitor gets loaded into the tubes while benzotriazole and 2-mercaptobenzothiazole are primarily deposited on the external defects of the halloysite. Loading efficiencies of the inhibitors were 4.0 %, 8.0% and 20.0% by weight for benzotriazole, 2-mercaptobenzothiazole and 2-mercaptobenzimidazole, respectively. High loading efficiency of the 2-mercaptobenzimidazole indicates that a significant amount of the inhibitor was loaded into the tube.
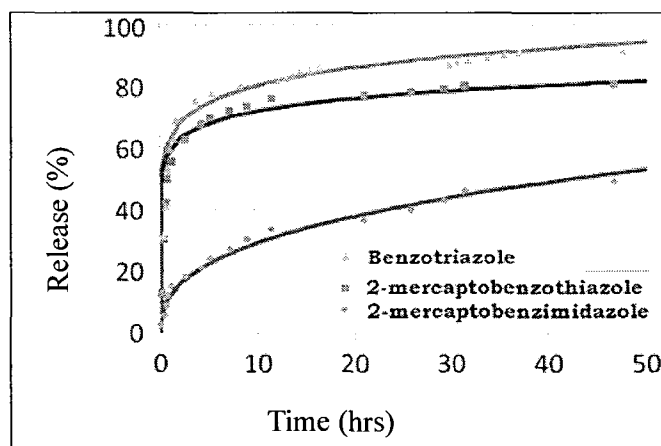
Figure 3.7 Release profiles of inhibitors; 2-mercaptobenzimidazole, 2-mercaptobenzothiazole and benzotriazole, from halloysite.

3.3.5. Corrosion test with halloysite-paint composite coating

Corrosion test was performed on copper wafers. For this purpose four copper wafers were coated with transparent polyurethane paint (this was chosen purposely in order to analyze the corrosion process underneath the paint) on one side and acrylic latex paint on the other side. One strip was coated with pure acrylic paint while three others were coated with the acrylic

paint containing the halloysite loaded with above mentioned corrosion inhibitors. Halloysite was admixed with paint as a dry powder by means of simple mechanical mixing. The paint was artificially scratched and exposed to salt water with a 30 g/L concentration of NaCl. The corrosion process was monitored by analyzing the copper concentration in the corrosive media.

The result for the corrosion test is displayed in Figure 3.8. The concentration of the copper ions is constantly increasing in the corrosive environment indicating the strong corrosion process taking place. The green patina underneath the paint that was observed by light microscope is also indicating a strong corrosion process. However, by adding halloysite, loaded with corrosion inhibitors, significantly reduced the corrosion rate. Some corrosion process took place in the initial stage, which was stopped by the release of corrosion inhibitors from the scratches. Small corrosion spots that are observed for these coatings are due to the initial corrosion process. Paint adhesion was checked after the corrosion test and the best adhesion was observed for the paint with benzotriazole loaded halloysite. Results indicate that the addition of inhibitor loaded halloysite into the paint significantly improved its anticorrosive performance.
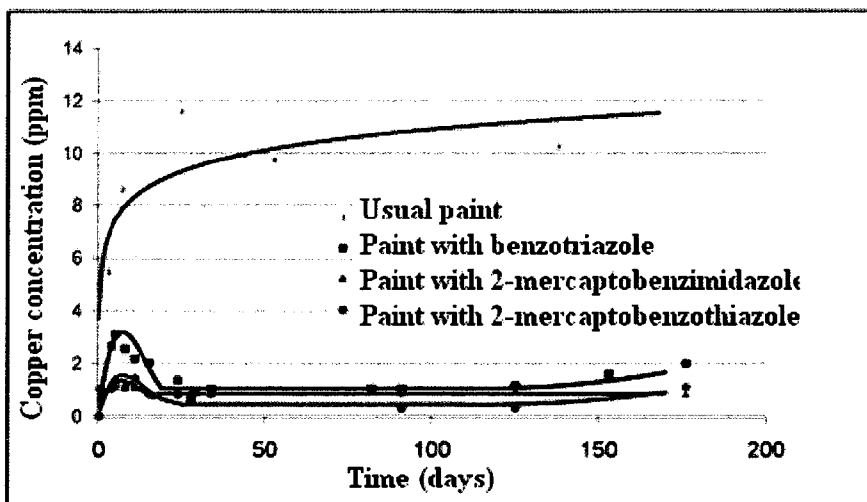
Figure 3.8 Variation of the copper concentration in the corrosive environment of the strips coated halloysite paint composite coating (a) and images of the strips taken by light microscope, usual acrylic paint (b), paint with halloysite loaded with benzotriazole (c), 2-mercaptobenzimidazole (d) and 2-mercaptobenzothiazole (e).

3.3.6. Self-healing effect by repairing the damaged coating

The second approach for improving the coating quality was achieved by repairing the damage of the coating by leakage of the monomer and curing agent from halloysite nanotubes in the cracks. This idea was tested on an epoxy coating. It is believed that during the curing process, the monomer of the epoxy resin does not mix with the hardener in the inner lumen of the tubes due to limited diffusion speed and thus remain unreacted. These agents (epoxy resin and curing agent) stay inside the tubes as long as there is no damage in

the coating since all the openings are blocked. As soon as there is damage in the coating some of the tubes get exposed to air (or other external environment) and start releasing their contents. Leaking monomer reacts with curing agent in the damage and repairs coating. In Figure 3.9, release of the epoxy resin, the main component of the epoxy coating, is shown. Eighty percent release was achieved within 10 hrs.
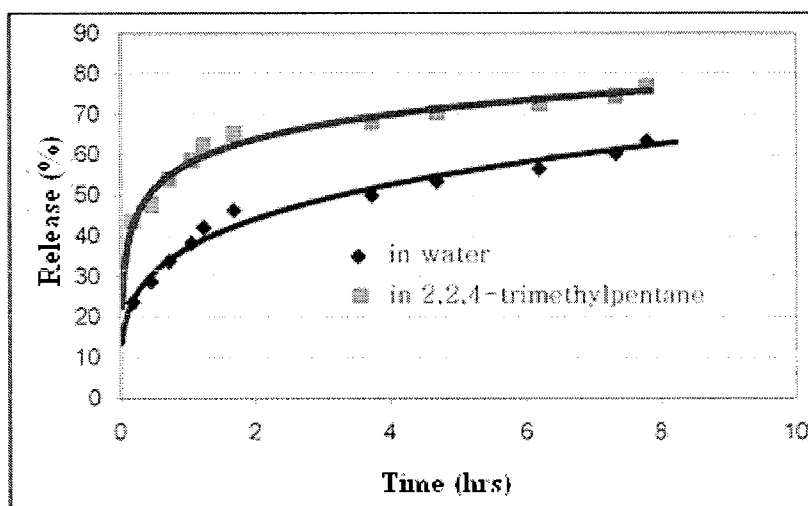
Figure 3.9 Release curves of the epoxy resin in water and 2,2,4-trimethylpentane.

The self-healing process for the artificially damaged epoxy coating was analyzed by exposing the damaged surface to the $CuSO_4$ solution as shown in Figure 3.10. For this purpose, a box with an opening in the bottom was placed onto the artificially scratched coating and sealed in order to avoid leakage of the solution. Then, 0.25 M copper sulfate solution was added to the box in order to allow the interaction of the metal underneath the scratch with the copper ions. In the case of the damaged surface, copper ions diffuse through the damaged area and interact with the iron underneath the paint by forming a thin copper film, which can be easily observed through the transparent coating. However, in the case of self-repairing coatings, copper ions cannot interact with the iron since its diffusion is effectively blocked by the paint.

In addition to the above mentioned technique, the self-healing process can be observed by measuring the potential difference between an electrode that is immersed into copper sulfate solution and a metal panel. Self-repair of the damage can be verified by zero potential in the voltmeter due to the isolation of the solution from the metal surface.

CuSO₄ solution

Paint with artificial scratch
Metal Panel

V
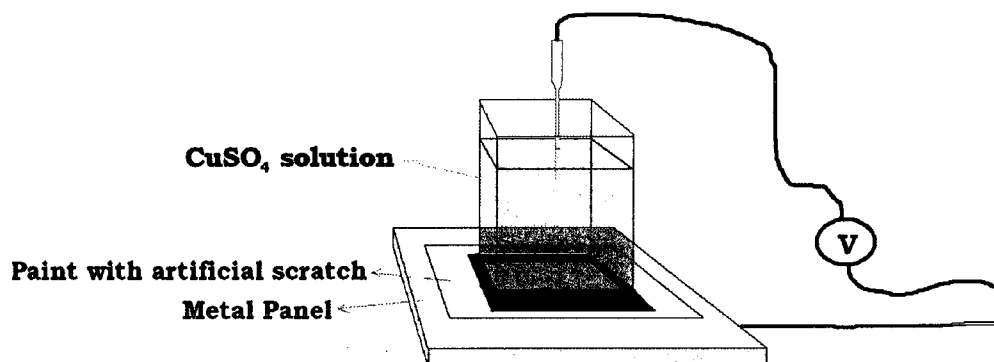
Figure 3.10 Experimental setup for analyzing self-repairing coating.

The result for the measurements is demonstrated in Figure 3.11. Coating with pure epoxy coating resulted in a significant amount of metallic copper formation underneath the paint, indicating that copper ions from the copper sulfate solution diffused through the scratch and interacted with the iron underneath the paint. In the case of paint with 5 wt% halloysites, no copper was observed underneath the paint visually. Readings of the voltmeter, however, showed the potential difference of 0.58 ± 0.01 V in both the cases, indicating that there was some electrical contact between the solution and the metal panel. These results show that partial diffusion of copper ions through the scratch took place in both cases, even though the speed of the diffusion was significantly reduced in the later case. Probably the coating was partially repaired by the leaching of the epoxy resin and curing agent, however, the amount of the epoxy resin was not sufficient for complete curing of the damage.

a)   b)
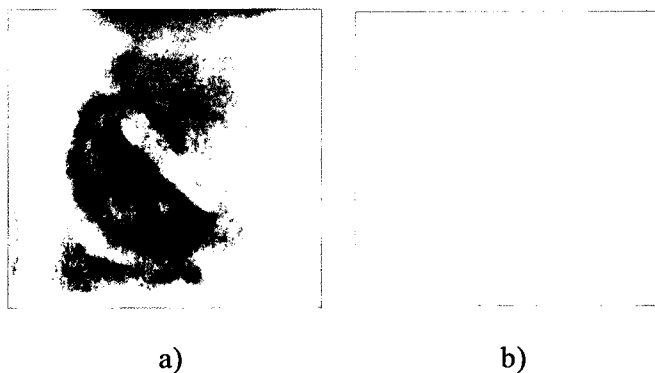
Figure 3.11 Epoxy coating; pure a) and with 5 wt% halloysite b), coated on A366 iron alloy and artificially scratched by knife. Repair of the coating was checked with 0.25 M CuSO4 solution.

3.4. Conclusion

Natural halloysite nanotubes were employed as inexpensive nanocontainers offering essential benefits for the entrapment of corrosion inhibitors into metal coatings. The improvement using the inhibitor loaded halloysite – paint coating was demonstrated on copper by direct exposure of the metal to highly corrosive media for six months. Corrosion was retarded at the initial stage due to the inhibitive action of the benzotriazole, 2-mercaptobenzothiazole and 2-mercaptobenzimidazole released from halloysite nanotubes in paint defects. Corrosion inhibitors form a protective complex on the metal surface isolating it from the corrosive media. Another approach was based on loading the main components of the liquid paint into the halloysite nanotubes for repairing the damaged coating. This idea was tested on the epoxy coating; however, it was only partially useful for the repair of the coating.

CHAPTER 4

ANTICORROSION COATINGS ON THE BASIS
OF INHIBITOR LOADED HALLOYSITE
NANOTUBES FOR THE PROTECTION
OF 2024 ALUMINUM
ALLOY

Some sections of this chapter were published in a paper written by the author of this thesis as "Halloysite Tubes as Nanocontainers for Anticorrosion Coating with Benzotriazole," in *ACS Applied Materials & Interfaces*, vol. 1(7), 2009, p. 1437–1443.

4.1. Introduction

Aluminum alloys are commonly used materials in the industry, especially in the aircraft industry. Corrosion losses are one of the main problems that manufacturers face and needs to be prevented. Several methods including protective coatings, corrosion inhibitors, and cathodic protection are applied to prevent metals from the corrosion process. Self-healing coatings offer great benefit for corrosion protection because of their high efficiency and cost effectiveness [8]. The advantage of a self-healing coating over normal coating is the ability to respond to any damaging of the coating that may occur due to external or internal stresses. The usual coatings quickly deteriorate and do not provide sufficient corrosion protection in most cases.

One way to provide, a self-healing effect is based on the concept of self-repairing polymeric materials. In this case microcapsules containing substances capable of rapid polymerization and curing agents are incorporated in the coatings. Such capsules rupture

upon formation of a scratch by releasing their content into the damaged area and provide the interaction of the monomers with the initiators to start the polymerization process that heals the damage [8, 104, 105]. One of the examples of such coatings was demonstrated by Brown, et al. [107]. They used dicyclopentadiene as polymerizing material and highly porous Ru catalyst to provide polymerization in epoxy coatings. Dicyclopentadiene was encapsulated by using 180 μm diameter urea-formaldehyde capsules and incorporated into the epoxy coatings with the quantity of 5% by volume [107]. The main disadvantage of this approach is the requirement for large amounts of materials to be embedded in the coatings and that the entire corrosion protection strategy is based on only passive corrosion protection. Large capsules will alter the mechanical and barrier properties of the coatings and, in many cases, may act as defect forming sites. On the other hand, an aqueous environment may significantly retard the polymerization process due to the inhibitive action of the water molecules.

Another approach is based on the incorporation of corrosion inhibitors into coatings. Corrosion inhibitors provide active corrosion protection in addition to the protective coatings. Many different types of the coatings were introduced by utilizing corrosion inhibitors, such as chromate containing coatings, cerium conversion coatings, lanthanides, and vanadates. Environmental issues and cost effectiveness restricted the usage of these coatings [8].

Organic corrosion inhibitors have gained more attention in recent years due to their high corrosion inhibition efficiency and environmental friendliness. Many different types of organic corrosion inhibitors, such as benzotriazole, benzimidazole and benzothiazole were studied by researchers and strong anticorrosive performance was demonstrated [98-100]. Direct addition of inhibitors into the paint is not effective since it is easily washed away with water, and leaves empty holes in the paint after washing out. Therefore, the introduction of inhibitors into paint with some kind of encapsulation seems to be the best solution for the problem. A lot of different capsule designs were introduced by researchers, such as

polyelectrolyte [8, 101] and polymer microcapsules [108], sol-gel nanoparticles [8, 102], and nanotubes [5, 8, 14-16, 56, 77]. However, very little work was done to explore the possibility of halloysite clay nanotubes to encapsulate corrosion inhibitors. Halloysite is an economically viable material and compatible with a great variety of metal coatings [1-5].

In this chapter we discuss the utilization of naturally available halloysite clay nanotubes as containers for the loading, storage and controlled release of the corrosion inhibitors, as well as improving the anticorrosion properties of the metallic coatings by the self-healing effect. Benzotriazole was used as a corrosion inhibitor. Halloysite nanotubes were applied to the metal surface by using sol gel coating as well as by polymeric paints. The influence of the halloysite nanotubes on the mechanical and barrier properties of the coatings was also studied.

4.2. Materials and Methods

4.2.1. Chemicals

Halloysite tube samples were obtained from the Dragon Mine in Eureka, Utah (Atlas Mining Co). Benzotriazole was purchased from Sigma-Aldrich, USA. All of the salts: $CuSO_4*5H_2O$, $CoCl_2*6H_2O$, $FeCl_2*4H_2O$, $FeCl_3*6H_2O$ were purchased from Fluka Chemika, Switzerland as dry powders. Industrial blue paint based on ECS-34 powder was purchased from Tru-Test Company and industrial epoxy and polyurethane paints were purchased from Rustoleum and Minwax Corporations, respectively. Acrylic latex paint was purchased from the Krylon Corporation.

4.2.2. Instrumentation

Halloysite samples were characterized by Scanning Electron Microscopy (Hitachi S 4800 FE-SEM) to observe nanotube external surface morphologies. The elemental composition of the halloysite samples was determined by using SEM EDX elemental analysis. The electron

beam acceleration voltage was 5-15 kV for imaging purposes and 25 kV for EDX elemental analysis. Halloysite samples were coated with 1.6 nm thick platinum using the Cressington Sputter coater (208HR) before each SEM experiment in order to avoid sample charging. Samples were coated at 80 mA current for 1 minute. The internal hollow lumen of the halloysite was analyzed by using Transmission Electron Microscopy (TEM, Zeiss EM 912) at a 120 kV accelerating voltage for the electron beam. Halloysite surface charge and average effective diameter in colloidal solutions are determined by using micro-electrophoresis with a ZetaPlus Potential Analyzer (Brookhaven Instruments). A UV-Vis spectrophotometer (Agilent 8453) was used to determine the benzotriazole concentration in aqueous media during release experiments. Solutions were calibrated relative to pure DI water before each experiment. The benzotriazole concentration was measured by the intensity of the signal at the 265 nm wavelength in the UV spectrum. Surface properties of the halloysite, as well as its compatibility with paint were verified by a Contact Angle Measurement System (Future Digital Scientific Co.). For this purpose, a tiny droplet of paint or water (~ 0.5 microliters) was dropped onto a pressed halloysite tablet and the contact angle of the droplet at the liquid - halloysite interface was measured. An eppendorf 5804R centrifuge was used to separate the halloysite nanotubes from the colloidal solutions. The solution was centrifuged at 7000 rpm for 2 minutes to achieve an effective separation. A light Microscope (Olympus, Japan) with video camera (Sony SSC DC 80) was used to observe corrosion spots on the scratched metal surface. The image was magnified by 10 – 15 times. A tensile stress instrument (ADMET, EP-0801161-M-48VAC) was used to determine tensile strengths and the stress – strain relationship of the halloysite – paint composites. Samples were pulled at a speed of 0.3 mm/min for obtaining the stress – strain curve. A Scanning Vibrating Electrode Instrument (SVET, Applicable Electronics) was used to detect corrosion current intensity originating from the corrosion spots on the coated metal samples.

4.2.3. Nanotubule loading procedure

To entrap benzotriazole, halloysite was mixed as a dry powder with a saturated solution of benzotriazole in acetone (80 mg/mL) (Figure. 4.1). A beaker containing benzotriazole and halloysite suspension was transferred to a vacuum jar, which was then evacuated using a vacuum pump. Slight fizzing of the suspension indicates that air is being removed from the core of the halloysite tubules and replaced with solution. Suspension was kept under vacuum for 1 to 5 hours, and then was cycled back to atmospheric pressure. The vacuum cycling process was repeated three times in order to increase the loading efficiency. Further repetitions did not cause significant changes in the loading efficiency. After loading, halloysite nanotubes were separated from solution by centrifugation and washed with water. Loading of benzotriazole from its melt and aqueous solutions were also performed but was found less efficient (probably, because of lower water benzotriazole solubility as compared with acetone).

| Nanotube in solution with benzotriazole | Vacuum removes air bubbles from lumen | When vacuum is broken solution enters into the pores | Washing | Drying loaded tubes |
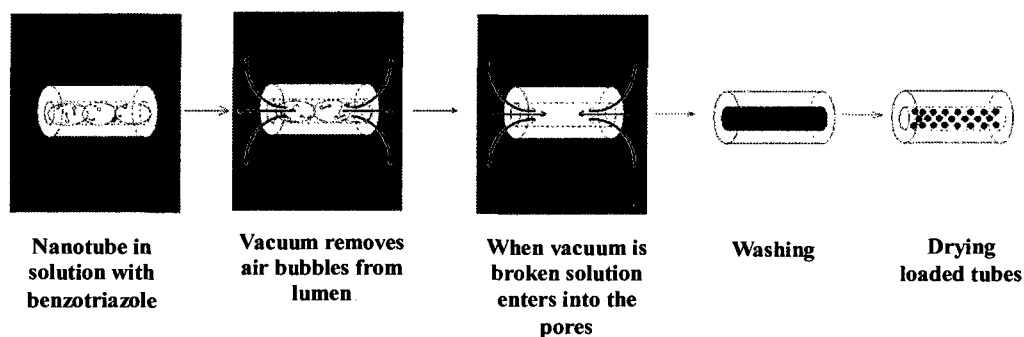
Figure 4.1 Loading procedure of halloysite nanotubes with benzotriazole.

4.2.4. Benzotriazole release kinetics

Release kinetics were investigated in water, pH 6-7, at room temperature. The suspension of halloysite nanotubes was constantly stirred with a magnetic stirrer during the release process in order to establish equilibrium conditions and to increase the release rate. Samples for analysis were separated from the tube suspension by centrifugation. The concentration of the benzotriazole was determined by UV-Vis spectrophotometry. Complete release was checked by sonication of the halloysite samples at the end of each release study.

4.2.5. Tube stopper formation

The formation of stoppers at the tube ends was based on the reaction between the loaded benzotriazole and transition metal ions which diffused into the tube openings to form insoluble metal-benzotriazole complexes that act as a stopper for the benzotriazole contained in the tubules. For this purpose, benzotriazole loaded halloysite samples were exposed for 1 min to a bulk aqueous solution containing Cu (II) or other ions. This suspension was constantly stirred with a magnetic stirrer. The processed nanotubes were separated from solution by centrifugation.

4.2.6. Corrosion resistance testing

The initial stage of the corrosion process on the metal surface was analyzed with the scanning vibrating electrode technique (SVET). Due to electrochemical reactions during corrosion, both anodic and cathodic sites develop on the substrate surface. A PtIr-electrode with Pt-blackened high capacitance microtip was positioned above the sample. A piezo-element generates the electrode vibration. An alternating current signal is induced due to the electrostatic potential gradient inside the electrolyte solution. The AC voltage was analyzed with a phase sensitive detector and amplifier (PSDA) and the amplitude was recorded for different horizontal positions of the tip above the sample. The Pt-blackened electrode tip had a diameter of 20 µm and a capacitance of 6.6 nF and was held at 0.3 mm

above the sample during scans. The metal plates were fixed on a glass holder and immersed into 0.1 M NaCl aqueous solution. An area of 3×3 mm^2 was scanned. Two metal strips made of 2024 aluminum alloy or copper were coated by ZrOx-SiOx sol-gel film or painted with and without benzotriazole loaded halloysite nanotubes and artificially scratched. The corrosion process was monitored by measuring corrosion current density from the scratched surface over 24 hours.

The corrosion process was also studied by optical microscopy of the corrosion development in the scratched area. In this study, 2024 Al alloy strips were coated with transparent polyurethane paint. Backsides of the strips were coated with acrylic latex paint. One of the samples was coated with commercially available acrylic paint, the other one with 5 wt% halloysite nanotubes. The samples were dried in air for 2 days, artificially scratched and dipped into a corrosive solution, simulating sea water and containing 30 g/L NaCl for four months. After four months, the scratched samples were analyzed with optical microscopy.

4.2.7. <u>Paint composite coating tensile stress</u>

Two different industrial paints; polyurethane paint (Minwax Co) and epoxy paint (Rustoleum Co) were used for studying tensile properties. Five different samples from each of the paints were prepared by the addition of halloysite at different loading ratios. Halloysite was mixed with paint by simple mechanical mixing. Thin aluminum foil was painted with the coatings which contained the different amounts of halloysite and dried for 1 week. The dried paint film was released by etching the foil in 0.1 M NaOH solution, dried in air for 3 more days and tested for tensile stress. Dimensions of the paint film samples were 8.5 ± 1.0 mm in width, 16.0 ± 1.0 mm in length, and of 0.50 ± 0.05 mm thickness.

4.3. Results and Discussion

4.3.1. Clay nanotube characterization

SEM analysis showed that the halloysite samples contain fine nanotubes with 50 ± 10 nm external diameter and 15 ± 3 nm internal diameter. The length of the tubes is 1000 ± 500 nm. A typical overage halloysite particle size, determined from light scattering (based on tube radius of gyration describing 3-D averaging), is 330 ± 10 nm, and polydispersity of 0.193. Halloysite nanotubes have an electrical zeta-potential of -42.6 ± 2 mV in water at pH 6.5 which predominantly corresponds to its silica outermost potential. Chemical composition of typical halloysite sample is as follows: 17.7% Al, 18.3 % Si, 63.7% O, and 0.3 % Fe.

4.3.2. Sustained benzotriazole release
from clay nanotubes

Loading of the halloysite nanotubes with anticorrosion agents was based on vacuum cycling of halloysite suspension in saturated solution containing benzotriazole, as was described earlier [8, 56]. The air located in the cores of the tubes was replaced by the anticorrosion solution during this process. To optimize the benzotriazole solvent for the most efficient loading, the solubility of the benzotriazole and low viscosity of the solution were taken into account. Besides, since halloysite nanotubes are hydrophilic (with SiO_2 outermost), the solvent has to be polar for better suspension stability. Loading of benzotriazole into the tubes was possible from its saturated solutions in water, acetone, and from melt benzotriazole. We found acetone to be the best solvent for loading in our process, and it allowed over 4 % of loading efficiency of halloysite by weight, which is approximately 80 % of the theoretical limit (tube lumen volume consists of 10 % of the total volume and halloysite density is 2.55 g/cm^3 [3]). Loading from water solution of benzotriazole or from its melt resulted in less benzotriazole content, being 2.1% and 0.25% by weight, respectively. In further experiments, we used acetone as a solvent for benzotriazole loading. Loaded halloysite may content

benzotriazole for a long time until it is exposed to water (for example, in the coating defect points). Once the coating integrity has been compromised the corrosive solution reaches the entrapped inhibitor and active release begins resulting in the initiation of benzotriazole inhibition.

In Figure 4.2, extended release profiles of benzotriazole from halloysite nanotubes in water are elucidated. For comparison, benzotriazole dissolution in water is also shown: it is almost a vertical line close to the Y-axis indicating very rapid dissolution. Benzotriazole release curves from two typical halloysite samples are close and demonstrate almost complete release of benzotriazole in water within 40 hours. About 30 % initial release of benzotriazole is typical for different molecules loaded into the clay nanotubes, and may be due to the fast dissolution of the material stored in tube fines and in the natural surface pockets formed at the ends of the loosely rolled sheets.
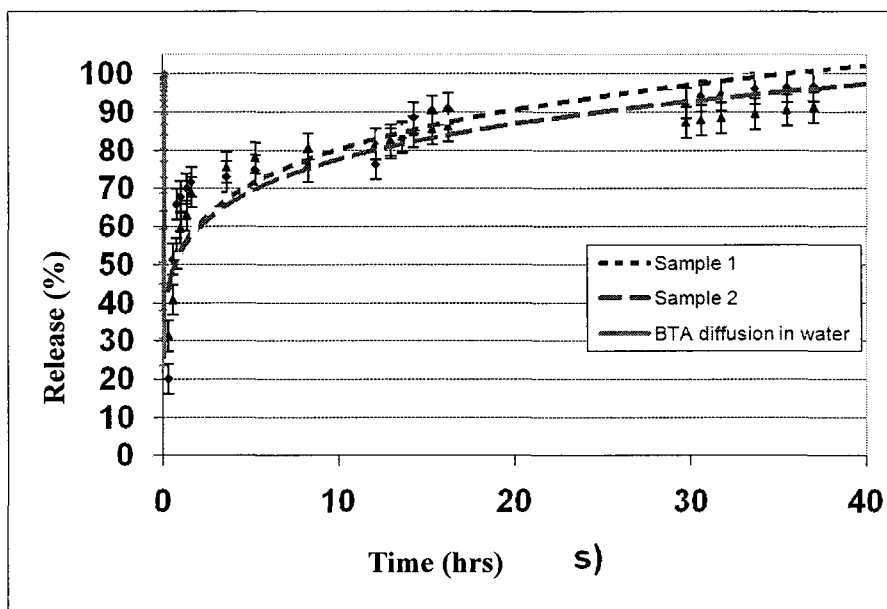
Figure 4.2 Benzotriazole release profiles from two halloysite samples from different batches (water, pH 6.5).

4.3.3. Halloysite / paint nanocomposite coating

In Figure 4.3, SEM micrographs of halloysite nanotubes in a scratched paint layer is shown. Nanotubes are exposed to the external environment at paint scratches or cracks. Benzotriazole loaded halloysite will start an enhanced release of the inhibitor when a crack occurrs, protecting the underneath metal from the development of the corrosion process.
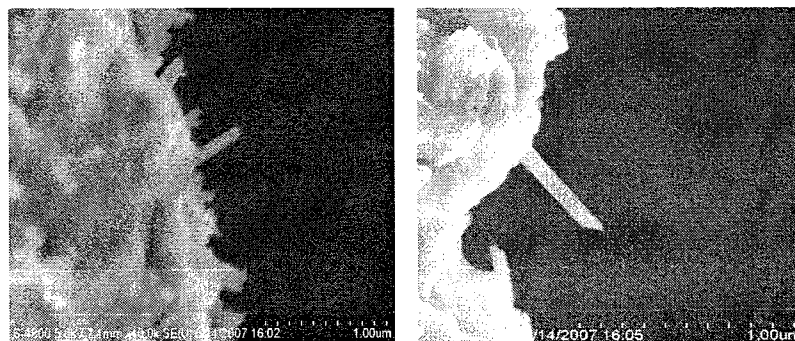
Figure 4.3 SEM micrograph of paint scratch containing 5 % of halloysite nanotubes.

Halloysite is readily mixed with a variety of metal protective coatings which is an important advantage of this material. The water contact angle for halloysite pressed into a tablet was found as low as $10 \pm 3°$ but it was still mixing well with paint, probably due to its highly porous surface. Surprisingly, for the paint droplet the contact angle was even less, of ca $3°$. The paint droplet spontaneously spreads over the halloysite tablet, which is an indication of good wettability of the halloysite tablet by paint. The reason for this could be due to specific chemical interactions between surface OH groups and paint CH groups or the presence of undisclosed surfactant additives in the paint.

The addition of nanotubes into epoxy paint significantly improved the strain − stress characteristics of the coating as is demonstrated in Figure 4.4a. A twofold increase in paint tensile strength was observed with addition of 5 wt % of halloysite (0.5 MPa for pure paint versus 1.0 MPa for 5 wt % halloysite loaded paint). The halloysite filler also increased the

hardness of the paint. The elastic moduli for the dried paint samples was 8.1 MPa for the layer of pure paint, and were 10.9, 13.2, 15.4, 19.7, and 49.8 MPa for 1 wt%, 2 wt %, 5 wt %, and 10 wt % and 30 wt% composite of halloysite with epoxy paint, respectively. However, paint films became brittle for more than 5 wt % halloysite loading. In the case of polyurethane paint, the addition of 1 wt% halloysite slightly increased the tensile strength of the coating; however, further addition of the halloysite reduced the tensile strength of the coating and increased its brittleness (Figure 4.4b). These data correspond to the results for the halloysite clay / polymer bulk composites. For example, incorporation of 5-13 % of halloysite in polypropylene resulted in a 30-50 % strength increase [26-27]. Therefore, from the point of view of paint cover strength, an optimal loading is below 10% by weight. In *Appendix B*, we give an estimation of the minimal halloysite concentration in paint which still provides a sufficient amount of anticorrosion agent for protection, and a sufficient amount is below this value for most of the cases.

a)   b)
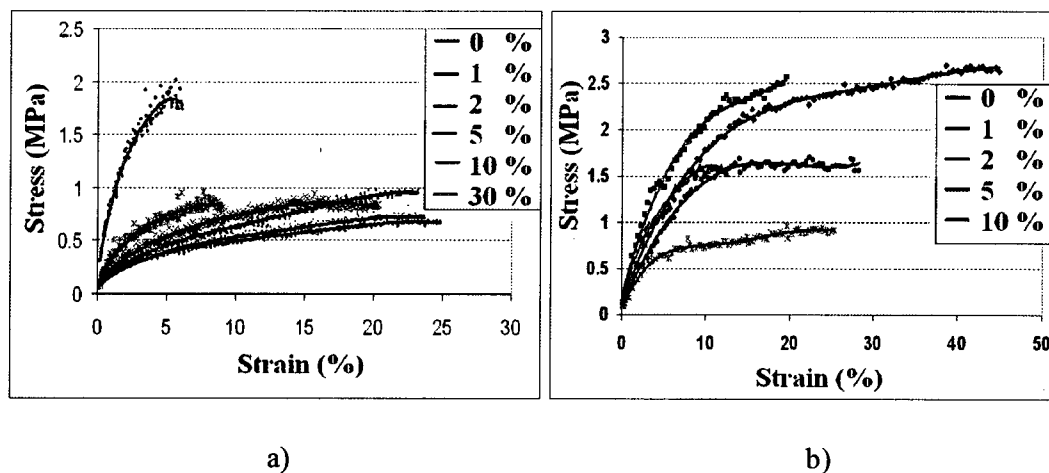
Figure 4.4 Stress strain relationship of two industrial paints, epoxy paint a) and polyurethane paint b) containing different amounts of halloysite nanotubes.

Another physical property of the anticorrosion coatings that one needs to consider is its surface properties, i.e. hydrophobicity. The coating needs to be hydrophobic in order to avoid

the formation of moisture on the metal surface. Contact angle of the water droplets on the paint surface is the simplest way to measure surface hydrophobicity. One may expect contact angles of the water droplets to decrease with increased addition of the halloysite into the paint due to its hydrophilic nature. In Figure 4.5, water contact angle measurements on epoxy and polyurethane coating with different amounts of the halloysite are shown. The addition of halloysite did not reduce the hydrophobicity of the epoxy coating indicating that halloysite does not affect the surface property of the coating up to 10 wt%. In the case of the polyurethane coating, the addition of halloysite slightly reduced the hydrophobicity of the coating.
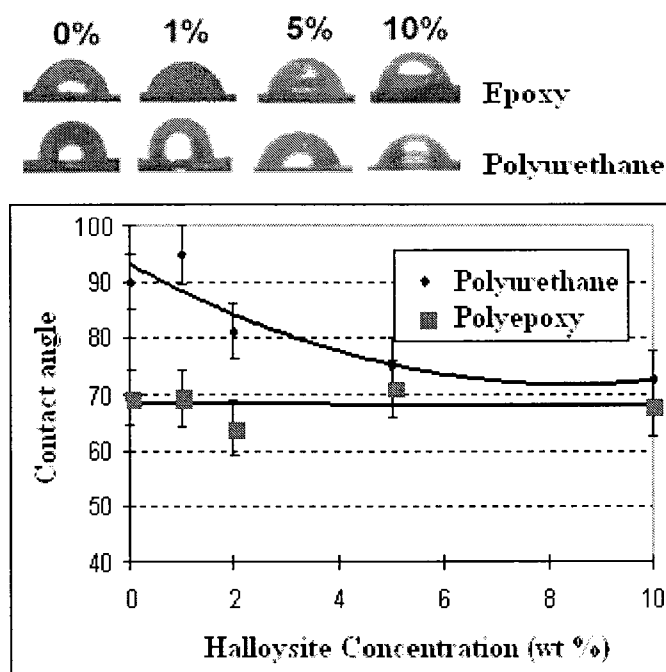
Figure 4.5 Water contact angles epoxy and polyurethane coatings containing different amounts of halloysite nanotubes.

4.3.4. Enhanced corrosion protection with benzotriazole loaded halloysite

The initial stages of corrosion development in metal coatings and self-healing ability of the halloysite-doped film were analyzed with the scanning vibrating electrode technique on

Aluminum alloy 2024 (taken as a substrate), which contains 4 wt % copper. Alloy plates were coated by the dip-coating procedure with ZrOx-SiOx sol-gel layer and artificially scratched in a similar way. Both samples with and without inhibitor-loaded halloysites were immersed in corrosion solution and corrosion development was observed over 24 hours as maps of the corrosion current.

Anodic corrosion activity on the aluminum alloy coated by a simple sol-gel layer was high and rapidly increased within several hours (Figure 4.6) in the scratched area. This indicates a fast pitting corrosion process taking place at the artificially introduced defect. In case of alumina coated with sol-gel containing halloysite tubes filled with benzotriazole, the progress of the corrosion at the defect points is strongly slowed down in the first moment of corrosion and almost no corrosion current (both cathodic and anodic) was developed. Compared to the pure sol-gel coating, the maximal current density in this case was 6 times smaller (ca. 3 μA/cm^2 for inhibitor containing sol-gel and 18 μA/cm^2 for pure sol-gel after 24 hours of immersion), which points out the very strong anticorrosion self-healing effect caused by controlled release of the inhibitor from the halloysite nanotubes in the cracked area.
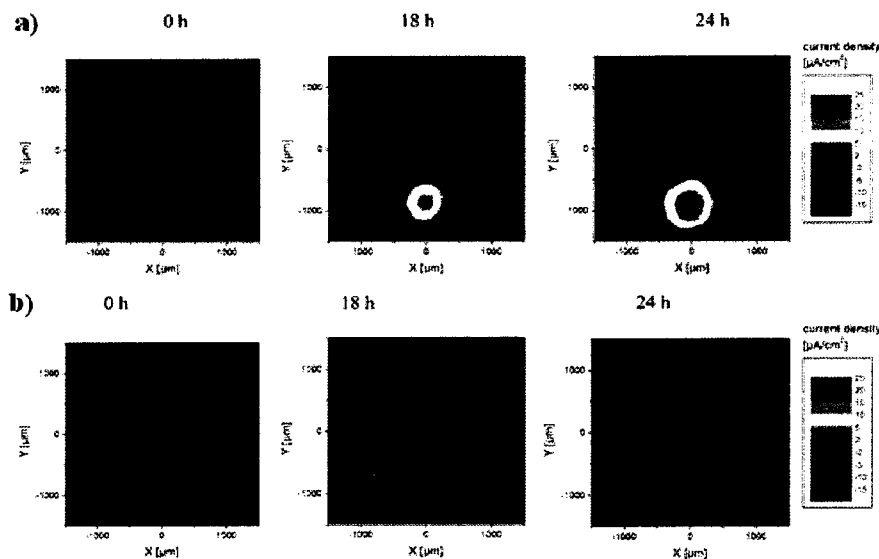
Figure 4.6 Corrosion current densities of 2024 Al alloy coated with pure sol-gel (a), and sol-gel particles containing halloysite loaded with benzotriazole (b), *Max Planck Institute of Colloids and Interfaces, Golm, Germany.*

In another experiment, aluminum strips coated with transparent polyurethane paint were exposed to 30g/L NaCl solution for 4 months. The backside of the aluminum wafers were coated with acrylic latex paint with or without containing halloysite nanotubes loaded with benzotriazole and artificially scratched. Images show that paint containing benzotriazole loaded nanotubes effectively slowed down aluminum corrosion, because no evidences of corrosion products is visible underneath the paint. A wafer coated with the usual acrylic paint shows severe corrosion pits under the paint (Figure 4.7).
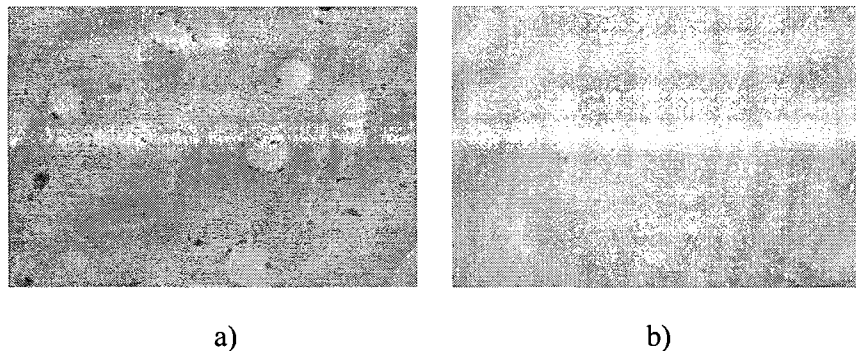
Figure 4.7 Images of the scratched aluminumstrips painted with transparent polyurethane paint, containing, loaded with benzotriazole, halloysite nanotubes a) and without these tubes b) after the exposure to the 30 g/L NaCl solution for 4 months.

4.3.5. Additional encapsulation of the loaded benzotriazole

Halloysite nanotubes provide excellent encapsulation for the loaded agents by significantly reducing their release rate. However, additional encapsulation is required for fast releasing substances or for the cases in which rapid circulation of water takes place in the external environment causing an acceleration of release of loaded agents. Two approaches were successfully demonstrated for additional encapsulation of the halloysite nanotubes:

1) Layer by Layer nanoassembly of the polyelectrolytes on halloysite nanotubes

2) Synthesis of artificial stoppers at tube endings

4.3.5.1. Layer by Layer nanoassembly: The first approach is based on Layer by Layer deposition of the polyelectrolytes on top of loaded halloysite nanotubes. Having negative surface potentials, halloysite nanotubes can be effectively coated by alternate adsorption of positively and negatively charged polyelectrolytes. Polyelectrolytes form a shell on the halloysite by covering the external surface including tube endings, and provide an additional diffusion barrier for the loaded agents.

In Figure 4.8, a brief schematic of the Layer by Layer encapsulation of the halloysite is shown. Halloysite originally has a negative surface charge; therefore, by interaction with

polycations (polyethyleneimine, polyallylaminehydrochloride, etc.) a thin layer of positively charged polyelectrolyte is formed on the halloysite surface. The efficiency of the coating process can be evaluated by measuring the zeta potential of the particles after deposition and strong positive charge indicates polycation layer being deposited on the halloysite surface.
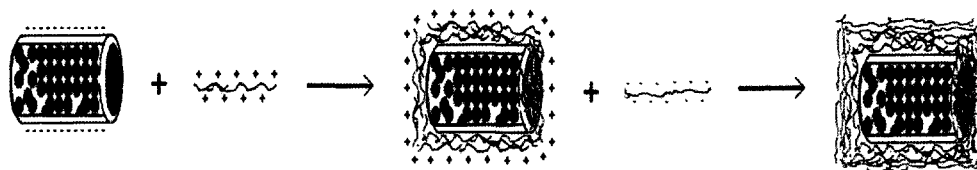
Figure 4.8 Schematic of the Layer by Layer deposition of the polyelectrolytes.

The polyelectrolyte multilayer shell did not slow down the benzotriazole release from the tube. Probably, benzotriazole molecules which have a molecular weight of 119 Dalton are too small and the wall of 4-5 polyelectrolyte monolayers is essentially too loose to decrease their diffusion. This is in contradiction to the results of Veerabadran, *et al.* on the entrapping of the higher molecular weight drug dexamethasone with Layer by Layer encapsulated halloysite [28, 43].

4.3.5.2. Synthesis of artificial stoppers: An alternative approach to encapsulate loaded substances is to synthesize stoppers at tube endings after loading the substance. Syntheses of the stoppers are based on the interaction of the leaking agent A with another substance B from the external solution by forming precipitate AB at tube endings which effectively seals the loaded agent. Substance A can be either the loaded agent of interest or another substance that is coloaded with the main agent.

A schematic of the stopper formation is briefly described in Figure 4.9. When halloysite nanotubes are exposed to the liquid, substance A starts leaking from the pores (Figure 4.9a). If there is a substance B in the external solution that forms precipitate with substance A, then

substances A and B interact at tube ending (Figure 4.9b) and seal it by forming precipitate

AB (Figure 4.9c). Efficiency of the sealing depends on the porosity of the precipitate,

concentrations of the substances A and B and strength of the interaction between precipitate

and halloysite nanotube walls. The requirements for the precipitate are; a) it has to form

quickly, and b) it has to stick to the walls of the halloysite nanotubes, in order to seal it.
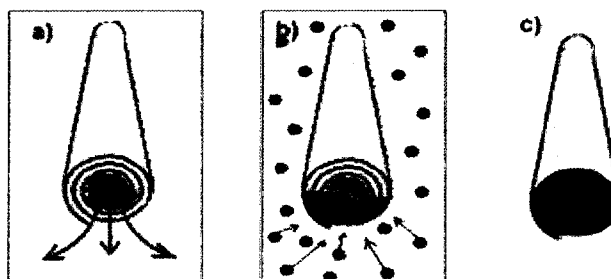
Figure 4.9 Stopper formation at halloysite tube endings by interaction of leaking agent and substance from external solution.

One of the possible ways to form stoppers at halloysite tube endings was achieved by

interaction of leaking benzotriazole (BTA) with transition metal ions. Benzotriazole is the

corrosion inhibitor that forms 2-D thin films with transition metal ions which covers the

entire halloysite external surface and provides additional encapsulation. The 2-D film is

similar to the one that is formed on the surface of the metals during corrosion inhibition by

benzotriazole. Leakage of the loaded benzotriazole occurs from the holes and openings in the

film. The formation of stoppers requires only the quick washing of the loaded tubes with

metal salt solution. Figure 4.10 shows that the benzotriazole release rate was significantly

reduced by encapsulating halloysite nanotubes with Co-BTA, Fe-BTA, and Cu-BTA films

and the best encapsulation was achieved by using Fe-BTA films. Desired release rate can be

obtained by varying the concentration of metal ions in the external bulk solution.
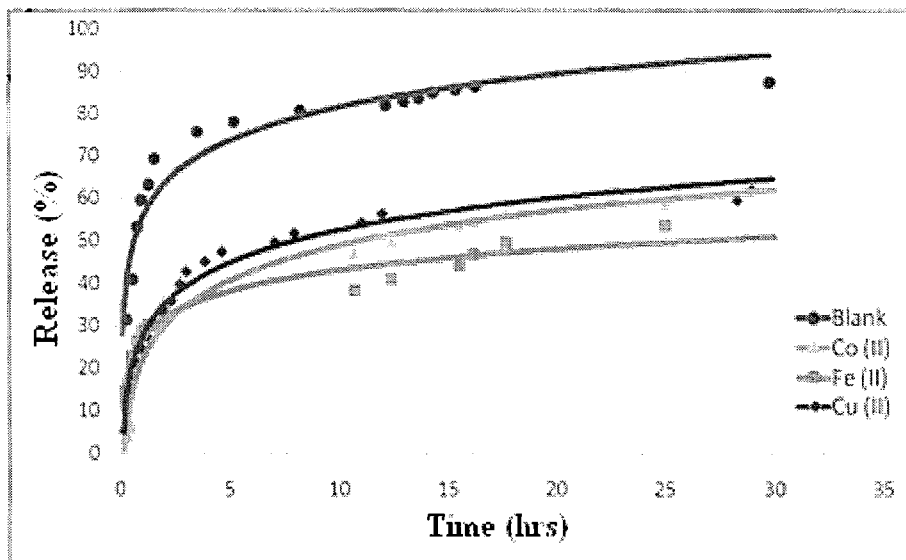
Figure 4.10 Release profiles of benzotriazole from halloysite nanotubes that was exposed to solution of transition metal salts to form stoppers at tube endings.

4.4. Conclusion

Halloysite nanotubes are a promising material for entrapment of corrosion inhibitors into paint. Benzotriazole was loaded in 50 nm diameter halloysite tubes and admixed to the paint coating in the amount 2-10 wt %. The tensile strength of this nanocomposite paint coating increased approximately 2-4 times. Benzotriazole release from raw halloysite nanotubes extended for ca 50 hours, and its kinetics was fitted to the power function model. The corrosion inhibition efficiency of halloysite nanocontainers was demonstrated by monitoring the localized corrosion current density on scratched metal, as well as visually, by exposure of the scratched metal sample to the highly corrosive environment showing a significant reduction in the metal corrosion rate. At the second stage of this tube nanocontainer development, the release rate of benzotriazole was controlled by formation of metal – benzotriazole stoppers at tube endings. This method provides high halloysite loading efficiency and longer release time, which gives the additional possibility for process optimization. Therefore, one can adjust the benzotriazole release rate from halloysite

nanotubes to achieve the best protective properties for metal coating. This is especially important when flow of the surrounding water takes place causing premature release of the corrosion inhibitors from the metal surface.

CHAPTER 5

CLAY NANOTUBES FOR CORROSION
INHIBITOR ENCAPSULATION
RELEASE CONTROL
WITH END
STOPPERS

Some sections of this chapter were published in papers written by the author of this thesis as "Halloysite Tubes as Nanocontainers for Anticorrosion Coating with Benzotriazole" in *ACS Applied Materials & Interfaces*, 2009, 1(7), p. 1437–1443 and "Clay Nanotubes for Corrosion Inhibitor Encapsulation: Release Control with End Stoppers," *Journal of Materials Chemistry*, 2010, 20, p. 6681–6687.

5.1. Introduction

There is a large variety of techniques to protect metals from corrosion. Chromate containing metal coatings is one of the most commonly used methods; however, toxicity of chromate compounds made this kind of coating impractical for metal protection [95]. Lanthanides as corrosion protection for aluminum and cerium conversion coatings were demonstrated, but these methods are complicated and expensive [62, 96]. An alternative class of corrosion inhibitors is organic corrosion inhibitors based on the triazole functional group, and benzotriazole is the most commonly used corrosion inhibitor in this family due to its environmental friendliness and cost effectiveness [98, 99, 101]. These inhibitors form a stable 2-D complex film through metal ion interaction, and this film covers the metal surface, isolating it from the corrosive media [99]. The inhibitive performance of benzotriazole was

analyzed for different transition metals including copper [98], iron [109], aluminum [8, 10, 16] and high corrosion protection efficiency was demonstrated.

The effectiveness of the corrosion protective layer is reduced in aggressive environments (especially in chlorine containing waters) due to the penetration of chlorine ions and the formation of tiny holes in the coating [110]. Therefore, a sustained supply of the corrosion inhibitors is required to increase the lifetime of the corrosion protection layer. An introduction of encapsulated corrosion inhibitors into metal coatings is the most promising method. Shchukin, et al. [8, 10] successfully demonstrated the Layer by Layer coated silica nanoparticles and polyelectrolyte capsules as possible carriers for corrosion inhibitors. An encapsulation of benzotriazole within an polyelectrolyte microshell significantly increased the inhibitive performance of benzotriazole. Naturally available halloysite clay nanotubes as nanocontainers for corrosion inhibitors were also proposed [8, 16]. These tubule nanocontainers offer great promise for encapsulating active agents because they are available in thousands of tons and are nontoxic to the environment [1-5, 27]. Halloysite significantly extended the release time of the corrosion inhibitor in an aqueous environment. Inhibitive efficiency of benzotriazole loaded halloysite tubes was demonstrated for copper and aluminum [5, 16, 62]. It was also shown that halloysite nanotubes are readily mixable with a variety of metal coatings (paints and polymers) [16, 64-71]. The addition of small amounts of halloysite significantly increases the tensile properties of the polymer coatings [16].

In this chapter, we show additional control over inhibitor release with stopper formation at the tube ends through interaction of loaded benzotriazole with bulk copper ion solutions. These tube caps are made of a Cu-benzotriazole complex, and it effectively seals the tube interior. It is a simple method which could provide tunable release of the corrosion inhibitor since the cap's thickness can be varied depending on the experimental conditions. The effectiveness of this encapsulation depends on the strength of the interaction between the

copper-benzotriazole complex and the halloysite tubule surface. These tube end stoppers may be opened by exposure to an ammonia solution. Six month corrosion protection performance of the halloysite / benzotriazole – paint composites was demonstrated on copper foil by exposure of the metal to chlorine containing aggressive media.

5.2. Materials and Methods

5.2.1. Chemicals

Halloysite samples were obtained from Applied Minerals Inc, Imerys Corp and China Clays Corp. Benzotriazole was purchased from Sigma-Aldrich, USA and $CuSO_4*5H_2O$ was purchased from Fluka Chemika, Switzerland as dry powder. Sodium diethyldithiocarbamate trihydrate was obtained from Sigma Aldrich, USA (for colorimetric determination of copper ions). Formaldehyde was purchased from Sigma Aldrich as a solution in water. Ammonia solution was purchased from Fluka as a saturated aqueous solution (28 wt. %). Industrial oil based blue paint based on ECS-34 powder was purchased from Tru-Test Company. Acrylic and polyurethane paints were purchased from the Krylon and Minwax Co., respectively.

5.2.2. Instrumentation

Halloysite nanotube surface morphology was characterized with a Scanning Electron Microscope (Hitachi S 4800 FE-SEM). The elemental composition of halloysite samples was determined by using SEM EDX elemental analysis. The electron beam accelerating voltage was 5-15 kV for imaging purposes and 25 kV for EDX elemental analysis. Halloysite samples were coated with 1.6 nm thick platinum using a Cressington Sputter coater (208HR) before each SEM experiment (coating regime: 20 mA current, 1 minute). The internal hollow lumen of the halloysite tubes was analyzed by using a Transmission Electron Microscope (TEM, Zeiss EM 912) at a120 kV accelerating voltage. Halloysite average effective size in

aqueous dispersion (derived from 3-D tube radius of gyration) was determined with micro-electrophoresis (ZetaPlus Potential Analyzer, Brookhaven Instruments). The specific surface area of the halloysite samples was determined by Nitrogen BET Adsorption isotherms (Nova 2000, Quantochrome Instruments). Halloysite samples were degassed in vacuum at 300 °C before each measurement. Thermo Gravimetric Analysis (TA Instruments) of the halloysite samples were performed in nitrogen atmosphere by using Alumina pans. Temperature was ramped from 50 °C up to 500 °C at a 3.0 °C/min rate.

UV-Vis spectrophotometer (Agilent 8453) was used to determine the benzotriazole and Cu (II) concentrations during the release experiments. Benzotriazole concentration was measured with peak wavelength at 265 nm. Copper (II) concentration was measured with sodium diethyldithiocarbamate at 450 nm, unless otherwise stated. Benzotriazole-copper complex thickness was monitored with a Quartz Crystal Microbalance (USI-System, Japan) using a 9 MHz QCM-resonator. A copper layer was plated on top of the original gold electrodes using electroless deposition with formaldehyde. An optical Microscope (Olympus, Japan) with a video camera (Sony SSC DC 80) was used to observe corrosion spots on the scratched metal surface. Images were magnified 10 – 15 times.

The tensile strength of the coating was tested with a tensile strength instrument (ADMET, EP-0801161-M-48VAC). Samples were pulled with a speed of 0.3 mm/min for obtaining the stress – strain curve.

5.2.3. Nanotube loading procedure

To entrap benzotriazole, halloysite was mixed as a dry powder with a saturated solution of benzotriazole in acetone (80 mg/mL). A beaker containing benzotriazole and halloysite suspension was transferred to a vacuum jar which was then evacuated using a vacuum pump. Slight fizzing of the suspension indicated that air was being removed from the core of the halloysite tubules and was being replaced with the benzotriazole solution. The suspension

was kept under vacuum for 3-5 hours and then cycled back to atmospheric pressure. This process was repeated three times in order to increase loading efficiency. Finally, halloysite nanotubes were separated from solution by centrifugation, washed with water and dried. Loading of benzotriazole from its melt and aqueous solutions was also checked but was found less efficient.

5.2.4. Benzotriazole release kinetics

All release experiments were performed in water, pH 6-7 at room temperature. The suspension of halloysite nanotubes was constantly stirred with a magnetic stirrer during the release process in order to establish equilibrium conditions. The concentration of benzotriazole was determined with UV-Vis spectroscopy at a 265 nm wavelength. For scaling release curves, at the end of each release experiment a complete release was determined with ultrasonication of the halloysite samples. Ultrasonication was continued until no benzotriazole was detected in the supernatant of the suspension.

Benzotriazole loading efficiency was also checked by Thermo Gravimetric Analysis. Weight loss of the loaded halloysite was compared with that of the unloaded halloysite sample and loading efficiency was calculated based on the difference of these measurements.

5.2.5. Tube stopper formation

Formation of stoppers at the tube ends was based on the reaction between loaded benzotriazole and copper ions from the bulk solution which diffused into the tube openings to form an insoluble metal-benzotriazole complex capping the tube ends. For this purpose, benzotriazole loaded halloysite was exposed for 1 min to the bulk aqueous solution containing Cu (II) ions (with continuous stirring). The processed nanotubes were separated from solution by centrifugation.

5.2.6. Stopper opening

To decompose the benzotriazole complex at the tube openings, we rinsed halloysite with a concentrated ammonia solution. Halloysite nanotubes, capped with stoppers were the added into the 28 wt % ammonia solution in water. Excess amounts of ammonia cause irreversible decomposition of the Cu – BTA complex which released $[Cu(NH_3)_4]^{+2}$ ions. Kinetics of the decomposition process was monitored by UV-Vis spectroscopy at 650 nm wavelength which corresponds to the absorption of the $[Cu(NH_3)_4]^{+2}$ ions.

5.2.7. Corrosion protection testing

The corrosion process was studied with visual microscopy of the corrosion development in the artificially scratched area. 110-Cu alloy strips were coated with ECS-34 True-Test oil based industrial blue paint. Copper samples were treated with nitric acid solution (20 % by weight) to remove impurities from the surface and to polish the metal surface. Then samples were washed with water and dried. After drying, one of the samples was coated with paint containing 10 wt % benzotriazole loaded halloysite and another sample was painted with normal paint. The samples were dried in air for two days, artificially scratched and dipped into a corrosive solution simulating sea water and containing 24 g/L NaCl, 3.8 g/L $CaCl_2$, and 2 g/L Na_2SO_4 for ten days, as described elsewhere [16]. Thickness of the coating was ~ 100 microns after drying. Scratched surfaces were analyzed with optical microscopy. A longer corrosion resistance (6 months) test was conducted on a sample coated with acrylic latex paint (purchased from Krylon Co.) and exposed to 30 g/L NaCl solution in water. Corrosion performance was evaluated based on the concentration of the Cu (II) ions in the corrosive environment. Halloysite was added to the liquid paint as a powder and dispersed by means of simple mechanical mixing in all of the cases.

5.3. Results and Discussion

5.3.1. Clay nanotube structure

Halloysite samples from four different deposits were analyzed. As seen in Figure 5.1, samples # 1, # 2 and # 3 have complete rolled nanotubular structures, with some variations of tubule diameters and lengths. The external diameters of most of the tubes is 50 nm. Few tubes with diameters as big as 150 nm also exist. Lengths of tubes vary in the range of 0.5 – 2.0 microns. Sample 3 also has some pieces of broken tubules and incompletely rolled tubules in addition. Sample 4 has a uniform distribution of lengths and diameters of the tubes. Tube diameter is ~ 40 nm and length is about 0.5 microns. Other physicochemical properties of the halloysite samples are described in Table 5.1.

a)　　　　　b)　　　　　c)　　　　　d)
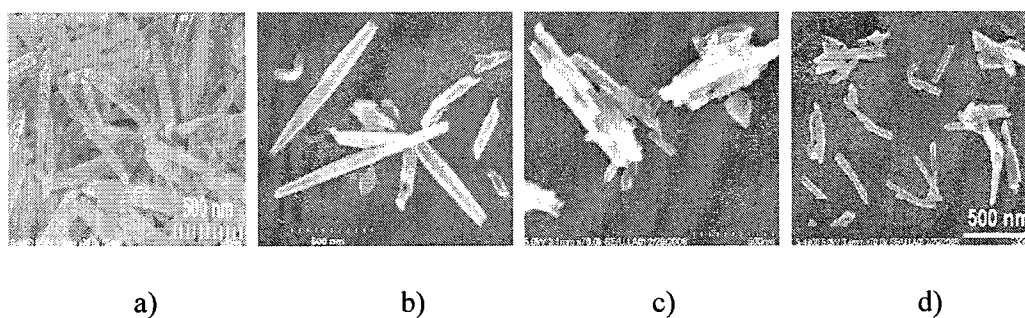
Figure 5.1 SEM images of halloysite samples; a) from Dragon mine, Utah (Applied Minerals, Inc), b), c) and d) from New Zealand (Imerys and China Clays Corp).

Table 5.1 Characteristics of the halloysite samples

Sample No	Overall particle size	Specific surface area (m²/g)	Elemental Composition (atomic %)	Constants of the release model	
				k	n
1	328 ± 7	153.0	17.7% Al, 18.3 % Si, 63.7% O	65.3	0.111
2	445 ± 23	127.0	17.1% Al, 16.7% Si, 63.3% O, 0.5% Fe, 1.6% Ca	66.7	0.095
3	382 ± 11	113.0	18.3% Al, 18.9% Si, 62.2% O	55.5	0.147
4	279 ± 3	121.8	18.7% Al, 18.7% Si, 62.1% O, 0.2% Fe	80.0	0.055

5.3.2. Benzotriazole release rate

In Figure 5.2, release profiles of benzotriazole from different halloysite samples are shown. Fast benzotriazole dissolution in water is also shown for comparison (the line close to the vertical axis). The release rates from different halloysite samples are close to each other, reaching 95 % release within 35-40 hours while complete dissolution of benzotriazole powder in water takes place within ten minutes.

Peppas model [106] was the best model describing the benzotriazole release profile from the halloysite samples ($M_t/M_\alpha = kt^n$, where M_t is the amount of substance released at time t, M_α is the amount released at infinite time, n is the exponential constant related to the release mechanism, and k is a constant). As it is seen from the Table 5.1 the values of k and n are very close for the samples 1-3 in spite of having slightly different chemical compositions (especially samples 1 and 2). This fact clearly indicates that the morphology of the tube is more significant in defining the release kinetics of the substances from the halloysite core rather than the chemical composition of the tubule walls. Typical loading efficiency of benzotriazole was in the range of 6 - 9 % by volume for these samples. On the other hand,

the 4th sample shows significantly faster release, which is evident from the larger value of k as compared to other samples. Having smaller tubule dimensions, does not allow enough room for benzotriazole to penetrate deeper into the pores and as a result all the loaded benzotriazole is collected at close proximity to the tubule external surface. Therefore, shorter diffusion pathway is required for benzotriazole release for this sample. This argument is further supported by the smaller loading efficiency of the benzotriazole into this sample compared to the previous samples (3 % by volume).

Figure 5.2 also gives the dissolution of benzotriazole from microcrystalline powder (simply adding powdered benzotriazole into water). Dissolution of benzotriazole in water fits to the same model with much larger parameters k and n, being equal to 514.4 and 0.64, respectively. This reflects different release mechanisms: 3-D release of benzotriazole during crystal dissolution as compared with one dimensional (1-D) benzotriazole release from halloysite tubules (so called, pore controlled diffusion [114]). Larger coefficients of k and n may indicate a higher diffusion coefficient of benzotriazole in bulk aqueous solution as compared to that inside halloysite nanotubule lumen.
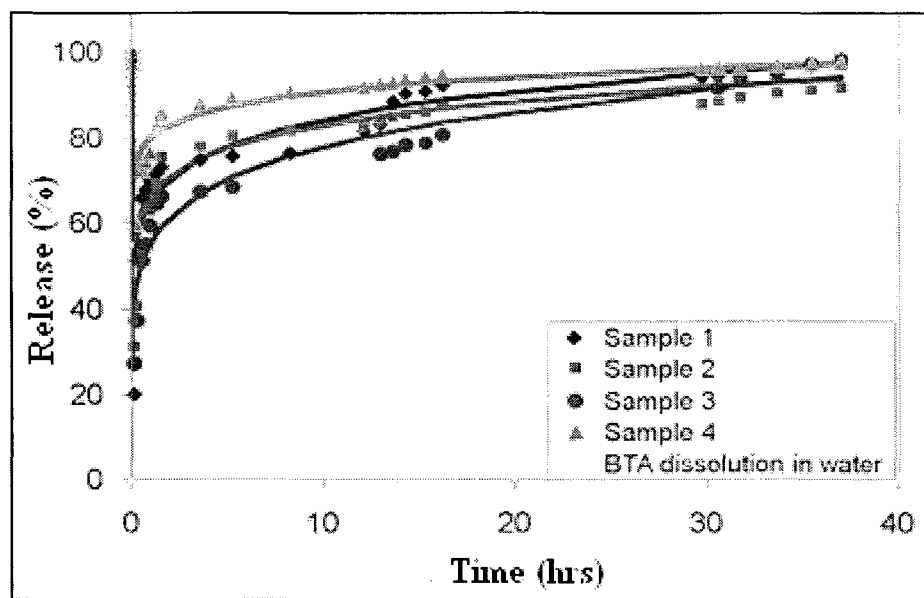
Figure 5.2 Benzotriazole (BTA) release profiles for different halloysite samples.

5.3.3. Benzotriazole corrosion inhibition process

Benzotriazole interacts with Cu (II) ions on the metal surface forming a thin 2-D complex film. The structure of this film depends on the conditions of the environment and was extensively analyzed in [99, 109-112].

Figure 5.3 gives the kinetics of the copper-benzotriazole complex formation as monitored by using copper plated Quartz Crystal Microbalance (QCM) electrode. Copper electrodes with total surface area of 12 mm^2 were deposited over the quartz chip, which resulted in an initial QCM resonance frequency of 8.6 MHz. Reaction of benzotriazole with the copper electrode resulted in an increase of the electrode mass, which was registered as a resonance frequency decrease. Increase in mass is related to the change in frequency by Sauerbrey's equation as $\Delta F = -0.87\Delta m$, where $\Delta F(Hz)$ is the shift in resonance frequency and $\Delta m(ng)$ is the change in mass due to the deposition of benzotriazole on the copper electrode surface [113].
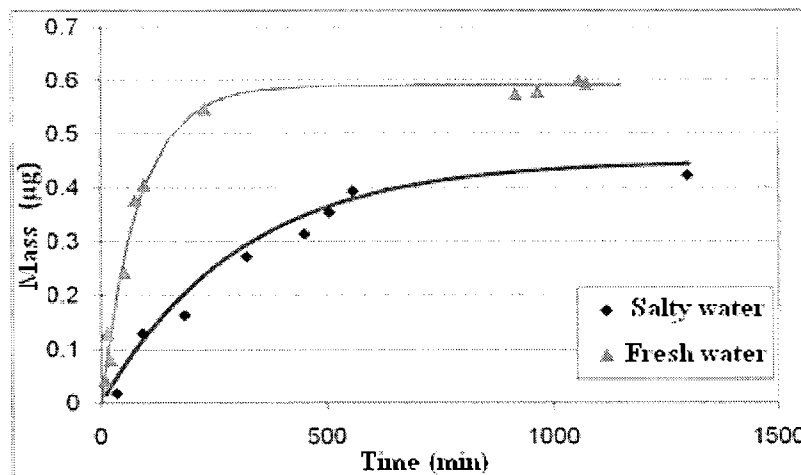
Figure 5.3 Benzotriazole complexation kinetics on copper electrode, monitored with QCM (deposited mass against time). Concentration of benzotriazole is 0.01 M and salty (simulated sea) water contains 30 g/L of NaCl.

Complexation of benzotriazole with copper shows a pseudo-first order reaction mechanism (in the presence of excessive amounts of benzotriazole). In the current experiment, a 0.01 M concentration of benzotriazole was used which is much higher than the 2-D surface concentrations of the Cu (II) ions. Kinetics of the complex formation on the copper surface can be described by $m(t) = m_0(1-e^{-kt})$, where $m(t)$ is the mass of the deposited benzotriazole on the surface at time t, m_0 is the mass of the benzotriazole when the surface of the copper electrode is completely covered with the film and no more Cu(II) ion is available for reaction, and k is the first order reaction rate constant. Values of m_0 were 0.59 and 0.45 micrograms for fresh and salt waters respectively, whereas the values of k were determined as 0.012 and 0.003 respectively.

These data indicate that the presence of chloride ions in the corrosive environment slows down the formation rate of the protective complex on the metal surface. Complete protective coverage of the copper surface was accomplished within ~ 6 hours in pure water while in salt water this process took more than 12 hours. Therefore, a continuous supply of benzotriazole is required for complete curing of the metal surface once corrosion is started, especially in a

sea water environment. As it was shown earlier, benzotriazole completely dissolves in water within a few minutes, while from halloysite tubes its release is extended for more than 40 hrs. This time interval corresponds to the time needed for the initiation of the corrosion protection in the metal coating defects where nanotubes become opened for benzotriazole release (Figure 5.4). This justifies the usage of halloysite tubes as nanocontainers to encapsulate corrosion inhibitors for their sustained release and for better and longer protection of metals against corrosion.

5.3.4. Analysis of corrosion development and inhibition process

Earlier, corrosion inhibition performance of the initial stags was studied with the Scanning Vibrating Electrode Technique as in [10, 16], and corrosion current density was found to be constantly growing due to the corroding scratch in the metal coated with pure sol-gel film while no corrosion current was observed for the metal coated with composite sol-gel film containing halloysite loaded with benzotriazole. This is an indication of the improvements to metal coatings embedded with halloysite.

In Figure 5.4, Cu (II) ion concentration profiles for the copper strips coated with commercially available acrylic paint and with the halloysite - paint composite are presented. Both of copper strips were scratched and exposed for six months to highly corrosive media with 30 g/L sodium chloride. The corrosion process was evaluated by determining the concentration of the Cu (II) ions in corrosive media with UV-Vis spectroscopy. One could see that the concentration of the copper ions was permanently increasing for the sample with commercial paint coating (an intensive corrosion process is developing in this case). However, in the media where copper is coated with halloysite-paint composites, copper ions concentration was reduced to below 1.0 ppm after 20 days of exposure and further. This indicates that a slow corrosion process was taking place only at the initial stage, but this

process was almost completely suppressed after isolation of the copper surface with the protective Cu-BTA complex film due to the benzotriazole release from the tubes.
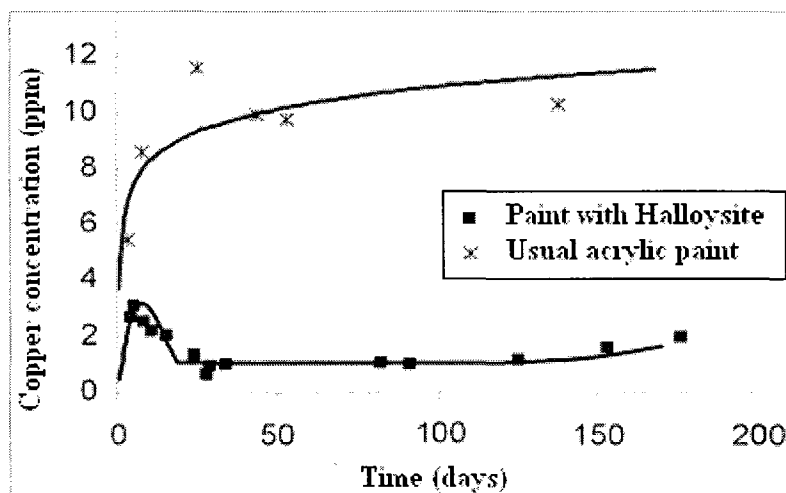
Figure 5.4 Copper (II) concentration profiles of the copper strips coated with acrylic paint and artificially scratched to induce corrosion process. Both samples were exposed to highly corrosive media containing 30 g/L NaCl. Composite paint contained 10 wt % halloysite loaded with benzotriazole.

In order to analyze the possibility of the deposited corrosion products underneath the paint during the corrosion test, the paint was removed and the surface of the metal was analyzed with optical microscopy after the completion of corrosion test. The surface underneath the paint was completely covered with green patina for the case of the commercial paint, while very little corrosion products were observed in the case of the paint with halloysite. It is believed that these corrosion products were formed at the initial stages of the corrosion process, which is also supported by the fact that the concentration of the Cu (II) ions was relatively high at the initial stages of the corrosion test and then reduced due to the inhibitive action of the leaking benzotriazole.

In Figure 5.5, scratches on the copper coated with industrial oil based paint with and without halloysite is demonstrated. Both samples were exposed to a highly corrosive environment for 10 days. Image (a) clearly demonstrates that paint containing 10 wt %

benzotriazole loaded nanotubes effectively slowed the copper corrosion rate because no signs of corrosion products are visible at the scratched area. Elemental analysis of the corrosive media also demonstrated that 128 ± 1 ppm of Cu (II) ions were dissolved by the environment for sample (b) while no copper ions were detected for sample (a). This result is a clear indication that entrapment of benzotriazole into the paint by using halloysite capsules is effective for metal corrosion inhibition, especially when the scratched surface is exposed to large amounts of a highly corrosive liquid, such as sea water. Besides, the addition of 2-5 % of halloysite into the paint increases the coating tensile strength by approximately 50-300%, which is an additional good feature of these protective nanocomposites [16, 66].

a)   b)
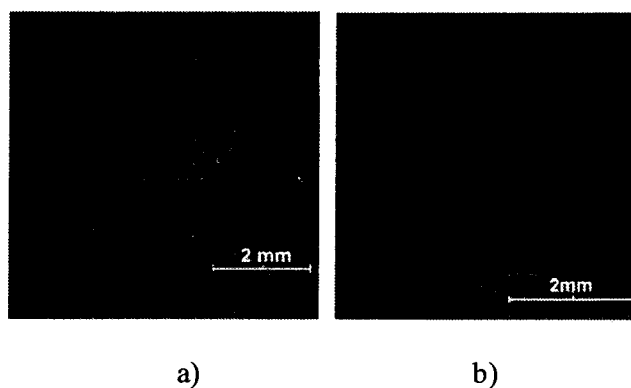
Figure 5.5 Images of the scratched copper strips painted with oil based blue paint, loaded with 5 % halloysite-benzotriazole nanotubes (a) and without any additives (b), after exposure to corrosive environment for 10 days.

5.3.5. Controlling release rates with the tube stoppers

Better encapsulation and control over the release rate is required in certain environmental conditions, especially in media where rapid convection of external water is taking place and in sea water where longer time is required for the initiation of the corrosion inhibition process (marine related industry). Tighter encapsulation of benzotriazole loaded into the tubes was achieved by exposing the dispersion of loaded nanotubes to the solution containing Cu (II) ions. Benzotriazole forms a complex film while it interacts with Cu (II) ions. This film clots

the tube endings and benzotriazole becomes entrapped into the tubes. In pure water benzotriazole is simply diffusing out from the tube openings, while in the presence of Cu (II) ions, leaking benzotriazole interacts with the copper and forms a stopper at the tube endings (Figure 5.6). Benzotriazole release from such closed tubes occurs through much smaller pores. The thickness of such stoppers depends on concentration of the Cu (II) ions in the solution, the amount of benzotriazole loaded in the tubes, and composition and morphology of the tubes. A higher concentration of Cu (II) ions leads to better encapsulation of the benzotriazole and, after a certain threshold value, no benzotriazole release was observed.

In the Figure 5.6, the formation of stoppers at the halloysite tube openings is demonstrated (using Cu(II) ions). Complex of copper ions and benzotriazole is well studied by various authors and described in the review by Cease, *et al.* [99]. Benzotriazole forms stable 2-D complexes with most of the transition metals and we tried Cu (II), Fe (II), Fe (III), and Co (II) salts for the stopper formation [99, 109, 112].

Cu(II) ions
Benzotriazole
Cu-BTA complex
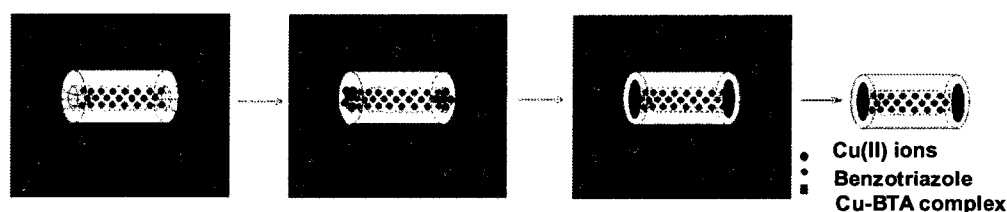
Figure 5.6 Illustration of stopper formation at halloysite tube endings by interaction of leaking benzotriazole at Cu (II) ions.

In Figure 5.7, an image of the shell formed on the halloysite external surface by nitrogen elemental mapping with TEM is described. 2-mercaptobenzimidazole was used in this case as a corrosion inhibitor and nitrogen atoms from the molecules of the corrosion inhibitor were imaged. As one can see from the image the shell covers the entire halloysite external surface (not on only tube endings) and thus provides excellent encapsulation. Oxygen mapping was used to visualize the halloysite particles.
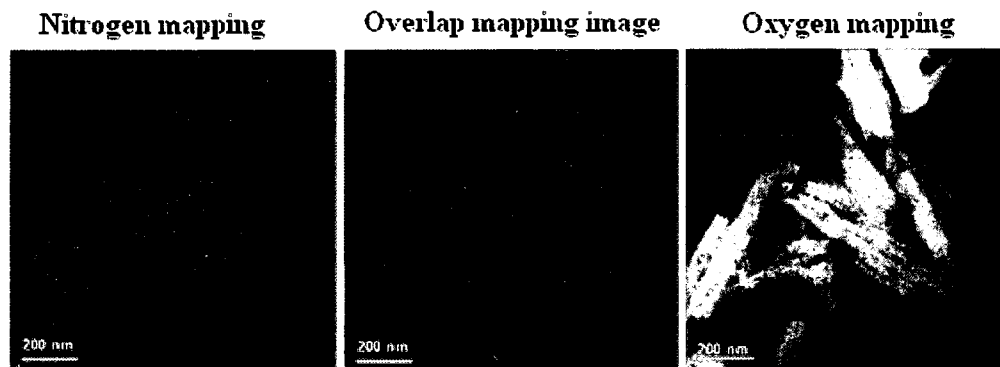
Figure 5.7 Visualization of the shells formed on halloysite external surface with interaction of corrosion inhibitors with copper (II) ions. Images were taken by TEM elemental mapping, *National Institute of Materials Sciences, Tsukuba, Japan.*

Benzotriazole release characteristics were studied in detail with the formation of stoppers with Cu (II) ions, which provided the best release control. The decrease in benzotriazole release rate depends on a number of parameters, such as the chemistry and morphology of the halloysite samples (we tried halloysite from two different deposits), the concentration and type of metal ion, and the concentration of benzotriazole available at tube openings.

One of the important parameters influencing benzotriazole release rates is the concentration of metal ions that are used for formation of metal – benzotriazole stoppers. In order to determine the influence of metal concentration in the bulk solution to the benzotriazole release rate, copper sulfate solution of six different concentrations was used to encapsulate benzotriazole inside halloysite tubes (Figure 5.8a). The benzotriazole release rate constantly decreased by using higher concentrations of copper sulfate solution. This is an indication that the efficiency of the encapsulation strongly depends on the concentration of the metal ions used for formation of the stoppers. This effect may be exploited to develop the desired release rate. For example, total release time for the sample process with 2 mM of $CuSO_4$ solution reached ca 100 hours.

Another important factor that influences the benzotriazole release rate is the concentration of benzotriazole at the tube endings that is available for formation of the metal-benzotriazole film. This can be controlled by the washing of loaded nanotubes with DI water after loading with benzotriazole and prior to processing with metal ions. To demonstrate this, nanotubes were washed two times in the first sample, and four times in another sample before exposure to 8 mM copper sulfate solution. Washing four times allowed less benzotriazole in halloysites external surface compared to that with two times washing, leading to"weaker" stopper formation with more number of voids or openings for benzotriazole leakage. Evidently, tubes washed four times with water showed faster release as compared to those washed two times before exposure to Cu (II) solution (Figure 5.8b).

a)   b)
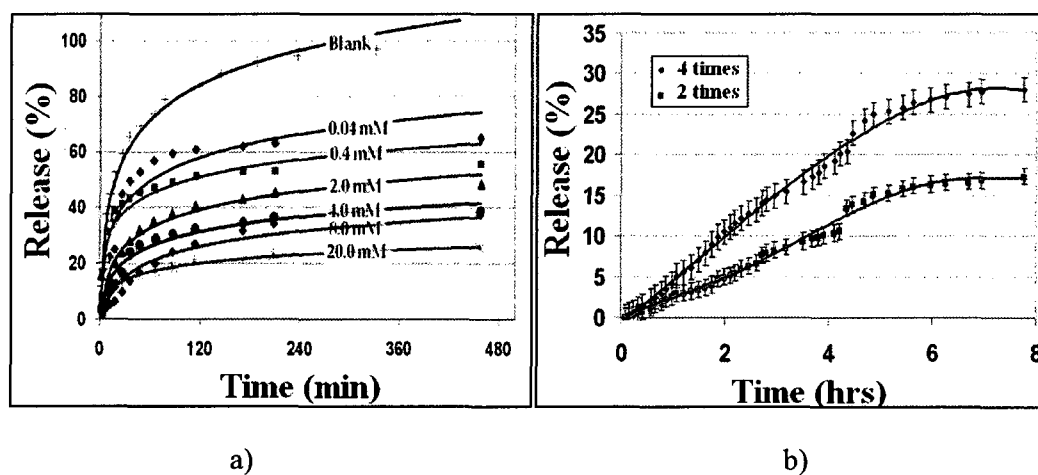
Figure 5.8 Release profiles of benzotriazole from halloysite washed with CuSO4 solution of different concentrations. Release of benzotriazole from untreated halloysite is also shown for comparison (a). Benzotriazole release profiles by halloysite having Cu-benzotriazole stoppers with 2 and 4 times washing stages (b).

It is interesting that the efficiency of the stopper formation was different for halloysite samples # 1 and # 2. (Table 5.1 and Figure 5.9). A significant reduction in the release rate was observed for halloysite sample # 2, while it was not as significant for the more typical halloysite sample #1. The difference in encapsulation efficiency might be related to the

irregular substitution of Al^{+3} with Fe^{+3} ions in octahedral sheets. This substitution gives rise to formation vacancies as well as an extra negative charge in the halloysite layer [2, 22, 35]. Therefore, iron rich halloysite samples are expected to have larger cation exchange capacities (CEC) [22], which results in the adsorption of Ca^{+2} ions from the soils (see Table 5.1, line 2). A stopper complex formation is based on the attraction of Cu^{+2} ions and the higher negative charge of halloysite sample # 2 attracts them more efficiently than sample # 1, which increases the efficiency of the benzotriazole complexation at the tube ends.

a)   b)
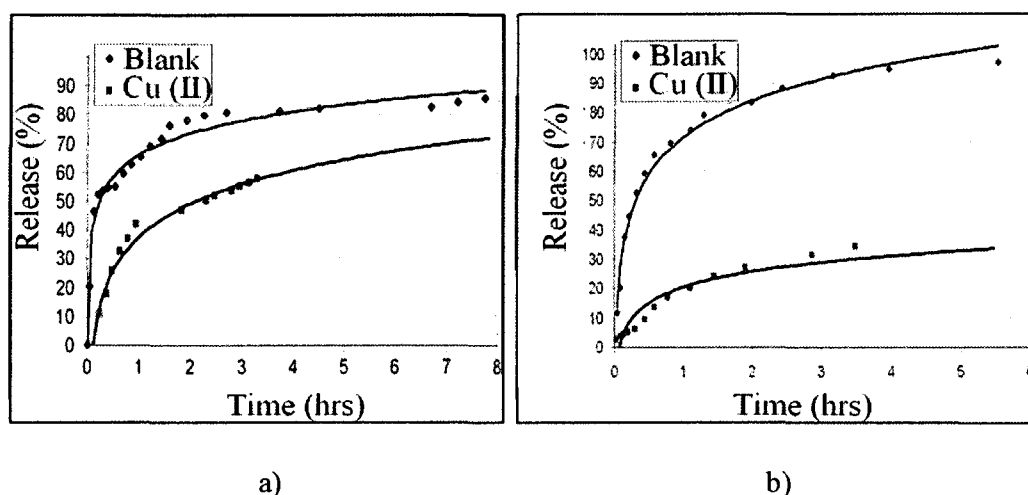
Figure 5.9 Influence of surface chemistry on stopper formation: comparison of halloysite samples # 1 (a) and sample # 2 (b) before and after stopper formation (1 min treatment with 0.09 ± 0.01 M $CuSO_4$).

5.3.6. Tube stopper opening

Formation of the Cu-BTA complex at the tube ends (and other possible leakage voids) decreased the benzotriazole release rate. One can assume that, in contrast, decomposition of the copper-benzotriazole complex conducted by addition of concentrated ammonia solution will reverse the situation and increase the release rate. Decomposition of the Cu-BTA complex takes place with the following reaction:

$$[Cu(BTA)_2]_n \quad + \quad 4nNH_3 \quad \longrightarrow \quad n[Cu(NH_3)_4]^{+2} + 2nBTA$$
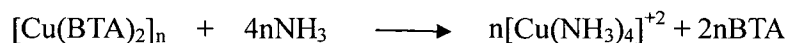
This reaction is reversible one, but in the presence of excessive amounts of ammonia the equilibrium is shifted toward the reaction products i.e. toward the decomposition of the complex.

In Figure 5.10, the switch of the benzotriazole release, based on the above reaction, is demonstrated. First, nanotubes were exposed to a concentrated $CuSO_4$ solution (0.8 M) in order to form the stoppers at the tube ends. As a result of the stopper formation, the release was almost completely stopped, as is evident from the initial part of the graph. However, concentrations of both copper and benzotriazole sharply increased after injection of ammonia solution. A saturated solution of ammonia in water dissolved the stoppers. With this method, one can switch on the release of the encapsulated materials.
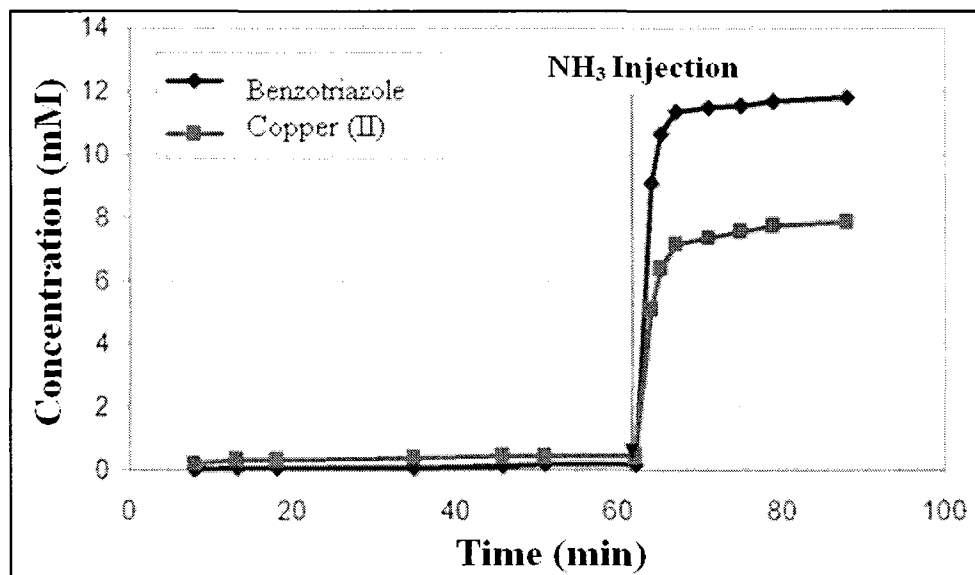
Figure 5.10 Switch of benzotriazole release rate from capped nanotubes: nanotubes clogged with Cu-BTA stopper before and after NH₃ injection.

Cu-BTA decomposition kinetics was different for halloysite samples # 1 and # 2 (Figure 5.11). The decomposition process follows pseudo - first order reaction kinetics in the

presence of excessive amounts of ammonia, which is described by the following formula;

$W_t/W_0 = e^{-kt}$, where W_t is the amount of Cu – BTA complex remaining at time t, W_0 is the initial amount of the complex, and k is the first order reaction rate constant. Constants of the reaction were $1.95 \cdot 10^{-3}$ and $6.28 \cdot 10^{-4}$ for the samples # 1 and # 2 respectively. This is a clear indication that the complex film interacts stronger with iron rich sample # 2. Figure 5.11 also indicates that about 25 % of the complex decomposed immediately after the exposure to ammonia solution.
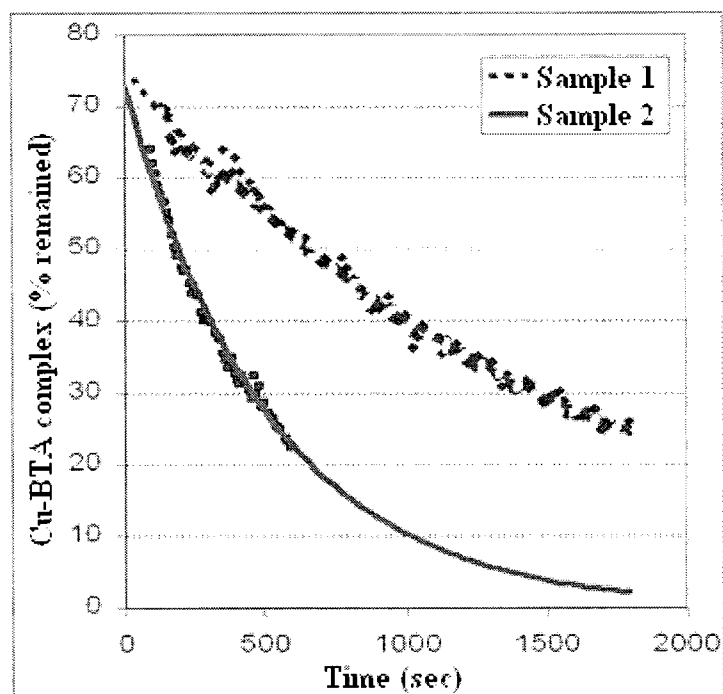
Figure 5.11 Decomposition kinetics of Cu-BTA complex by ammonia solution: sample #1 and sample #2 (with 0.5 % iron). Halloysite was added to ammonia solution as a dry powder and reaction started at 0th second.

5.4. Conclusion

Natural halloysite nanotubes were employed as inexpensive nanocontainers offering essential benefits for the entrapment of corrosion inhibitors into metal coatings. An improvement of inhibitor loaded halloysite – paint coating was demonstrated on copper by

direct exposure of the metal to highly corrosive media for six months. Corrosion was retarded at the initial stage due to the inhibitive action of the benzotriazole released from the halloysite nanotubes in paint defects. Benzotriazole forms a protective complex on the metal surface isolating it from the corrosive media. An analysis of the complexation kinetics showed that the protective layer formation took c.a. 6 hours in pure water, and chloride ions from simulated sea water significantly reduce this speed. Therefore, a sustained supply of corrosion inhibitor from nanocontainers is required for complete protection of the metals. Better encapsulation of benzotriazole in the nanotubes was demonstrated through formation of tube end stoppers by complexation of leaking benzotriazole with external copper ions. The efficiency of the stoppers depended on the chemical composition of the halloysite: tubes with higher Fe^{+3} content showed lower benzotriazole release rate. The stoppers can be dissolved and release rate restored with ammonia treatment.

CHAPTER 6

STRUCTURAL AND BIOCOMPATIBILITY INVESTIGATION OF HALLOYSITE NANOTUBES

This chapter was published in a paper written by the author of this thesis as "Cytocompatibility and uptake of halloysite clay nanotubes," *Biomacromolecules*, vol. 11, p. 820-828, 2010.

6.1. Introduction

Inorganic materials and biomaterials are apparently on opposite sides of the materials' world. Proteins, nucleic acids, and lipids are soft and often show incredible functionality with high specificity and efficiency which cannot be easily replicated. The best way to utilize the high functionality and stability of bio-related materials is to create hybrids consisting of materials of biological origin and inorganic materials. Halloysite is defined as a two-layered aluminosilicate, chemically similar to kaolin, which has predominantly hollow tubular structure with the dimensions in the submicron range [1-5]. Halloysite nanotubes are capable of entrapping a range of active agents within the inner lumen, followed by their retention and slow release [5].

There is an increasing amount of on-going research activity to produce multifunctional nanometer-scale containers, and a growing demand for their use in sophisticated applications. Such containers should be inexpensive materials with a simple means of fabrication and thus, natural resources and nanotubes are good candidates. Typically thin tubular systems are highly preferred, because they have better loading efficiency and retention of the loaded

agents compared to spherical nanoparticles or nanocapsules. The lumen diameter of the halloysite tube fits ideally to globular protein diameters, allowing for their incasement in the tube and feeding them with low molecular compounds for biocatalysis [43]. These tubes are especially attractive because of the different chemistry of the inner and outer surfaces and because of their tunable inner diameter. Halloysite is also a "green" material and, due to the fact that it is a natural product will not present an added risk to the environment. Halloysite was found to be a viable and inexpensive nanoscale container for the encapsulation of biologically active molecules, which was first demonstrated by Price, Lvov and Kelly, *et al.* [3, 36, 45]. Polymer-halloysite composites are prospective materials for medical implants [115].

However, a comprehensive study of halloysite biocompatibility has not yet been done. Are there health risks associated with halloysite? Currently, there is no research on cytotoxicity caused by cellular exposure to halloysite in concentrations viable for commercial applications. Halloysite nanotubes are rolled versions of kaolin, and they are just as chemically stable and as widely used in household products as kaolin clay. However, concern over the use of fine particles rich in silica is understandable. Many diseases, such as fibrosing collagenous pneumoconiosis and silicosis, are related to prolonged lung exposure to fine crystalline silica particles. Studies associate pathogenesis of these diseases to (1) generation of free radicals by the particles and (2) overactive inflammatory response by intra-alveolar/interstitial macrophages.

In this chapter, we focused on studying halloysite interaction (both untreated and fluorescently labeled) with cells. We analyzed halloysite toxicity and visualized the process of cell uptake of fluorescently labeled clay nanotubes with using a confocal laser scanning microscopy (CLSM). Intracellular uptake by cells of different origins (cervical adenocarcinoma, HeLa, or breast cancer cells, MCF-7) and cytoviability tests (MTT and

Trypan blue) demonstrated halloysite cytocompatibility and potential as biofriendly cargo nanocontainer for biomaterials.

6.2. Materials and Methods

6.2.1. Chemicals

The sources of the chemicals are as follows: poly(sodium 4-styrene-sulfonate) (PSS, Sigma), poly (allylamine hydrochloride) (PAH, Sigma), fetal bovine serum (FBS, Sigma), penicillinstreptomycin solution (Sigma), sodium pyruvate (Sigma), Dulbecco's Modified Eagle Medium, DMEM (Sigma), thiazolyl blue tetrazolium bromide >97.5% TLC (Sigma), phosphate-buffered saline, Dulbecco A (PBS, Oxoid), sephadex G25 (Sigma), fluorescein isothiocyanate isomer I (FITC, Aldrich), triton X-100 (Sigma), aminopropyltriethoxysilane (APTES, 99%, Aldrich). Purified dehydrated Halloysite samples were obtained from Applied Minerals, Inc.

6.2.2. Halloysite fluorescence staining

6.2.2.1. Layer by Layer coating. Halloysite nanotubes were coated by using a Layer by Layer technique.   1000 µL of halloysite dispersed in DI water was dispersed in a solution containing the polycation (PAH). The dispersion was continuously shaken for 10 min. The excess polycation was removed by three centrifugation/washing steps with ultrapure water. Thereafter, 1 mL of a 0.5 M NaCl solution containing the polyanion (PSS) was added and the dispersion was continuously shaken for 10 min, followed again by three centrifugation/washing steps. This procedure was repeated three times for each polyelectrolyte resulting in the deposition of five polyelectrolyte layers on the halloysite nanotubes. An FITC-labeled PAH layer was inserted between non-labeled layers in order to follow the halloysite nanotubes uptake by cells. In order to prepare PAH-FITC, two solutions (PAH and FITC) were mixed at a ratio of 1:5 (PAH:FITC) and incubated over 2-3 days. After

being dialyzed against water for 1-2 h, followed by drying in a lyophilisator and dissolving in water, remove the free FITC with a sephadex G25 column in ammoniac buffer (pH 8.5), drying within the lyophilisator and stored at + 4 °C.

6.2.2.2. Fluorescence staining by APTES functionalization. Halloysite nanotubes (HNTs) were modified according to the procedure generally applied for the grafting of silica-based materials. In a typical run, 500 µL of APTES was dissolved in 6.25 mL of dry toluene. Approximately 0.15 g of clay powder was added, and the suspension was dispersed ultrasonically for 30 min. The suspension was then refluxed at 120 °C for 20 h under constant stirring. The resultant mixture was extensively washed six times with fresh toluene to remove the excess organosilane, and then dried overnight at 120°C for further curing. The mixture was washed 10 times with water, and the sample was freeze-dried overnight. 3 mg of the amino functionalized HNTs was dissolved in 1.5 ml of 0.1 M carbonate buffer (pH 8.0). To this solution, 100 µL of 13 mM solution of FITC in DMSO was added. The mixture was allowed to react for two days under constant stirring at room temperature and protected from light. The solution was dialyzed and lyophilized overnight.

6.2.3. Cell culture

The human epithelial carcinoma cell line (HeLa) and human breast cancer cell line (MCF-7) were maintained in DMEM medium supplemented with FBS (10%), penicillin (100 U/mL culture medium), streptomycin (100 µg/mL culture medium), glutamine (5%) and sodium pyruvate (5%). Cells were grown in a humidified incubator at 37°C, 5% CO_2, and 95% relative humidity.

6.2.4. Microscope observations

6.2.4.1. Transmission Electron Microscope (TEM). Low-resolution TEM images were recorded with a Jeol Jem 1011 microscope operated at an accelerating voltage of 100 kV. Sample analysis were performed on carbon-coated copper grids.

6.2.4.2. Scanning Force Microscope (SFM). SFM micrographs were obtained by means of a Bioscope II and Multimode-Picoforce (Veeco Instruments Inc., Santa Barbara, CA, USA) in air at room temperature using contact mode with MLCT-AUNM cantilevers with a 0.01 k\N spring constant and in Tapping Mode using TESPA cantilevers with a 4N\m spring constant. A drop of sample suspension was applied to a freshly cleaved mica support. Halloysite nanotubes were imaged after dehydration. Images were analysed by Nanoscope software (Vers. 7.30).

6.2.4.3. Confocal Laser Scanning Fluorescence Microscope. Confocal micrographs were taken with a Leica confocal scanning system mounted to a Leica TCS SP5 (Leica Microsystem GmbH, Mannheim, Germany) and equipped with a 63X oil immersion objective. Z scan and XY scans images were acquired to demonstrate internalization of nanotubes into the cells.

6.2.5. Cytotoxicity analysis

6.2.5.1. MTT test. All cells lines were used in the general cytotoxicity test. The MTT system measures the activity of living cells via mitochondrial dehydrogenase activity. Mitochondrial dehydrogenases of viable cells cleave the tetrazolium ring, yielding purple MTT formazan crystals which are insoluble in aqueous solutions. The crystals have been dissolved in acidified isopropanol. The resulting purple solution is measured by spectrophotometer. An increase in cell number results in an increase in the amount of MTT formazane formed and an increase in absorbance.

The halloysite suspension at different concentration (from 1 µg/ml up to 1mg/ml) was diluted with complete culture medium. The MTT method of cell determination is most effective when cultures are prepared in multiwell plates. HeLa and MCF-7 cells (10^5 cells/mL) were added to 6-well culture plates at 2 mL/ well and incubated at 37°C in 5% CO_2, 95% relative humidity for 24-48-72 hours with the nanotubes suspension. The control was a complete culture medium. After an appropriate incubation period, the cultures were removed

from incubator and an MTT solution in an amount equal to 10% of the culture volume was aseptically added. Cultures were returned to the incubator and incubated for 3 hours. After the incubation period, cultures were removed from the incubator and resulting MTT formazane crystals were dissolved with acidified isopropanol solution an equal culture volume. Plates were ready within 1 hour after adding acidified isopropanol solution. After the incubation time, pipetting up and down was required to completely dissolve the MTT formazane crystals. Absorbance at wavelength of 570 nm was spectrophotometrically measured. Subtract background absorbance was measured at 690 nm. The percentage viability was expressed as the relative growth rate (RGR) by equation:

$$RGR = (D_{sample}/D_{control}) *100\% ,$$ (4.1)

where D_{sample} and $D_{control}$ are the absorbances of the sample and the negative control (sodium chloride).

6.2.5.2. Trypan Blue test. Trypan Blue is one of the dye exclusion procedures for viable cell counting. This method is based on the principle that live (viable) cells do not take up certain dyes, whereas dead (non-viable) cells do. Staining facilitates the visualization of cell morphology.

Live cells, with intact cell membranes, are not coloured. Since cells are very selective to the compounds that pass through the membrane, in a viable cell Trypan blue is not absorbed; however, it traverses the membrane in a dead cell. Hence, dead cells are shown as a distinctive blue colour when viewed under a microscope. Therefore living cells are excluded from staining.

For the Trypan Blue assay, HeLa and MCF-7 cells (10^5 cells/mL) were added to 6-well culture plates at 2 mL/ well and incubated at 37°C in 5% CO_2, 95% relative humidity for 24-48-72 hours with the nanotubes suspension. The halloysite suspension at different concentration (from 1 μg/ml up to 1mg/ml) was diluted with complete culture medium which

is used as the control. After the appropriate incubation period, the medium of each well was collected; after trypsinization the cells were collected and centrifuged. The pellet was resuspended in an appropriate amount of medium. The collected cells were mixed with the same volume of 0.4% trypan blue solution.

Cells were allowed to stand from 5 to 15 minutes. Later, 10 µl of stained cells were placed in a hemocytometer and the number of viable (unstained) and dead (stained) cells was counted with a light microscope. The viability percentage was expressed using the following equation:

$$Cell\ Viability\ (\%) = N_{viable}/N_{total}*10\ ,\qquad\qquad (4.2)$$

where N_{viable} is the amount of total viable cells (unstained) and N_{total} is the total amount of all cells (stained and unstained).

6.2.6. Nanotubes uptake by cell line: Qualitative study

To determine the cellular uptake of the nanotubes, we seeded 10^5 cells/mL in a sterile glass-culture slide coated with poly-L-Lysine. The cells were incubated with the microcapsule dispersions at a ratio of 1:5 (cell:nanotubes). After 3 hours of incubation at 37°C, the culture medium was removed, the cells were washed three times with phosphate buffered saline and fixed. Cells were analyzed with Confocal Laser-Scanning Fluorescence Microscope.

6.3. Results and Discussion

6.3.1. Characterization of halloysite clay nanotubes

Halloysite nanotubes form stable colloids in water over a wide pH range. Halloysite is negatively charged above pH 2.5 [4, 5]. Due to different outside and inside chemistry (which comprise to silica (SiO_2) and alumina (Al_2O_3) sheets correspondingly), the lumen is charged positively while the external surface is charged negatively. This allows the selective loading of negative molecules into the lumen over the range of pH from 2.5 to 8.5 [5].

Figure 6.1 shows electron microscopy images, SEM (A) and TEM (C), obtained from halloysite spread on a flat support, and (B) a halloysite cross-section obtained from a slice of halloysite embedded into PMMA. One can see that the majority of the sample consists of cylindrical shaped tubes of 40-50 nm diameter and a relatively short length of 500 to 1000 nm. Halloysite nanotubes appear rather polydispersed in size. TEM images clearly indicate the empty lumen of halloysite with 15 – 25 nm diameters, whereas SFM images (Figure 6.2) reveal the surface morphology of the tubes. All of these results demonstrate the rolled nature of the tubes.

a)   b)   c)
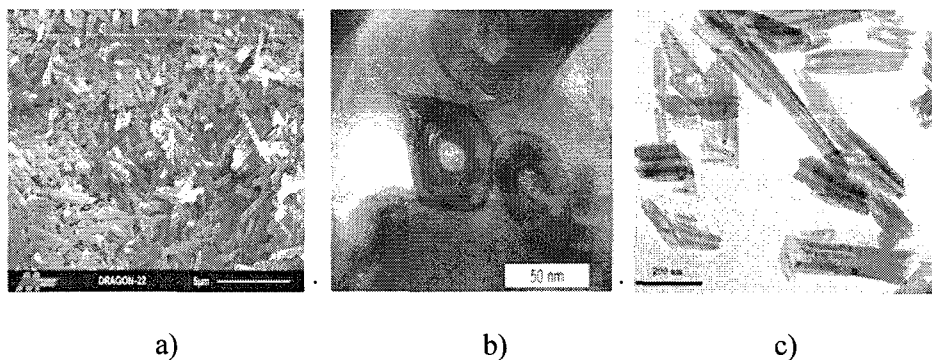
Figure 6.1 SEM (a) and TEM (b,c)   images of halloysite nanotubes powder as supplied from Dragon Mine, Atlas Mining Company.

Scanning force microscopy micrographs are acquired both in tapping mode (Figure 6.2a) and in contact mode (Figure 6.2b). In particular, Figure 6.2b shows a deflection (error signal mode) contact mode SFM image of two isolated tubes, enhancing the morphological details. The hollow tubes appeared rolled cylindrically as shown in the three-dimensional view of a long isolated tube in Figure 6.2c. The tube diameter measured from SFM is ca 100 nm (see section in inset of Figure 6.2c) which is larger than the one measured from TEM images which may be related to SFM tip size (which has a radius of curvature of around 20nm) convolution. Another reason for larger SFM diameter may be in the presence of external loosely packed

aluminosilicate layers which are not resolved in the TEM image but may be detected with scanning force microscopy. An additional argument for this could be the very small value of elasticity modulus measured in preliminary experiments (ca 200 kPa). Halloysite nanotubes (HNTs) elasticity is considerably smaller than carbon nanotubes (CNTs) which have usually a Young's modulus of around 1 Tera Pascal [124]. Such large differences in elastic properties between CNTs and HNTs could facilitate HNTs internalization into cellular compartments, enhancing spontaneous penetration.

a)   b)   c)
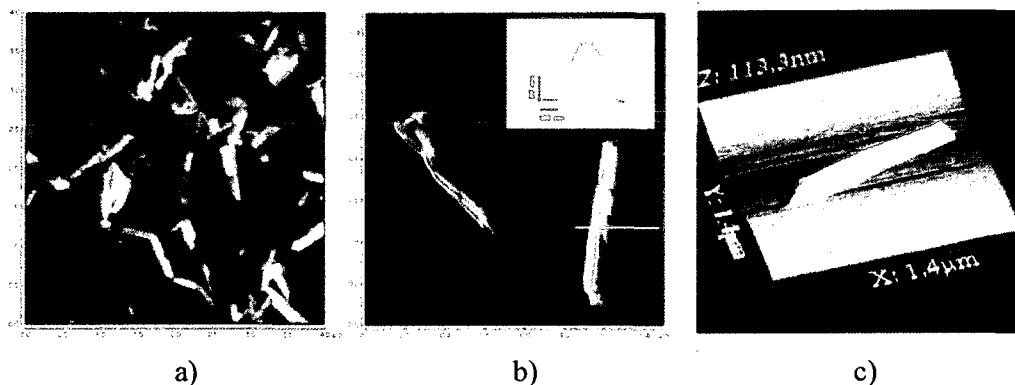
Figure 6.2 Tapping Mode SFM a) image of halloysite clay nanotubes (Z scale 700nm). Contact Mode (deflection) b) image of two isolated nanotubes. A typical height profile of a single nanotube is shown in the inset. Three dimensional view c) of a single long nanotubes, *Italian Institute of Technology, Lecce, Italy*

6.3.2. Imaging halloysite nanotubes uptake
by cancer cells

To study halloysite cytotoxicity we added these clay nanotubes to two model cell cultures (MCF-7, breast and HeLa, cervice cancer cells). Figures 6.3 and 6.4 demonstrate halloysite uptake by cancer cells. In Figure 6.3 are shown two orthogonal XZ sections of a Z-stack for MCF-7 (Figure 6.3a) and HeLa (Figure 6.3b). In the bottom and right sides of Figure 6.3a, the MCF-7 cell membrane (red, TRITC-labelled) with co-localised HNTs (yellow, merging from FITC-labelled HNTs (green)) and phalloidin-TRITC labelled membrane (red) are shown.

Similarly, in the bottom and right sides of Figure 6.3b, the localisation of HNTs (green) outside HeLa nuclei (blue, Hoechst staining) is illustrated. These images demonstrate the effective internalisation of HNTs in cancer cells.

a)   b)
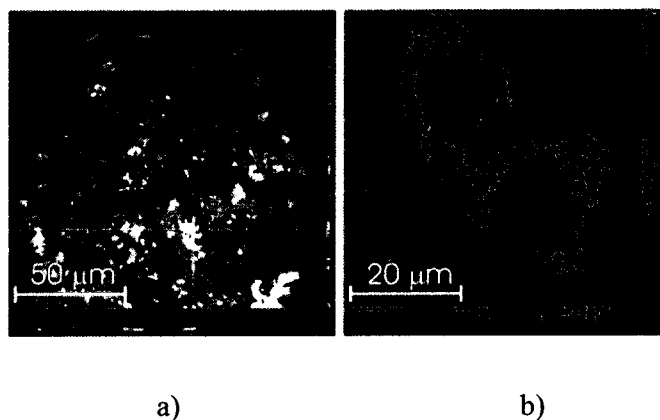
Figure 6.3 CLSM image of halloysite nanotubes intracellular uptake by MCF-7 cells(a). Sections of a z-stack FITC-Fluorescence (green) and Phallloidin-TRITC Fluorescence overlayed images (image size: 108μm). CLSM image of HNTs (functionalised by APTES) intracellular uptake by HeLa cells (b). Sections of a z-stack FITC-Fluorescence of HNTs+APTES (green) and Hoechst-fluorescence stained HeLa nuclei (blue) overlayed images (image size: 42μm), *Italian Institute of Technology, Lecce, Italy*

To further support our observation, we report in Figure 6.4 the confocal micrographs of MCF-7 (a-c) and HeLa (d-f) cells interacting with HNTs (fluorescent-labelled) showing co-localisation of HNTs aggregates (green) around cell nuclei (blue). One can see in both cases that labelled halloysite readily penetrate the cells (green area around blue cell nuclei). In Figure 6.4 (a-c), Layer by Layer coated HNTs containing an FITC-labelled layer (green) was analyzed relative to breast cancer cells, MCF-7. HNTs are readily uptaken by cells, predominantly in the cytoplasmatic region (outside nuclear regions, blue). A similar result was obtained for APTES-functionalised halloysite nanotubes (green) as well (Figure 6.4(e-f)) by using HeLa instead of MCF-7.
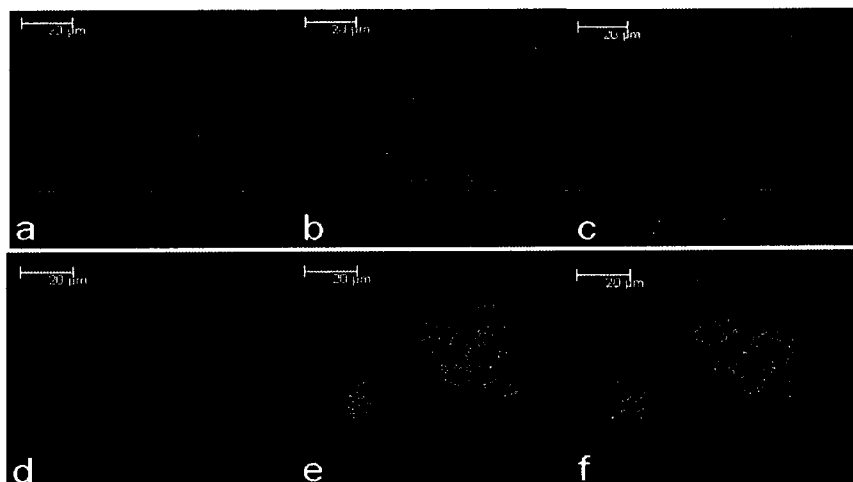
Figure 6.4 CLSM images of halloysite nanotubes (HNTs) intracellular uptake by cancer cells. CLSM images of HNTs (a-c) (coated by polyelectrolyte multilayers with a FITC labelled layer embedded herein) spontaneous intracellular uptake by MCF-7 cells. Hoechst-f fluorescence of nuclei (blue) (a), FITC-fluorescence (green) of HNTs coated with a FITC layer embedded in polyelectrolyte multilayers (b). FITC-fluorescence of HNTs with a FITC layer and MCF-7 nuclei (blue) (c) overlayed images; CLSM images of HNTs (d-e) (functionalised by APTES) spontaneous intracellular uptake by HeLa cells. Hoechst-fluorescence of nuclei (blue) (d), FITC-fluorescence (green) of HNTs+APTES (e), FITC Fluorescence HNTs+APTES and HeLa nuclei (f) (blue) overlayed images, *Italian Institute of Technology, Lecce, Italy.*

6.3.3. Halloysite nanotubes cytotoxicity

6.3.3.1. Uncoated halloysite. Figures 6.5 and 6.7 summarize the data on the cytotoxicity of halloysite studied with human cell models: breast cancer cell line (MCF-7) and cervical cancer cell (HeLa). We performed MTT tests at different time intervals (24 to 48 to 72 h) and at different concentrations (from 1 μg/mL to 1 mg/mL). The halloysite powder was dispersed in DI water and added to the cell cultures. In both cell lines, the HNTs exhibited growth inhibition in a concentration dependent manner. The cell viability was preserved (~ 70% of cells survived) up to a halloysite concentration of 75 μg/mL (Figures 6.5 and 6.7). With increasing tube concentration up to 1000 μg/mL, there is a clear decrease in cell vitality (less
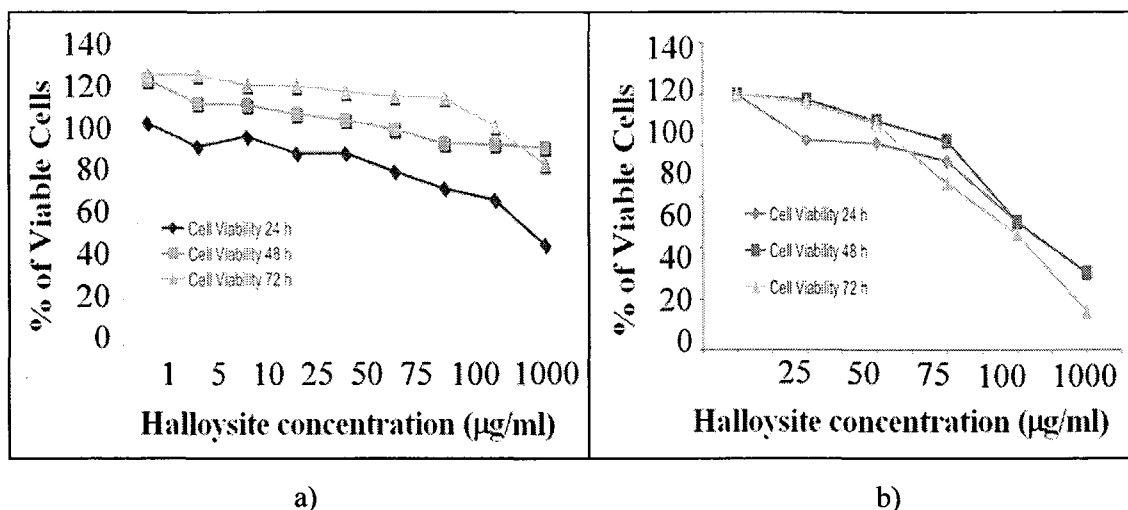
Figure 6.5 MTT assay of: HNTs taken up by HeLa (a) and MCF-7 cells (b) % Cell Viability vs HNTs concentration for 24-48-72 hours (Error bar is STD, Standard deviation, not visible), *Italian Institute of Technology, Lecce Unit, Lecce, Italy.*

6.3.3.2. FITC-Labeled halloysite. To follow halloysite localization into the cells and to study

its uptake, we used nanotubes functionalized with FITC, as described above. Figure 6.6 gives

the toxicity of APTES-FITC-functionalized HNTs for two cell lines. HeLa and MCF-7 cell

mortality increases with increasing concentration for both cells in a similar manner with

uncoated nanotubes. Therefore, uncoated and APTES-functionalized HNTs did not affect the

cell viability, and the trends in the cell viability were the same (Figures 6.5 and 6.6). These

toxicity data were also confirmed by Trypan blue tests performed under the same conditions

as those for nonfunctionalized nanotubes (Figure 6.7). These data show that nanotubes were

taken up by the cells, and their viability is maintained at >70% for HNT concentrations upto

75 μg/mL, suggesting high biocompatibility for halloysite. With increasing halloysite

concentration, there is a significant reduction in vitality.
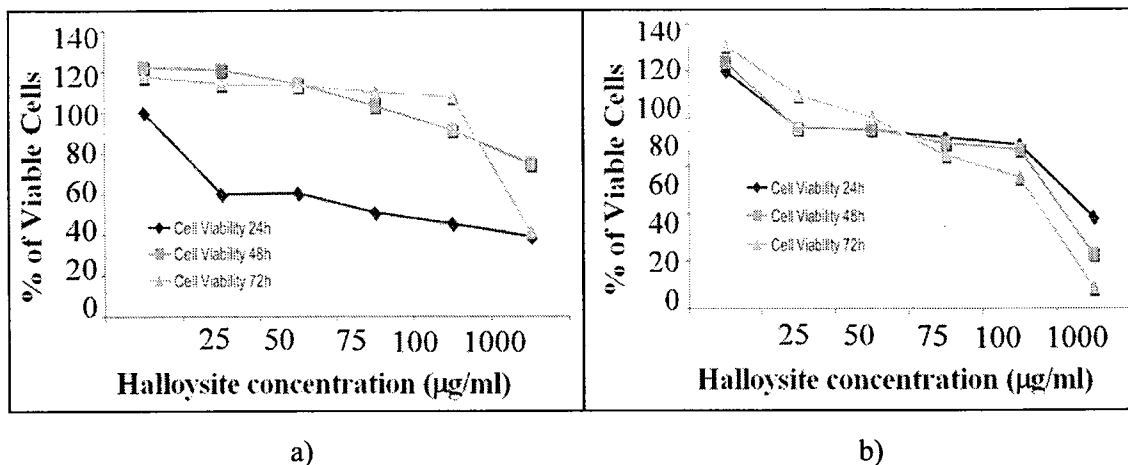
Figure 6.6 MTT test of HNTs functionalized with APTES on HeLa (cervice cancer) (a) and MCF-7 cells (b). % Cell Viability vs HNTs+APTES concentration for 24-48-72 hours. (Error bar is STD, Standard deviation, not visible), *Italian Institute of Technology, Lecce, Italy.*
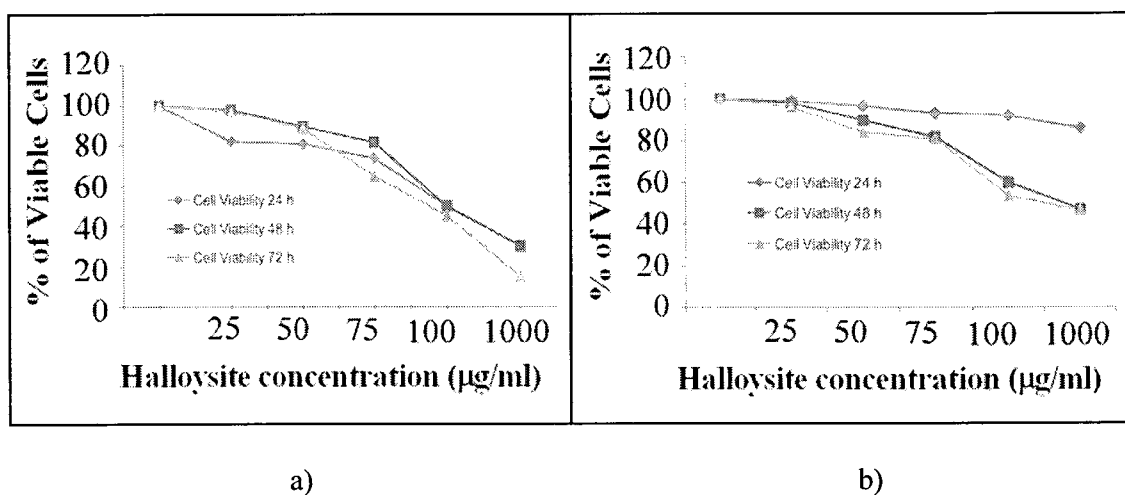
Figure 6.7 Trypan Blue test of HNTs in MCF-7 (a) and HeLa Cells (b). % Cell Viability vs HNTs concentration for 24-48-72 hours, *Italian Institute of Technology, Lecce, Italy.*

6.4. Discussion

First biocompatibility experiments were performed on a halloysite multilayer assembled on plastic or glass surface via the layer-by-layer process with alternated adsorption with cationic poly(ethyleneimine) or poly(lysine) [117]. Such very thin halloysite multilayer of ca 100 nm improved the adhesion of human dermal fibroplasts and these cells maintained their cellular phenoptype on this coating. Fibroblast cell attachment and spreading was faster

on the halloysite coated substrate as compared with silica and montmorillonite clay coating or on bare glass [117]. Later, similar results endorsing osteoblast and fibroblasts cell proliferation were obtained for composites of poly(vinyl alchool) and halloysite containing up to 5 wt % of HNTs [115]. Neverthelss, in all these tests, biological cells were seeded on halloysite containing surfaces and no data on HNTs penetration into cells were provided.

Much more biological tissue exposure is expected if one applied halloysite nanocontainers for drug delivery or medical implants (such as tooth fillers or bone cements) [3, 28, 45, 117]. For example, in the case of bone implants with a typical size of 1 cm^2 of polymetmethacrylate based cement loaded with 5 wt % of halloysite, the amount of nanotubes is ca 10^{10} within a 10 micrometer vicinity of the surface. Eventually, over months of the degradation process, these clay nanoparticles may be released to the surrounding biological tissue having a mass of few grams. Still this concentration is at least one hundred times less than the data given above indicated for safe halloysite concentration. In [118], the toxicity of halloysite was tested after a 24 - 48 hour incubation time for fibroblast and human breast cells. It was observed that halloysite is non-toxic to the cells and is even much less harmful than ordinary table salt (NaCl). The percentage of live cells as determined by celltiter-96 reagent and was measured for various concentration of testing agents (raw halloysite was added 0.1 up to 100 mg/mL of culture, and sodium chloride was a negative control). The data showed that the addition of even as much as 0.1 wt % of halloysite to the cell culture did not kill tested cells. For comparison, addition of only 0.005 wt % of ordinary NaCl completely killed all the cells. Neverthless, unlike table salt halloysites can not be injected to the body due to its non-biodegradability.

Confocal microscopy data revealed that the cells accumulate halloysite in their interiors but this does not prevent their proliferation. We were able to visualize the process of cellular uptake and have shown that halloysite nanoparticles penetrate into the cells and concentrate around cell nucleus.

Studying halloysite toxicity, we always had in mind blick data on asbestos toxicity and its danger for living organisms [119-120]. The main difference of halloysite, as compared with asbestos fibers, is that HNTs are much shorter and fit the size window (0.5-1 micrometer) which is generally considered not toxic for silicate nanoparticles [121]. Halloysite is just a rolled version of widely adopted in human life kaolin clay (alumosilicate) and is chemically different from asbestos, which is magnesium-silicate (chrysolite), or the less common Na and Fe, Mg silicates (amphiboles). The danger of asbestos is based on its very long fiber structure (several tens of microns). In the review on mechanisms of asbestos pathogenesis [120], it is indicated that asbestos fibers shorter than 5 micrometers are safer. Long thin fibers are more potent inducers of cell injury and inflammation. Compared with asbestos fibers, HNTs are much shorter and fits the size window (0.5-1 micrometer) and can easily be removed by macrophages.

The third point is the safe concentration range: in our experiments, halloysite concentration of ca 1 mg/mL (e.g., ca 10^{11} particles per gram) was safe for the cells while asbestos disease is characterized by much less asbestos fibers per gram of lung (10^{8} particles per gram). Therefore, already a thousand times less of a particular concentration of asbestos, as compared with halloysite, causes the disease. Generally speaking, there was a dramatic increase in cytotoxicity for asbestos fibers compared to other minerals, including respirable quartz. There are many different forms of natural silica-rich minerals, and Hart and Hesterberg [120] carried out studies showing moderate cytotoxic effect for different minerals. There is a little inconsistency with different literature sources as to what the threshold is for

silica particle size for cytotoxic or fibrogenic effects, but, in all publications, particles larger than 5μm were found more fibrogenic than particles of 1μm in diameter or less [119-121].

Toxicity of halloysite may be compared with silica nanoparticles because its external surface being exposed to intracellular media is silica. Our results have shown that even large amounts of added halloysite (up to 1 mg/mL) did not show toxicity, and at least 90 % of the cells survived while, from fluorescent laser confocal images, one could see that nanotubes were taken up by the cells. From our point of view, direct toxicity of halloysite to cells will not be the issue in applications, unlike carbon nanotubes which immedately killed cells [122-123]. Secondary effects of HNTs on tissue may be important, such as increased fibrogenicity. As the collective research stands, experimentation with macrophage exposure to HNTs seems appropriate and, ultimately, logical as the next research step. Although there is a little discrepancy in size-related toxicity, current research suggests that HNTs are safe for use in biological systems for overskin and dental applications.

6.5. Conclusions

With TEM, SEM and SFM microscopy, we characterized halloysite clay as tubule nanoparticles of ca 50 nm external diameters and 500-1000 nm in length. For a wide range of pH, it has a negative electrical zeta-potential, which for allowed its good dispersibility and colloidal stability in water. An addition of halloysite to three different cell lines allowed to demonstrate that it is nontoxic up to a concentrations of 1 mg/mL, and parallel laser confocal microscope visualization of cell uptake of fluorescently labelled halloysite identified its location within the cells.

CHAPTER 7

NATURAL NANOCONTAINER FOR THE CONTROLLED DELIVERY OF GLYCEROL AS A MOISTURIZING AGENT

7.1. Introduction

Halloysite is a naturally occurring two-layered (1:1) aluminosilicate mineral, which mostly exhibits a hollow tubular structure in the submicron range [1-5]. The halloysite structure allows selective internal loading of a wide range of active agents, such as cosmetics, fragrances, pharmaceuticals, cosmeceuticals, antifouling paint, antiscalants, herbicides, and other functional agents [5, 43].

Only a few research groups have been interested in controlling the delivery of active materials using tubular halloysites. The Price and Lvov group studied in-vitro release of both hydrophilic and hydrophobic agents with a few tens of nanometer halloysite [3]. They showed that halloysite could be used for loading poorly soluble drugs up to a maximum loading of 12 vol% and for sustaining their release for 5-10 h [28]. The Shchukin group modified halloysite nanotubes by coating polyelectrolyte on their outer surface to control release and reloading efficiency of corrosion inhibitors [10]. The Deasy group carried out physicochemical characterization of halloysite to use as a drug delivery carrier [44]. They revealed that the halloysite surface tends to be anionic and easily adsorbs cationic polymers from the solution. Based on this property, cationic drugs of highly water soluble and less soluble were adsorbed onto the halloysite surface resulting in sustained release [46]. They

125

also demonstrated that coating the halloysite with cationic polymers onto its negatively charged surface can further enhance the retardation of drug release [45].

Although the possible application of halloysite in cosmetics has already been known, no research on the release control of them using halloysite has yet been reported. In U.S. Patent Application 2007/0202061, a cosmetic skincare application of halloysite for glycerol loading was claimed but specific data showing the performance of release control were not given [126]. So a well-designed study on the cosmetic application of halloysite is required to realize its potential for everyday usage. Glycerol, which is widely used in cosmetics, is a good candidate for that purpose. It is a skin-friendly humectant which promotes retention of moisture in the skin. It also helps to maintain the water balance in the intercellular matrix and in so doing it maintains the skin's homeostasis. In this work, we used natural halloysite nanotubes with about 15 nm internal lumen as a cosmetic nanocontainer for slowing down the release of glycerol. Halloysite was filled with glycerol in water to estimate its capability for retention of the cosmetic ingredient. Also, glycerol-loaded halloysite was Layer by Layer coated with polyelectrolytes to additionally reduce the releasing rate.

7.2. Materials and Methods

7.2.1. Chemicals

Halloysite samples were obtained from Applied Minerals, Inc. (Former Atlas Mining Co.), and Imerys Corporation. Glycerol was obtained from Sigma Aldrich with 99% purity. Low molecular weight polythyleneimine (PEI) with Mw = 2000 was obtained from Aldrich as 50% solution in water. Low molecular weight polyacrylic acid (PAA) with Mw = 5100 was obtained from Fluka as a dry powder of sodium salt. Potassium bichromate ($K_2Cr_2O_7$) was obtained from Aldrich with 99 % purity.

7.2.2. Glycerol loading and release

Glycerol loading was accomplished by suspension of the halloysite in a solution of glycerol in deionized (DI) water. The concentration of glycerol was 40% by volume. The purpose of using this solution instead of pure glycerol was to reduce its viscosity. After adding halloysite, the suspension was sonicated for 1 h and placed into a vacuum jar for 20 min, which was then replaced by atmosphere. The vacuum process was repeated 3-4 times to increase the loading efficiency. After vacuum process, the sample was kept for a few days under atmospheric pressure, which is believed to further increase loading efficiency. After the loading procedure, the halloysite was separated from the solution by centrifugation and washed two times with DI water. Release was conducted by constant stirring of halloysite in 1 ml DI water. At certain time intervals, supernatant of the suspension was collected by centrifugation for analysis and fresh DI water of the same amount was added.

7.2.3. Determination of glycerol concentration

Concentrations of glycerol in supernatants were analyzed by UV-Vis spectrophotometer (Agilent 8453). The principle behind the analysis was the discoloration of potassium dichromate ($K_2Cr_2O_7$) solution by glycerol. For this purpose, the solution of potassium dichromate with a certain concentration was mixed with collected supernatants with a certain ratio of volume. A droplet of concentrated sulfuric acid was also added in order to make solution acidic. After mixing, the samples were left overnight to complete the reaction.

$$5K_2Cr_2O_7 + 3CH_2(OH)CH(OH)CH_2OH + 24H_2SO_4 \longrightarrow 5K_2SO_4 + 5Cr_2(SO_4)_3 + \\ + 3HOOC\text{-}CO\text{-}COOH + 27H_2O$$
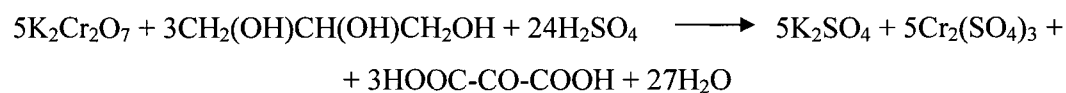
The concentration of glycerol in the supernatants were calculated based on the reduction of the intensity of the potassium dichromate signal at 350 nm in the UV spectrum compared to its signal in the control solution (without glycerol). A similar procedure was also applied to

three different glycerol solutions with known concentrations in order to obtain the relationship between the UV signal intensity and glycerol concentration.

7.2.4. Layer by Layer nanoencapsulation

Layer by Layer nanoassembly was implemented for extending the glycerol release rate from loaded halloysite nanotubes. We used polyethylenimine (PEI) and Polyacrylic acid (PAA) to encapsulate the halloysite nanotubes. Initially, negatively charged halloysite particles were suspended in the solution containing 5 mg/ml low molecular weight (~ 2,000 g/mol) PEI for 20 min, followed by removal of the halloysite from the solution by centrifugation and its resuspension in 5 mg/ml PAA solution. Halloysite samples were washed with water before resuspending them in a consecutive polyelectrolyte solution. Three bilayers of PEI/PAA were deposited over the surface of halloysite filled with glycerol. The assembly of the polyelectrolytes was monitored by using surface (electrokinetic) potential (ZetaPlus Potential Analyzer, Brookhaven Instruments). The thickness of the polyelectrolyte layers was determined by using the Quartz Crystal Microbalance method (USI Systems, Japan).

7.3. Results and Discussion

Halloysite nanotubes from two sources, Utah, USA and New Zealand were used to encapsulate glycerol, a skin friendly moisturizing agent. The biocompatible nature of the halloysite nanotubes were checked in the previous study [118]. Average particle sizes were 420 nm and 660 nm for Utah and New Zealand halloysites respectively. The surface electrokinetic potentials of the particles in water suspension were -30.0 ± 2.0 mV in both cases. The same range of zeta potential may provide the same behavior for adsorption of active agents on the surface of the tubules.

The morphology of tubules is much different from each other, as shown in Figure 7.1. USA samples in Figure 7.1(a) are highly uniform in particle size and are well-developed hollow tubules; while NZ samples in Figure 7.1(b) appear irregular in shape and many particles appear to have no open ends. As a result, most of the glycerol loaded in the NZ halloysite should be located in the edge pockets, leading to the initial burst of the release pattern (Figure 7.2). In addition, the loading capacity of NZ halloysite was much lower than that of USA samples due to the same reason.
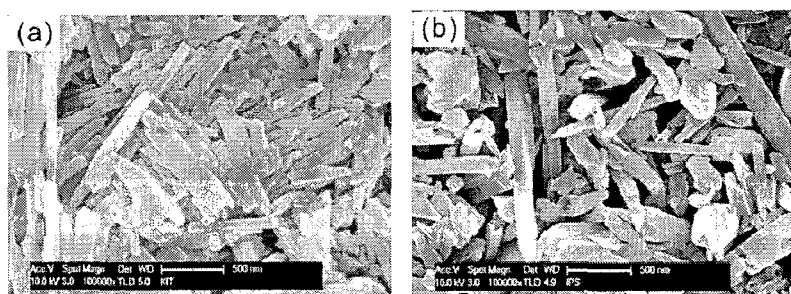
Figure 7.1 Scanning electron microscope images of (a) USA and (b) New Zealand halloysite, *Korean Institute of Geosciences and Applied Materials, Dijeon, South Korea.*

Glycerol loading occurs through two mechanisms: the entrapment of the glycerol inside the hollow tubules and the adsorption onto the surface of the tubules. The active agent releases initially by desorption mainly from the exterior surface of the halloysite and then by diffusion from the ends of the microtubules [3]. Viseras, *et al.* [47] also suggested that overall adsorption consists of two separate processes: initial rapid adsorption on the external surface and slow adsorption inside the lumen. They proved this by studying kinetics and thermodynamics of the adsorption of a drug onto halloysite. So the adsorbed portion of glycerol was washed off a few times to examine only the release from the inside lumen [47].

Release profiles of glycerol from two different halloysite samples are shown in Figure 7.2. Loading efficiencies of the glycerol were 19 ± 3 wt% and 2.3 ± 0.5 wt% for USA and

New Zealand (NZ) halloysite samples, respectively. The release was much faster in the case of NZ halloysite, with an initial 60 % burst and 80% within first 5 h. Therefore, the halloysite sample from USA appears to be a better container for glycerol sustained release compared to the sample from New Zealand. Furthermore, the USA sample displayed no initial burst, which means that most glycerol was loaded within the nanotubes. Total release time of glycerol from the USA halloysite nanotubes exceeded 20 h, which is considered enough time for cosmetic applications.
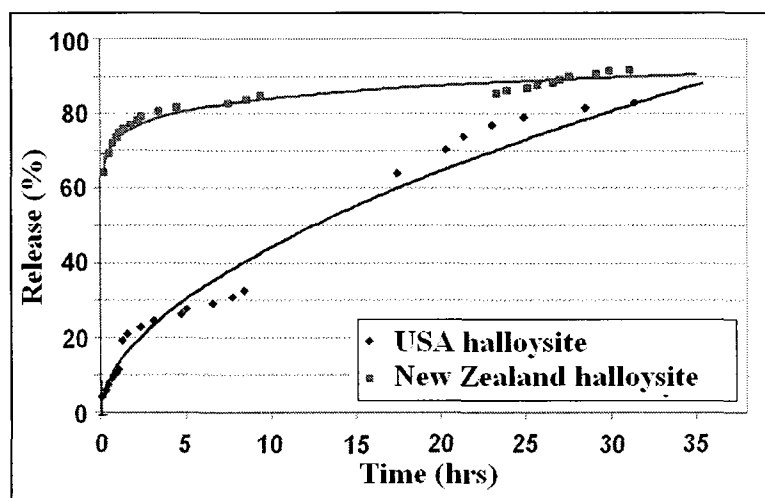
Figure 7.2 Release profile of glycerol from halloysite nanotubes. Release was conducted for more than 30 h.

To further retard the release, the halloysite filled with glycerol was coated with a few layers of polyionic polymers. Glycerol must diffuse out through the polymer shells following travelling through the narrow lumen to reach the open ends of the halloysite. The polymer shells provide an additional barrier through which glycerol must diffuse and in turn slow down its release. Halloysite has a tubular structure with a silica layer exposed on its surface, leading to isoelectric point at 1.0–1.7 pH range [4]. The silica surface tends to have an anionic surface with hydroxyl ions adsorbed on it, except at very low pH, and should readily

bind to cationic polymers from the solution. Hence, an initially negatively charged halloysite surface was adsorbed with cationic polymer (PEI) and then anionic polymer (PAA). The Layer by Layer process was monitored by measuring the surface potential of the halloysite periodically during the assembly process. Figure 7.3a shows the change in the zeta potential for the samples generated according to the polymer charge, demonstrating that multi layers of polymers were coated on the halloysite surface. Alteration of the positive and negative surface charge indicates the successful adsorption of the polyelectrolytes on the halloysite surface. The thickness of the polyelectrolytes layers were measured by using the Quartz Crystal Microbalance (QCM) method, which employs a quartz chip with silver electrodes resonating at a resonance frequency of 9.0 MHz. Layer thicknesses were measured by using Sauerbrey's equation ($\Delta l=-0.017\Delta F$, Δl layer thickness, ΔF resonance frequency shift) which relates the thickness of the polyelectrolyte layers with the shift in resonance frequency [113]. The average thickness of the PEI/PAA polyelectrolyte bilayer was about 2.0 nm (Figure 7.3b).

a)   b)
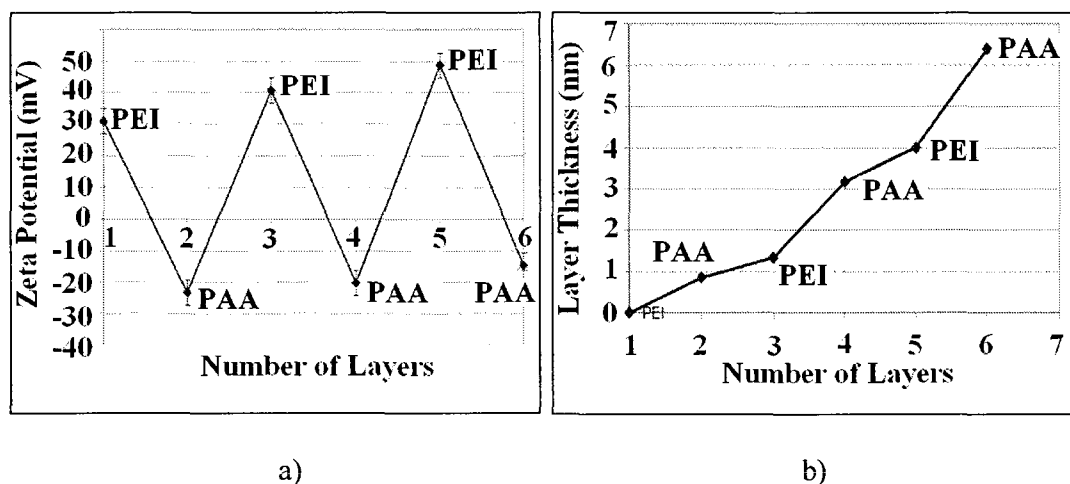
Figure 7.3 Change of surface charge during LbL assembly of polyelectrolytes on halloysite nanotubes (a) and monitoring of the layer thickness by using Quartz Crystal Microbalance Technique (b).

Glycerol release characteristics from coated USA halloysite nanotubes were tested by using a similar procedure to that which was used for the uncoated halloysite nanotubes. In Figure 7.4, release profiles of glycerol from coated and uncoated halloysite nanotubes are depicted. Glycerol release rates from both of the tubes were close to each other, if one considers the errors in the determination of the glycerol concentration. This result indicates that LbL nanoassembly does not have a significant influence on the glycerol release rate. This is partially related to the smaller molecular weight of glycerol, i.e., being a small and mobile molecule, glycerol can easily pass from the openings of the LbL nanoshells. It could also be attributed to a higher solubility of glycerol in water thus helping glycerol molecules to diffuse through water due to a high concentration gradient [46]. The layers of higher molecular weight polymers like chitosan or gelatin may give higher retardation to the release rate of glycerol [118].
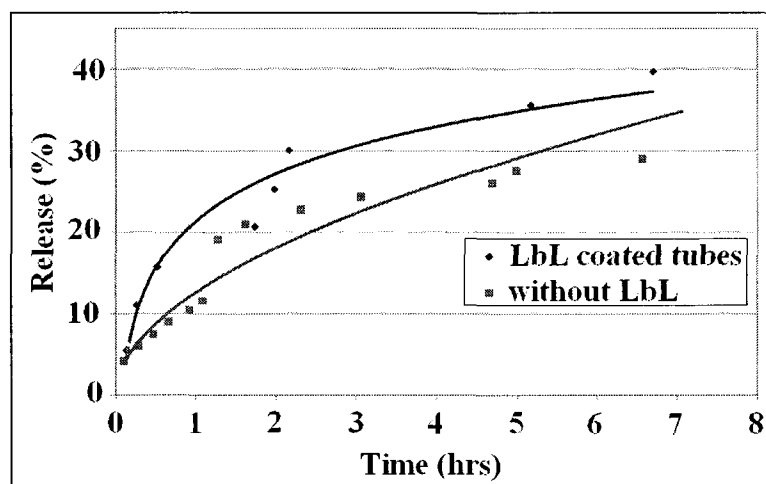
Figure 7.4 Release profiles of glycerol from coated and uncoated halloysite nanotubes. The first 7 h portions of the release curves are described.

7.4. <u>Conclusions</u>

Halloysite minerals having tubular geometry are excellent materials for encapsulation of biologically active agents. Glycerol was successfully encapsulated by halloysite nanotubes, showing extended release rates in aqueous environments. This phenomenon can drastically increase its biological activity for pharmaceutical applications. The possibility of further encapsulation of tubules by using layer-by-layer nanoassembly was also tested. LbL nanoassembly has insignificant influence on the glycerol release rate partially due to the smaller molecular weight of glycerol or its higher solubility in water.

CHAPTER 8

CONCLUSIONS AND FUTURE WORK

8.1. Conclusions

In this dissertation, the capability of halloysite nanotubes for encapsulation of chemically and biologically active agents was explored. Encapsulation of the corrosion inhibitors by halloysite nanotubes shows great promise in the production of self-healing anticorrosion coatings. Three different types of corrosion inhibitors, benzotriazole, 2-mercaptobenzothiazole and 2-mercaptobenzimidazole were used to provide anticorrosion coatings for 2024 aluminum alloy and copper. Anticorrosive performance was checked by using the Scanning Vibrating Electrode Technique as well as visually by direct exposure of the metal strips to the chlorine containing corrosive media. High efficiency of the coatigs, based on halloysite nanotubes embedded in the paint, was demonstrated in all of the cases.

Tunable controlled release of the loaded corrosion inhibitors was achieved by synthesizing stoppers at tube endings based on the interaction of the leaking corrosion inhibitor from the tube endings and transition metal ions from the external bulk solution. The high efficiency of the encapsulation was demonstrated for Cu(II), Co(II) and Fe(III) ions. These stoppers provide the release of corrosion inhibitors with the desired rate, which is especially useful when high circulation of the water takes place in the external environment. Some details of the stopper formation and stopper-halloysite interaction was studied by using Cu(II) ions.

A biocompatibility study of the halloysite nanotubes was also performed by analyzing cellular uptake of the bare and modified halloysite nanotubes. HeLa and MCF-7 cells were

used for the biocompatibility study and the results indicated that halloysite has a biocompatible nature and can be used for external medical applications.

Finally, halloysite nanotubes were used to encapsulate glycerol, a skin moisturizing agent, which is one of the main components of cosmetic products. Successful encapsulation of the glycerol by using halloysite from two different deposits was demonstrated. The possibility for further encapsulation by using Layer by Layer nanoassembly of polyelectrolytes was also analyzed and results showed no significant effect of Layer by Layer encapsulation on the glycerol release rate.

8.2. Future Work

Results clearly indicate that the halloysite nanotube is a promising material for loading and release of active agents and this may significantly improve the quality of many products that benefit from chemical and biological agents. In this work, we attempted to explore the the loading and release capability of halloysite nanotubes for certain active agents namely corrosion inhibitors and pharmaceutic agents. However, many other active agents such as drugs, antifouling agents, and antiseptics need to be analyzed as a future extension of this work.

In first section of this work, we focused on self-healing agents and indicated the high performance of the coatings on the basis of halloysite-paint nanocomposites. Further analysis of the paint halloysite interaction and influence of the halloysite to the key physical properties of the paints, such as adhesion, tensile and impact strength, viscosity, oxygen and water permeability needs to be analyzed for a wide range of the coatings.

Encapsulation of the active agents by the formation of stoppers at tube endings offer great benefit in terms of providing tunable controlled release of the loaded agents. In the current work we used this approach in the example of interaction between loaded corrosion

inhibitors and transition metal ions. This approach can further be extended to other substances. Practically any two substance that form a precipitate with sufficiently high speed can potentially be used for synthesizing artificial stoppers for controllable release of the loaded agents. A study in this direction can reveal many new agents with the capability of providing controllable release of the loaded agents.

Another extension of this work can be done for the pharmaceutical industry. A study of glycerol release kinetics and the highly biocompatible nature of the halloysite nanotubes indicate that halloysite nanotubes can find application in the pharmaceutical industry. A large variety of different active agents is used in current cosmetic products which can effectively be encapsulated by halloysite nanotubes.

Finally, halloysite nanotubes can find applications in the improvement of artificial bone cements and in dental applications. Addition of halloysite into bone cement may significantly improve its mechanical properties which is crucial for bone implants. In addition, active agents that need to be embedded into bone cement (such as growth hormone or antibiotics) can effectively be encapsulated by halloysite nanotubes to provide long time effect without drug overdose.

APPENDIX A

DERIVATION OF THE REACTION RATE
EQUATIONS FOR THE INSULATIVE
LAYER FORMATION
ON THE COPPER
SURFACE

Kinetics of the isolation layer formation process follows second order reaction kinetics, i.e. the reaction rate depends on both inhibitor concentration and the concentration of the unreacted copper atoms at the surface of the metal. We assume that only a monolayer of the corrosion inhibitor deposits on copper surface and the isolating film covers the metal surface uniformly. Equation of the reaction is as follows

$$Cu^{+2} + Inh \xrightarrow{k_1} [Cu(Inh)]_n$$
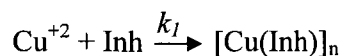
By applying reaction rate law, we can obtain the following equation:

$$Reaction\ rate = k*[Cu]*[Inh]. \tag{A.1}$$

We also have the following boundary conditions:

$$a(t) = a_0, \quad \theta(t) = 1.0 \quad when \quad t = 0 \tag{A.2}$$

$$a(t) = a_0 - x_\infty = a_\infty, \quad \theta(t) = 0 \quad when \quad t = \infty, \tag{A.3}$$

where, $a(t)$ and $\theta(t)$ are the molar concentration of inhibitor and portion of the unreacted copper ions at the metal surface, respectively, and $x(t)$ is the amount of reacted inhibitor at time t. The first condition appears from the fact that all the Cu^{+2} ions are unreacted before the reaction starts and the initial concentration of the corrosion inhibitor is a_0. The second condition states that the corrosion inhibitor is in excessive amounts and all the copper ions at the metal surface are consumed after the reaction completely stopped. In addition to the boundary conditions, we have following equation:

$$a(t) = a_0 - x(t), \quad \theta(t) = 1 - n*x(t) \quad when \quad t \in [0, \infty]. \tag{A.4}$$

This equation appears from the assumption that inhibitor forms monolayer coverage on the copper surface and the complex covers the surface uniformly, where n corresponds to the amount of surface copper atoms covered by inhibitor film, while 1 mole of inhibitor is absorbed. We obtain the following differential equation for the reaction rate:

$$v = \frac{dx}{dt} = k*[Cu]*[Inh] = k*\theta*a = k(1-nx)(a_0 - x) \tag{A.5}$$

$$\frac{dx}{dt} = k(1 - nx)(a_0 - x) \tag{A.6}$$

$$kdt = \frac{dx}{(1 - nx)(a_0 - x)} \tag{A.7}$$

$$kt = \int \frac{dx}{(1 - nx)(a_0 - x)} = \frac{1}{(1 - a_0 n)} \left(\int \frac{dx}{(a_0 - x)} - \int \frac{dnx}{(1 - nx)} \right) =$$

$$= \frac{1}{(1 - a_0 n)} \ln \left(\frac{1 - nx}{a_0 - x} \right) + C, \tag{A.8}$$

where, C is the constant. By applying 1st boundary condition ($A.2$) we can find C.

$$\frac{1}{(1 - a_0 n)} \ln \left(\frac{1 - n * 0}{a_0 - 0} \right) + C = k * 0 \tag{A.9}$$

$$\frac{1}{(1 - a_0 n)} \ln \left(\frac{1}{a_0} \right) + C = 0 \tag{A.10}$$

$$C = \frac{1}{(1 - a_0 n)} \ln(a_0). \tag{A.11}$$

From ($A.8$) and ($A.11$) we obtain:

$$kt = \frac{1}{(1 - a_0 n)} \ln \left(\frac{1 - nx}{a_0 - x} \right) + \frac{1}{(1 - a_0 n)} \ln(a_0) = \frac{1}{(1 - a_0 n)} \ln \left(\frac{a_0 - na_0 x}{a_0 - x} \right) \tag{A.12}$$

$$(1 - a_0 n)kt = \ln \left(\frac{a_0 - na_0 x}{a_0 - x} \right) \tag{A.13}$$

$$\frac{a_0 - na_0 x(t)}{a_0 - x(t)} = \frac{a_0 - na_0 (a_0 - a(t))}{a(t)} = \exp[(1 - a_0 n)kt] \tag{A.14}$$

$$a(t) = \frac{a_0 (1 - na_0)}{\exp[(1 - a_0 n)kt] - na_0}. \tag{A.15}$$

By applying equation ($A.3$) we calculate the value of n as follows:

$$a(t) = a_0 - x_\infty = a_\infty \Rightarrow x_\infty = a_0 - a_\infty$$

$$\theta(t) = 1 - n * x_\infty = 1 - n * (a_0 - a_\infty) = 0 \Rightarrow n = \frac{1}{a_0 - a_\infty}. \tag{A.16}$$

From equations ($A.15$) and ($A.16$) we obtain:

$$a(t) = \frac{a_0(1 - a_0/(a_0 - a_\infty))}{\exp[(1 - a_0/(a_0 - a_\infty))kt] - a_0/(a_0 - a_\infty)} =$$

$$= \frac{a_0 a_\infty}{a_0 - (a_0 - a_\infty)*\exp[(-a_\infty/(a_0 - a_\infty))kt]}. \qquad (A.17)$$

APPENDIX B

EESTIMATION OF THE AMOUNT OF
HALLOYSITE TO BE MIXED
WITH THE PAINT FOR
CORROSION
PROTECTION

A piece of copper strip was painted with blue paint containing halloysite loaded with the corrosion inhibitor, benzotriazole. The thickness of the paint is 1 mm (Figure B.1). Let's calculate the minimum concentration of halloysite that is required to add into the paint so that the metal underneath the scratch is totally covered with a Copper-benzotriazole thin film once the scratch has occurred. The following data are useful:

1) Paint thickness – 1.0 mm.

2) Halloysite parameters: external diameter-50 nm, internal diameter-15 nm, length- 1.0 microns, density-2.65 g/cm^3 [19-21].

3) Benzotriazole parameters: Molecular weight-119 g/mole, density-1.3 g/cm^3 [3-17].
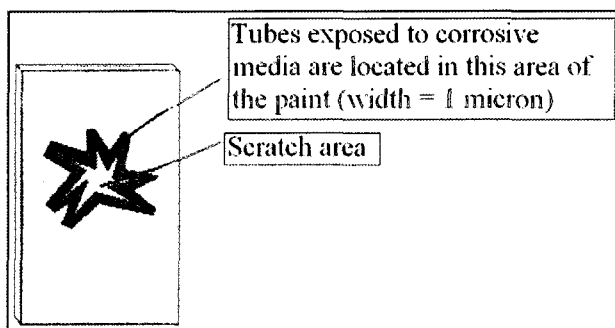
Figure B.1 A piece of painted copper strip with a scratch on it.

Amount of benzotriazole required for the coverage of copper surface by Cu-BTA film was measured by using the Quartz Crystal Microbalance technique and it was found that 2.7 micrograms of benzotriazole is required for complete coverage of a 1 cm^2 copper surface with the isolating film. For this purpose in a QCM chip with copper electrode having 0.22 cm^2 electrode area was exposed to 0.012M benzotriazole solution and complete film growth was established within 3 hours. The amount of benzotriazole required for corrosion inhibition of the scratch with area of s will be equal to:

$$M_{Benzotriazole} = 2.7 * 10^{-6} * s. \qquad\qquad (B.1)$$

Mass and volume of the halloysite nanotubes that are required to provide this amount of benzotriazole is:

$$M_{Halloysite} = \frac{M_{Benzotriaole}}{w} * 100 \qquad\qquad (B.2)$$

$$V_{Halloysite} = \frac{M_{Halloysite}}{d_{Halloysite}}, \qquad\qquad (B.3)$$

where, w is the loading efficiency of halloysite with benzotriazole(i.e. weight fraction of benzotriazole in loaded halloysite in %) and d is the density of halloysite. By combining equations $B.1$-$B.3$ and by substituting all the variables with their values we get the following formula for the amount of halloysite:

$$V_{Halloysite} = \frac{M_{Benzotriazole} * 100}{d_{Halloysite} * w} = 2.55 * 10^{-5} s \ cm^3. \qquad\qquad (B.4)$$

When a scratch occurred, only the tubes locating within a certain vicinity of the paint will be exposed to the corrosive environment (Figure. B.1). The volume of the dry paint from which halloysite nanotubes are exposed into the corrosive environment is calculated as follows:

$$V_{Paint}^{dry} = h * r * l, \qquad\qquad (B.5)$$

where: h is the thickness of the paint, r is the vicinity within the paint where the halloysite nanotubes are exposed to the corrosive environment. Clearly, this has to be not more than the lengths of the tubes, which is 1 micron. l is the perimeter of the scratch. When paint gets dried, all the solvent is evaporated by leaving only a dry film on the metal, which is mainly composed of binders. For simplicity we will assume that dry paint contains only binder besides halloysite. Then the volume of original wet paint before drying will be:
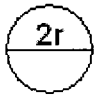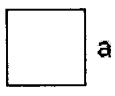
$$V_{Pa\,int}^{wet} = \frac{V_{Pa\,int}^{dry}}{W_{binder}} * 100 = \frac{h * r * l}{W_{binder}} * 100 = 5 * 10^{-5} l \ cm^3, \qquad (B.6)$$

where, W_{binder} is the concentration of binder in wet paint. In conventional paints concentration of the binder ranges from 20 to 40 % by volume. In equation B.6 W_{binder} was considered as 20%. By using equations $B.1$-$B.6$ following relationship for the concentration of halloysite in the wet paint:

$$w(Halloysite) = \frac{V_{Halloysite}}{V_{Pa\,int}^{wet}} * 100 = 50.94 * (s/l) \ \% , \qquad (B.7)$$

where, s and l are the area and perimeter of the scratch respectively. We see that minimum concentration of halloysite that is required in the paint depends on area as well as from the shape of the scratch. Table B.1 describes the relationship between s and l for different areas.

Table B.1 Perimeter area relationships for various figures.

Shape	Figure	Area - s	Perimeter - l	Relationship between s and l
Circle	2r	$\pi * r^2$	$2\pi * r$	$l = 3.545\sqrt{s}$
Square	a	a^2	$4a$	$l = 4\sqrt{s}$
Real case				$l \approx 20 - 50\sqrt{s}$

The following equation can be obtained for maximum and minimum concentration of the halloysite for metal corrosion protection:

$$w(Halloysite) = (1 - 2.5)\sqrt{s} \ \%, \qquad (B.8)$$

where, s is the area of scratch in cm^2. This equation is calculated based on the assumption

that all of the benzotriazole that is loaded into the tubes is consumed for corrosion protection. However, in real situations a significant amount of benzotriazole is leaked into the environment without interaction with the metal. Therefore, an extra amount of benzotriazole is required. Table B.2 describes the amount of halloysite required to mix with wet paint by assuming that five-fold extra amounts of benzotriazole is required for efficient corrosion protection. In most cases, the scratch area does not exceed 10 mm^2, which corresponds to 1 – 5% of halloysite in paint by volume. For paint having same density as halloysite, this value will be equal to the halloysite weight fraction as well.

Table B.2 Amount of halloysite powder needed for corrosion protection of copper

Scratch area (mm^2)	Halloysite concentration (vol %)	
	Min	Max
100	5.00	12.50
50	3.54	8.84
25	2.50	6.25
12.5	1.77	4.42
6.25	1.25	3.13

REFERENCES

[1]   Bates T.; Hildebrand, F.; Swineford, A., "Morphology and Structure of Endellite and Halloysite," *The American Mineralogist,* 1950, 35, 463-484.

[2]   Joussein, E.; Petit, S.; Churchman, J.; Theng, B.; Righi, D.; Delvaux, B., "Halloysite clay minerals – a review," *Clay Minerals,* 2005, 40, 383 – 426.

[3]   Price, R.; Gaber, B.; Lvov, Y., "In-vitro release characteristics of tetracycline HCl, khellin and nicotinamide adenine dineculeotide from halloysite; a cylindrical mineral,"*Journal of Microencapsulation,* 2001, 18, 713-722.

[4]   Tari, G.; Bobos, I.; Gomes, C. S. F.; Ferreira, J. M. F., "Modification of Surface Charge Properties during Kaolinite to Halloysite – 7A Transformation," *Journal of Colloids and Interface Science,* 1999, 210, 360-366.

[5]   Lvov, Y. M.; Shchukin, D. G.; Mohwald, H.; Price, R. R., "Halloysite Clay Nanotubes for Controlled Release of Protective Agents," *ACS Nano,* 2008, 2, 814-820.

[6]   Kennedy B. A., *Surface Mining. 2nd Edition,* 1990, Port City Press, Baltimore, MD.

[7]   Wilson, I. R., Kaolin and halloysite deposits of China, *Clay Minerals,* 2004, 39, 1 – 15.

[8]   Shchukin, D.; Mohwald, H., "Self-Repairing Coatings Containing Active Nanoreservoirs," *Small,* 2007, 3, 926–943.

[9]   Niezgoda, S.; Gupta, V.; Knight, R., Cairncross, R. A.; Twardowski, T. E., "Effect of Reinforcement Size on the Scratch Resistance and Crystallinity of HVOF Sprayed Nylon-11/Ceramic Composite Coatings," *Journal of Thermal Spray Technology,* 2006, 15, 731-738.

[10]   Shchukin, D.; Mohwald, H., "Surface-Engineered Nanocontainers for Entrapment of Corrosion Inhibitors," *Advanced Functional Materials,* 2007, 17, 1451–1458.

[11]   Pinto, R. C.; Ribeiro, A. J.; Neufeld, R. J.; Veiga, F., "Alginate Microparticles as Novel Carrier for Oral Insulin Delivery," *Biotechnology and Bioengineering,* 2007, 96, 977-989.

[12]   Baral, S.; Brandow, S.; Gaber, B. P., "Electroless Metalization of Halloysite, a Hallow Cylindrical 1:1 Aluminosilicate of Submicron Diameter," *Chemistry of Materials,* 1993, 5, 1227 – 1232.

[13]   Reis, C. P.; Neufeld, R. J.; Ribeiro, A. J.; Veiga, F., "Nanoencapsulation I. Methods for Preparation of Drug-Loaded Polymeric Nanoparticles," *Nanomedicine: Nanotechnology, Biology and Medicine,* 2006, 2, 8-21.

[14] Brown, G.; Bailey, S.R.; Novotny, M.; Carter, R.; Flahaut, E.; Coleman, K. S.; Hutchison, J. L.; Green, M. L. H. and Sloan, J., "High yield incorporation and washing properties of halides incorporated single walled carbon nanotubes," *Applied Physics A: Materials Science and Processing*, 2003, 76, 457-462.

[15] Hilder, T. A.; J. M. Hill, "Theoretical comparison of nanotube materials for drug delivery," *Micro Nano Letters*, 2008, 3, 18-24.

[16] Abdullayev, E.; Price, R.; Shchukin, D.; Lvov, Y., "Halloysite Tubes as Nanocontainers for Anticorrosion Coating with Benzotriazole," *ACS Applied Materials and Interfaces*, 2009, 1, 1437-1443.

[17] Alexander, L. T.; Faust, T. G.; Hendricks; S. B., Insley; H.; McMurdie, H. F., "Relationship of the clay minerals halloysite and endellite," *The American Mineralogist*, 1943, 28, 1-18.

[18] MacEwan, D. M. C., "The nomenclature of the halloysite minerals," *Mineralogical Magazine*, 1947, 28, 36-44.

[19] Churchman, G. J.; Aldridge, L. P.; Carr, R. M., "The relationship between the hydrated and dehydrated states of an halloysite," *Clays and Clay Minerals*, 1972, 20, 241 – 246.

[20] Keller, W. D.; Da Costa, L. M., "Comparative chemical compositions of aqueous extracts from representative clays," *The American Minerologist*, 1989, 74, 1142-1146.

[21] Williams, K. A.; Dreyer, D. R.; Bielawski, C. W., "The Underlying Chemistry of Self-Healing Materials," *MRS Bulletin*, 2008, 33, 759 – 765.

[22] Soma, M.; Churchman, G. J., Theng, B. K. G., "X-Ray Photoelectron Spectroscopic Analysis of Halloyites with Different Composition and Particle Morphology," *Clay Minerals*, 1992, 27, 413-421.

[23] Bennet, R. H.; Bryant, W. R; Hulbert, M. H., *Microstructure of Fine-Grained Sediments*, 1991, Springer-Verlag New York, Inc.

[24] Singh, B., "Why Does Halloysite Roll?-A New Model," *Clay and Clay Minerals*, 1996, 44, 191-196.

[25] Jackson, M. L.; Abdel-Kader F. H., "Kaolinite Intercalation Procedure for all Sizes and Types with X-Ray Diffraction Spacing Distinctive from other Phyllosilicates," *Clay and Clay Minerals*, 1978, 26, 81-87.

[26] Lee, S. Y.; Kim, S. J., "Adsorption of Naphtalene by HDTMA modified kaolinite and halloysite," *Applied Clay Science*, 2002, 22, 55-63.

[27] Vergaro, V.; Abdullayev, E.; Lvov, Y. M.; Cingolani, R.; Rinaldi R.; Leporatti, S., "Cytocompatibility and Uptake of Halloysite Clay Nanotubes," *Biomacromolecules*, 2010, 11, 820-828.

[28] Veerabadran, N.; Price, R.; Lvov, Y., "Clay nanotubes for encapsulation and sustained release of drugs," *NANO Journal*, 2007, 2, 215-222.

[29] Yuan, P.; Southon, P. D.; Liu, Z.; Green, M. E. R.; Hook, J. M.; Antill, S. J.; Kepert, C. J., "Functionalization of Halloysite Clay Nanotubes by Grafting with γ-Aminopropyl – triethoxysilane," *Journal of Physical Chemistry C,* 2008, 112, 15742 – 15751.

[30] Abdullayev, E.; Abbasov, V.; Lvov, Y., "Halloysite Clay Nanotubes; Structural Study and Technological Applications," *Processes of Petrochem. & Oil Refining,* 2009, 10, 260 – 273.

[31] Abdullayev, E.; Lvov, Y., "Clay Nanotubes for Controlled Release of Protective Agents," Ch. 3 in book: *Active Coatings Based on Nanocontainers,* Eds. D. Shchukin, H. Mohwald, Wiley Publ., London, Berlin, 2011 *in press.*

[32] Rodoslovich E. W., "The Cell Dimensions and Symmetry of Layer-Lattice Silicate. VI. Serpentine and Kaolin Morphology," *The American Minerologist,* 1963, 48, 368-378.

[33] Singh, B.; Mackinnon, I. D. R., "Experimental Transformation of Kaolinite to Halloysite," *Clays and Clay Minerals,* 1996, 44, 825-834.

[34] Newman, R.; Childs, C.; Churchman, J., "Aluminum Coordination and structural Disorder in Halloysiote and Kaolinite by ^{27}Al NMR spectroscopy," *Clays and Clay Minerals,* 1994, 29, 305 – 312.

[35] Kirkman, J. H., "Morphology and Structure of Halloysite in New Zealand Tephras," *Clays and Clay Minerals,* 1981, 29, 1-9.

[36] Schukin, D. G.; Sukhorukov, G. B.; Price, R. R.; Lvov, Y. M., "Halloysite Nanotubes as Boimimetic Nanoreactors," *Small,* 2005, 1, 510 – 513.

[37] Wada, K., "A Structural Scheme of Soil Allophane," *The American Minerologist,* 1967, 52, 690-708.

[38] Krivovichev, S., *Minerals and Advanced Materials I,* 2008, Springer-Verlag, Berlin Heidelberg.

[39] Yamamoto, K., Otsuka, H., Takahara, A., "Preparation of Novel Polymer Hybrids from Imogolite Nanofiber," *Polymer Journal,* 2007, 39, 1-15.

[40] Sudo, T., Shimoda, S., *Developments in Sedimentology. Vol 26: Clays and Clay Minerals of Japan,* 1978, Elsevier Scientific Publishing Company (Copublished by Kodansha, Ltd.), Japan.

[41] Bonelli, B; Bottero, I.; Ballarini, N.; Passeri, S.; Cavani, F.; Garrone, E., FT-IR and Catalytic Characterization of the Acidity of Imogolite-Based Systems, *Presented in 21st North American Catalysis Society Meeting* 2009, San Francisco, CA.

[42] Aomine, S.; Yoshinaga, N., Clay Minerals of Some Well Drained Volcanic Ash Soils of Japan, *Soil Science,* 1955, 79, 349-358.

[43] Ruiz-Hitzky, E., Ariga, K., Lvov, Y., *Bio-Inorganic Hybrid Nanomaterials,* 2008, Wiley-VCH Verlag GmbH & Co. KGaA, Weinheim.

[44] Levis, S. R.; Deasy, P. B., "Characterization of Halloysite for Use as a Microtubular Drug Delivery System," *International Journal of Pharmaceutics*, 2002, 243, 125 – 134.

[45] H. M. Kelly, P. B. Deasy, E. Zaika, N. Claffey, "Formulation and Preliminary in vivo Dog Studies of a Novel Drug Delivery System for the Treatment of Periodontitis," *International Journal of Pharmaceutics*, 2004, 274, 167 – 183.

[46] S. R. Levis, P. B. Deasy, "Use of Coated Microtubular Halloysite for the Sustained Release of Ditiazem Hydrochloride and Propanolol Hydrochloride," *International Journal of Pharmaceutics*, 2003, 253, 145 – 157.

[47] Viseras, M. T.; Aguzzi, C.; Cerezo, P.; Viseras, C.; Valenzuela, C., "Equilibrium and Kinetics of 5-Aminosalicylic Acid Adsorption by Halloysite," *Microporous and Mesoporous Materials*, 2008, 108, 112- 116.

[48] Zhao, M.; Liu, P., "Adsorption Behavior of Methylene Blue on Halloysite Nanotubes," *Microporous and Mesoporous Materials*, 2008, 112, 419-424.

[49] Mellouk, S.; Cherifi, S.; Sassi, M.; Marouf-Khelifa, K.; Bengueddach, A., "Intercalation of Halloysite from Djebel Debagh (Algeria) and Adsorption of Copper Ions," *Applied Clay Science*, 2009, 44, 230-236.

[50] Carr, R. M.; Chaikum, N.; Patterson, N., "Intercalation of salts in halloysite," *Clays and Clay Minerals*, 1978, 26, 144 – 152.

[51] Frost, R. L.; Kristof, J., "Intercalation of Haloysite: A Raman Spectroscopic Study," *Clays and Clay Minerals*, 1997, 45, 551-563.

[52] Joussein, E.; Petit, S.; Delvaux, B., "Behavior of Halloysite Under Formamide Treatment," *Applied Clay Science*, 2007, 35, 17-24.

[53] Hillier, S.; Ryan, P. C., "Identification of Halloysite (7A) by Ethylene Glycol Solvaiton: the 'MacEwan' Effect," *Clay Minerals*, 2002, 37, 487-496.

[54] Antill, S. J., "Halloysite: A Low-Cost Alternative Nanotube," *Australian Journal of Chemistry*, 2003, 56, 723.

[55] Churchman, G. J., Whitton, J. S., Claridge, G. G. C., Theng, B. K. G, "Intercalation Method Using Formamide for Differentiating Halloysite From Kaolinite," *Clays and Clay Minerals*, 1984, 32, 241-248.

[56] Abdullayev, E.; Shchukin, D.; Lvov, Y., "Halloysite Clay Nanotubes as a Reservoir for Corrosion Inhibitors and Template for Layer-by-Layer Encapsulation," *Polymeric Materials Science and Engineering*, 2008, 99, 331–332.

[57] Abdullayev, E., Lvov, Y., 2007, *unpublished data*.

[58] Suh, Y.; Kil, D.; Chung, K.; Abdullayev, E.; Lvov, Y.; Torchilin, V., "Natural Nanocontainer for the Controlled Delivery of Glycerol as a Moisturizing Agent," *Journal of Nanoscience and Nanotechnology*, 2010, *in press*.

[59] Lu, Z.; Eadula, S.; Zheng, Z.; Xu, K.; Grozdits, G.; Lvov, Y., "Layer-by-Layer Nanoparticle Coatings on Lignocellulose Wood Microfibers," *Colloids and Surfaces A: Physicochemical and Engineering Aspects*, 2007, 292, 56 – 62.

[60] Wilson, I. R., "Kaolin and Halloysite Deposits of China," *Clay Minerals*, 2004, 39, 1 – 15.

[61] Hardy, A., "Green Light for Nanotech," *Biopack News*, 2008, 2, 5-6.

[62] Fix, D.; Andreeva, D. V.; Lvov, Y. M.; Shchukin, D. G.; Mohwald, H., "Application of Inhibitor-Loaded Halloysite Nanotubes in Active Anti-Corrosive Coatings," *Advanced Functional Materials*, 2009, 19, 1720 – 1727.

[63] Zheng, Q. H.; Yu, A. B.; Lu, G. Q., Paul, D. R., "Clay Based Polymer Nanocomposites: Research and Commersial Development,"*Journal of Nanoscience and Nanotechnology*, 2005, 5, 1574 – 1592.

[64] Wagner, A.; Cooper, S.; Riedinger, M., "Natural Nanotubes Enhance Biodegradable and Biocompatible Nanocomposites," *Industrial Biotechnology*, 2005, 1, 190 – 193.

[65] Guo, B. C.; Lei, Y. D.; Chen, F.; Liu, X. L.; Du, M. L.; Jia, D. M., "Styrene-Butadiene Rubber/Halloysite Nanotubes Nanocomposites Modified by Metacrylic Acid", *Applied Surface Science*, 2008, doi: 10.1016/j.apsusc. 2008.07.188.

[66] Du, M.; Guo, B.; Jia, D., "Newly emerging applications of halloysite nanotubes: a review," *Polymer International*, 2010, 59, 574 – 582.

[67] Liu, M. X.; Guo, B. C.; Du, M. L.; Cai, X. J.; Jia, D. M., "Properties of halloysite nanotube epoxy resin hybrids and the interfacial reactions in the system," *Nanotechnology*, 2007, Article number: 455703.

[68] Du, M. L.; Guo, B. C.; Liu, M. X.; Jia, D. M., "Preparation and characterization of polypropylene grafted halloysite and their compatibility effect to polypropylene/halloysite composite," *Polymer Journal*, 2006, 38, 1198 – 1205.

[69] Du, M.; Guo, B.; Jia, D., "Thermal stability and flame retardant effects of halloysite nanotubes on poly(propylene)," *European Polymer Journal*, 2006, 42, 1362-1369.

[70] Du, M.; Guo, B.; Liu, M.; Jia, D., "Thermal Decomposition and Oxidation Ageing Behaviour of Polypropylene/Halloysite Nanotube Nanocompocites," *Polymer & Polymer Composites*, 2007, 15, 321-328.

[71] Liu, M.; Guo, B.; Du, M.; Jia, D., "Drying induced aggregation of halloysite nanotubes in polyvinyl alcohol/halloysite nanotubes solution and its effect on properties of composite film," *Applied Physics A*, 2007, 88, 391-395.

[72] Laurence, McK. W., *Fluorinated Coatings and Finishes Handbook -The Definitive User's Guide and Databook*, William Andrew Publication, 2006.

[73] Lambourne, R.; Strivens, T. A., *Paint and Surface Coatings - Theory and Practice (2nd Edition)*, Woodhead Publishing, 1999. (ISBN 978-1-884207-73-0).

[74] Price, R., Gaber, B. Controlled Release of Active Agents Using Inorganic Tubules. *U.S. Patent 5,651,976.*

[75] Abdullayev, E.; Patel, S.; Lvov, Y., 2010, *unpublished data.*

[76] Abdullayev, E.; Benson, K.; Wei, W.; Lvov, Y., 2010, *unpublished data.*

[77] Abdullayev, E.; Lvov, Y., "Clay Nanotubes for Corrosion Inhibitor Encapsulation: Release Control with End Stoppers", *Journal of Materials Chemistry,* 2010, DOI: 10.1039/ c0jm00810a.

[78] Oltra, R.; Maurice, V.; Akid, R.; Marcus, P., *Local Probe Techniques for Corrosion Research Pages,* Woodhead Publishing Ltd., 2006, Cambridge, UK.

[79] Oskin, M.; Chong, F. T.; Chuang, I. L.; Kubiatowicz, J., "Building Quantum Wires: The Long and the Short of it," *Proceedings of the 30th International Symposium on Computer Architecture, ISCA* 2003, San Diego, CA.

[80] Prasad, P. N., *Nanophotonics.* 2004, John Wiley & Sons, Inc, Canada.

[81] Georgakilas, V.; Tzitzios, V.; Gournis, D.; Petridis, D., "Attachment of Magnetic Nanoparticles on Carbon Nanotubes and Their Soluble Derivatives," *Chemistry of Materials,* 2005, 17, 1613 – 1617.

[82] Guo, Y. G.; Hu, J. S.; Liang, H. P.; Wan, L. J.; Bai, C. L., " Highly Dispersed Metal Nanoparticles in Porous Anodic Alumina Films Prepared by a Breathing Process of Polyacrylamide Hydrogel," *Chem. Mater,* 2003, 15, 4332-4336.

[83] Schnur, J. M., "Lipid Tubules: A Paradigm for Molecularly Engineered Structures," *Science,* 1993, 262, 1669 – 1676.

[84] Niemeyer , C. M.; Simon, U., "DNA-Based Assembly of Metal Nanoparticles," *European Journal of Inorganic Chemistry,* 2005, 3641 – 3655.

[85] McShane, M.; Lvov, Y., Layer-by-Layer Electrostatic Self-Assembly, in book: *"Dekker Encyclopedia of Nanoscience & Nanotechnology,"* Ed. Schwartz, J.; Contescu, C., Taylor & Francies Publ., NY, p. 1-21, 2005, (ISBN: 978-0-8247-5055-8).

[86] Fu, Y.; Zhang, L., "Simultaneous deposition of Ni nanoparticles and wires on a tubular halloysite template: A novel metallized ceramic microstructure," *Journal of Solid State Chemistry,* 2005, 178, 3595-3600.

[87] Wagner, A.; Price, R., Radiation absorbtive composites and production, *U. S. Patent Appl. Publ.* 2007 / 0148457 A1.

[88] Geckeler, K. E.; Shamsi, M. H., Gold nanoparticles-Halloysite nanotube and method of forming the same, *U.S. Patent Appl. Publ. 2009/0092836 A1.*

[89] Kutsuna, S.; Ibusuki, T.; Takeuchi, K., "Heterogenous Photoreaction of Tetrachloroethene – Air Mixture on Halloysite Particles," *Environmental Science and Technology,* 2000, 34, 2484 – 2489.

[90]   Tae, J. W.; Jang, B. S.; Kim, J. R.; Kim, I.; Park, D. W., "Catalytic degradation of polystyrene using acid treated halloysite clays," *Solid State Ionics*, 2004, 172, 129-133.

[91]   Offutt, W. C.; Whitaker, A. C., Catalytic Conversion Process Employing as Catalyst, a Halloysite Clay Activated with Magnesium Oxide, *U. S. Patent* 1956 / 2744056.

[92]   Santilli, D. S., Residual Oil Processing Catalyst, *U. S. Patent* 1982 / 435840.

[93]   Robson, H., Synthetic Halloysite as Hydrocarbon Conversion Catalysts, *U. S. Patent* 1978 / 4098676.

[94]   Gary, J. H.; Handwerk, G., *Petroleum Refining Technology and Economics 4th Edition* 2001, Marcel Dekker, Inc., NY.

[95]   Twite, R. L.; Bierwagen, G. P., Review of Alternatives to Chromate for Corrosion Protection of Aluminum Aerospace Alloys,   *Progress in Organic Coatings* 1998, 33, 91-100.

[96]   Kobayashi, Y.; Fujiwara, Y., "Corrosion Protection of Cerium Conversion Coating Modified with a Self-Assembled Layer of Phosphoric Acid Mono-n-Alkyl Ester," *Electrochemical and Solid-State Letters*, 2006, 9, B15-B18.

[97]   Gichuhi, T.; Novelli, W., "The efficiency of corrosion inhibitors," *Presented at the Waterborne Symposium* 2008, New Orleans, LA.

[98]   Faltermeier, R. B., "A corrosion inhibitor test for copper-based artifacts," *Studies in Conservation*, 1998, 44,121 – 128.

[99]   Sease, C., "Benzotriazole a review for conservators," *Studies in Conservation*, 1978, 23, 76 – 85.

[100] Assouli, B.; Srhiri A.; Idrissi, H., "Effect of 2-Mercaptobenzimidazole and Its Polymeric Film on the Corrosion Inhibition of Brass (60/40) in Ammonia Solution," *Corrosion*, 2004, 60, paper no: 04040399.

[101] Shchukin, D. G.; Zheludkevich, M.; Yasakau, K.; Lamaka, S.; Ferreira, M. G. S.; Mohvald, H., "Layer-by-Layer assembled nanocontainers for self-healing corrosion protection," *Advanced Materials*, 2006, 18, 1672-1678.

[102] Zheludkevich, M. L.; Shchukin, D. G.; Yasakau, K. A.; Mohwald, H.; Ferreira, M. G. S., "Anticorrosion Coatings with Self-Healing Effect Based on Nanocontainers Impregnated with Corrosion Inhibitor," *Chemistry of Materials*, 2007, 19, 402-411.

[103] Cho, S. H.; Andersson, H. M.; White, S. R.; Sottos, N. R.; Braun, P. V., Polydimethylsiloxane-Based Self-Healing Materials, *Advanced Materials,*2006, 18, 997–1000.

[104] Caruso, M. M.; Blaiszik, B. J.; White, S. R.; Sottos, N. R.; Moore, J. S., Full Recovery of Fracture Toughness Using a Nontoxic Solvent-Based Self-Healing System, *Advanced Functional Materials*, 2008, 18, 1898–1904.

[105] Yelleswarapu, C. S.; Gu, G.; Abdullayev, E. ; Lvov, Y.; Rao, D.V.G.L.N., Nonlinear optics of nontoxic nanomaterials, *Optics Communications,* 2010, 283, 438–441.

[106] Peppas, N. A., Analysis of Fickian and non-Fickian Drug Release from Polymers, *Pharmaceutica Acta Helvetiae,* 1985, 60, 110-111.

[107] Brown, E. N.; White, S. R.; Sottos, N. R., "Microcapsule induced toughening in a self-healing polymer composite," *Journal of Materials Science,* 2002, 39, 1703-1710.

[108] K. M. Yin, "Electrochemical Impedance study of copper corrosion in chloride ion contained solution at the presence of benzotriazole," *Presented at 208th ECS Meeting,* 2005, Los Angeles, CA.

[109] Sanad, S. H., "Effect of Benzotriazole on acid corrosion of steel," *Surface Technology,* 1984, 22, 29 – 37.

[110] Magnussen, O. M.; Behm, R. J., "Atomic scale processes in Cu corrosion and corrosion inhibition," *MRS bulletin,* 1999, 15 – 23.

[111] Li, J.; Lampner, D., "In-situ AFM study of pitting corrosion of Cu thin films," *Colloids and Interfaces A: Physicochemical and Engineering Aspects,* 1999, 154, 227 – 237.

[112] Cao, P. G.; Yao, J. L.; Zheng, J. W.; Gu, R. A.; Tian, Z. Q., "Comparative study of inhibition effects of benzotriazole for metals in neutral solutions as observed with Surface-Enhanced Raman Spectroscopy," *Langmuir,* 2002, 18,100 – 104.

[113] Lvov, Y.; Ariga, K.; Ichinose, I.; Kunitake, T., "Assembly of multicomponent protein films by means of electrostatic layer-by-layer adsorption," *Journal of American Chemical Society,* 1995, 117, 6117-6122.

[114] Berg, M. C.; Zhai, L.; Cohen, R. E.; Rubner, M. F., "Controlled Drug Release from Porous Polyelectrolyte Multilayers," *Biomacromolecules,* 2006, 7, 357-364.

[115] Zhou, W.; Guo, B.; Liu, M.; Liao, R.; Rabie, A.; Jia, D., "Poly(vinyl alcohol)/Halloysite Nanotubes Bionanocomposite Films,"*Journal of Biomedical Materials Research, Part A,* 2009, 2, 1456–1463.

[116] Liu, M; Guo, B; Zou, Q; Du, M; Jia, D; "Interaction between halloysite nanotubes and 2,5-bis(2-benzoxazolyl) thiophene and their effect on reinforcement of polypropylene nanocomposites," *Nanotechnology ,*2008, 19, article 205709.

[117] Kommireddy, D; Ichinose, I; Lvov, Y; Mills, D, "Nanoparticle Multilayer: Surface Modification for Cell Attachment and Growth," *Journal of Biomedical Nanotechnology,* 2005, 1, 286-290.

[118] Veerabadran, N.; Mongayt, D.; Torchilin, V.; Price, R.; Lvov, Y., "Organized Shells on Clay Nanotubes for Controlled Release of Macromolecules," *Macromolecular Rapid Communications,* 2009, 30, 94–99.

[119] Mossman, B.; Churg, A., "Mechanisms in the Pathogenesis of Asbestosis and Silicosis,"*American Journal of Respiratory and Critical Care Medicine,* 1998, 157, 1666–1680.

[120] Hart, G.; Hesterberg, T., "In Vitro Toxicity of Respirable-Size Particles of Diatomaceous Earth and Crystalline Silica Compared with Asbestos and Titanium Dioxide," *Journal of Occupational and Environmental Medicine,* 1998, 40, 29–42.

[121] Wiessner, J.; Mandel, N.; Sohnle, P.; Mandel, G., "Effect of Particle Size on Quartz-induced Hemolysis and on Lung Inflammation and Fibrosis," *Experimental Lung Research,* 1989, 15, 801–812.

[122] Porter, A.; Gass, M.; Muller, K.; Skepper, J.; Midgley, P.; Welland, M., "Direct Imaging of Single-Walled Carbon Nanotubes in Cells," *Nature Materials,* 2007, 2, 713–718.

[123] Nel, A.; Xia, T.; Madler, L.; Li, N, "Toxic Potential of Materials at the Nanolevel," *Science,* 2006, 311, 622–628.

[124] Treacy, M.; Ebbesen, T.; Gibson, J., "Exceptionally High Young's Modulus Observed for Individual Carbon Nanotubes," *Nature,* 1996, 381, 678–680.

[125] Byrne, R. S.; Deasy, P. B., "Use of porous aluminosilicate pellets for drug delivery," *Journal of Microencapsulation,* 2005, 22, 423-437.

[126] Redlinger, M.; Corkery, R., "Cosmetic Skincare Applications Employing Mineral Derived Tubules for Controlled Release," *US Patent* 2007 / 0202061 A1.

VITA

Elshad Abdullayev finished his high school in Baku, Azerbaijan in 2001 and earned his Masters of Science degree in Chemistry at M. Lomonosov's Moscow State University in 2006. During 1999 – 2006 Mr. Abdullayev was recognized more than 20 times by the school or university administration as well as by the Ministry of Education of Azerbaijan Republic for his successes in studies and research. He is a National and International Chemistry Olympiad winner for multiple times (gold (2001), silver (1999) and bronze (2000) medal winner from Azerbaijan National Chemistry Olympiads, and silver (2000) and bronze (2001) medal winner from 34th and 35th Mendeleyev's International Chemistry Olympiads). He made an internship at British Petroleum, Azerbaijan Strategic Performance Unit for two times on summers of 2004 and 2005. Mr. Abdullayev was included into the database of best Russian students upon his completion of the Masters Degree in Moscow, Russia. In the winter of 2006, he was enrolled into Engineering PhD program at Louisiana Tech University under the supervision of Dr. Yuri Lvov. Mr. Abdullayev's area of interest is the development of protective coatings for different purposes such as anticorrosion coatings for metals or insulation coatings for conductive surfaces in micro-devices, etc. He was selected to the "Who's Who Among Students" honors program for academic award in 2009. Mr Abdullayev has had many publications and attended many conferences during his graduate studies. His publications are listed as follows.

Book Chapter

E. Abdullayev, Y. Lvov, "Clay Nanotubes for Controlled Release of Protective Agents," Ch. 3 in book: *"Active Coatings Based on Nanocontainers,"* Eds. D. Shchukin, H. Möhwald, Wiley Publ., London, Berlin, 2011 *in press.*

Disclosures to Louisiana Tech University

E. Abdullayev, Y. Lvov, "Microreservoir with End Plugs for Controlled Release of Corrosion Inhibitors," Disclosure to Louisiana Tech University, submitted in May, 2009 and patent was filed to USPTO in June, 2010.

Peer-Reviewed Journals

E. Abdullayev, D. Shchukin, R. Price, Y. Lvov, "Halloysite Tubes as Nanocontainers for Anticorrosion Coating with Benzotriazole," *ACS Applied Materials & Interfaces,* v. 1(7), 2009, p. 1437–1443.

E. Abdullayev, V. Abbasov, Y. Lvov, "Halloysite Clay Nanotubes; Structural Study and Technological Applications," *Processes of Petrochem. & Oil Refining,* v.10 (3-4), 2009, p. 260 – 273.

C. S. Yelleswarapu, G. Gu, E. Abdullayev, Y. Lvov, and D.V.G.L.N. Rao, "Nonlinear optics of nontoxic nanomaterials," *Optics Communications,* v. 283, 2010, p. 438–441.

V. Vergaro, E. Abdullayev, Y. M. Lvov, R. Cingolani, R. Rinaldi and S. Leporatti, "Cytocompatibility and Uptake of Halloysite Clay Nanotubes," *Biomacromolecules,* v. 11, 2010, p. 820-828.

Y. Suh, D. Kil, K. Chung, E. Abdullayev, Y. Lvov, V. Torchilin, "Natural Nanocontainer for the Controlled Delivery of Glycerol as a Moisturizing Agent," *J. Nanoscience and Nanotechnology,* v.10, 2010, *in press.*

E. Abdullayev, Y. Lvov, "Clay Nanotubes for Corrosion Inhibitor Encapsulation: Release Control with End Stoppers,"*J. Mater. Chem,* 2010, DOI: 10.1039/ c0jm00810a.

Conference Proceedings

E. Abdullayev, D. Shchukin, Y. Lvov, "Halloysite Clay Nanotubes as a Reservoir for Corrosion Inhibitors and Template for Layer-by-Layer Encapsulation," *Polymer Mater. Science Engin.,* v. 99, 2008, 121-122, (*Proceedings of 236[th]National American Chemical Society Meeting, Aug 17-21, 2008, Phildelphia, PA*).

E. Abdullayev, Y. Lvov, "Hallosite clay nanotubes as "Green" Nanocontainers for Anticorrosion Metal Coatings," Advanced Coatings and Surface Treatments for Corrosion Protection, 2010, *in press* (*proceedings of International Materials Science & Technology 2010 Conference, Oct. 17-21, 2010, Houston, TX*).

Conference Talks and Posters

N. Veerabadran, E. Abdullayev, S. Balkundi, R. Price, Y. Lvov, "Tunable controlled release of active agents from tubular nanoclay," *10th International Conference on Advanced Materials*, Bangalore, KA, India, Oct 8th, 2007.

E. Abdullayev, N. G. Veerabadran, Y. M. Lvov, Dmitry Fix, Dmitry Shchukin, "Anticorrosion Coatings for Metals using Nanotubular Clay Composite," *The Waterborne Symposium - 35th Annual International Symposium on Advances in Sustainable Coating Technologies*, New Orleans, LA, Jan 30th – Feb 1st, 2008.

E. Abdullayev, D. Shchukin, Y. Lvov, "Halloysite Clay Nanotubes as a Reservoir for Corrosion Inhibitors and Template for Layer-by-Layer Encapsulation," *236th National American Chemical Society Meeting*, Philadelphia, PA, Aug 17th -21st, 2008.

E. Abdullayev, Y. Lvov, "Halloysite clay nanotubes as a reservoir for corrosion inhibitors and template for layer-by-layer encapsulation," *264 Southwest Regional American Chemical Society Meeting*, Little Rock, AR, Oct 1st -4th, 2008.

Y. Lvov, E. Abdullayev, and K. Stokes, "Halloysite Clay Nanotubes as Smart Nanocontainers," *Annual AMRI Mardi Gras Symposium*, New Orleans, LA, Feb 19th -20th, 2009.

E. Abdullayev, Y. J. Suh, Y. Lvov, "Biocompatible halloysite clay nanotubes, a self-responsive container for the delivery of bioactive agents," *American Society for Biomaterials' 2009-Annual Meeting*, Houston, TX, Apr 23rd -25th, 2009.

Y. Lvov, E. Abdullayev, Z. Zheng, "Smart nanocontainers for delivery of chemical agents: architectural capsules and tubes," *83rd ACS Colloid & Surface Science Symposium and 13th International Conference on Surface Science*, Columbia University, New York, NY, Jun 16th, 2009.

E. Abdullayev, R. Price, Y. Lvov, "Halloysite clay nanotubes - smart capsules for corrosion inhibitors in metal coatings," *83rd ACS Colloid & Surface Science Symposium and 13th International Conference on Surface Science*, Columbia University, New York, NY, Jun 14th -19th, 2009.

E. Abdullayev, S. Leporatti, V. Vergaro, B. Antonazzo, P. Cozzoli, R. Cingolani, Y. Lvov, "Halloysite nanotubes as biocompatible container for sustained release of protective agents," *14th International Clay Conference*, Castellaneta, Italy, Jun 15th -20th, 2009.

V. Vergaro, A. Zacheo, S. Bonsegna, I. E. Palama, Z. Zheng, E. Abdullayev, G. Giovinazzo, R. Cingolani, R. Rinaldi, Y. M. Lvov, A. Santino, S. Leporatti, "Cytomechanical modifications induced by drug- loaded carriers uptake by breast cancer cells," *7th European Biophysics Congress*, Genoa, Italy, Jul 11th – 15th, 2009.

V. Vergaro, E. Abdullayev, Y. Lvov, G. Giovinazzo, A. Santino, R. Cingolani, R. Rinaldi, S. Leporatti, "Scanning Force Microscopy (SFM) Investigation of Cytomechanical Changes Induced by Drug-loaded Carriers Uptake by Neoplastic Cells," *Nanoscale-VII Veeco International Conference*, Santa Barbara, CA, Jul 28th -31st, 2009.

Y. J. Suh, D. S. Kil, Kang S. Chung, E. Abdullayev and Yuri M. Lvov "Biocompatible Smart Nanocontainer for the Delivery of Bioactive Agents," 1st *Nano Today Conference*, Singapore, Aug 2nd-5th, 2009.

V. Vergaro, E. Abdullayev, Y. Lvov, D. Mills, A. Santino, R. Cingolani, R. Rinaldi, S. Leporatti "Halloysite Clay Nanotubes: Characterization, Biocompatibility, and Use as Drug Carriers," *European TNT-2009 Conference (Trends in NanoTechnology)*, Barcelona, Spain, Sept 7th-11th, 2009.

V. Vergaro, E. Abdullayev, D. Mills, G. Giovinazzo, A. Santino, R. Cingolani, Y. M. Lvov and S. Leporatti, "Halloysite Clay Nanotubes: Characterization, Biocompatibility and Use as Drug Carriers," 2nd *National Nanomedicine Conference*, Università degli Studi di Pavia, Pavia, Italy, Sept 21st-22nd, 2009.

V. Vergaro, Z. Zheng, E. Abdullayev, Y. M. Lvov, G. Giovinazzo, A. Santino, R. Cingolani, R. Rinaldi and S. Leporatti, "Nanotechnology for cancer therapy: cytomechanical changes induced by drug-loaded carriers uptake by neoplastic cells," 2nd *National Nanomedicine Conference*, Università degli Studi di Pavia, Pavia, Italy, Sept 21st-22nd, 2009.

Y. Lvov, E. Abdullayev, "Halloysite Clay Nanotubes for Controlled Release of Protective Agents," 29th *Biennial Western Coating Symposium*, Las Vegas, NV, Oct 25th-28th, 2009.

E. Abdullayev, D. Shchukin, R. Price, Y. Lvov, "Halloysite- benzotriazole nanocomposites, low cost additives to metallic coatings for corrosion protection," 29th *Biennial Western Coating Symposium*, Las Vegas, NV, Oct 25th-28th, 2009.

V. Vergaro, E. Abdullayev, D. Mills, R. Cingolani, Y. Lvov, S. Leporatti, "Halloysite Clay Nanotubes: Characterization and Biocompatibility Study," *International Conference NanoSmart-2009*, Rome, Italy, Oct 20th, 2009.

E. Abdullayev, Y. Lvov, "Halloysite Clay Nanotubes as "Green" Nanocontainers for Controlled Release of Corrosion Inhibitors," *Annual AMRI Mardi Gras Symposium*, New Orleans, LA, Feb 10th-12th, 2010.

V. Vergaro, E. Abdullayev, G. Giovinazzo, A. Santino, R. Cingolani, Y. M. Lvov and S. Leporatti, "Halloysite Nanotubes and Nanocolloids: High Payload Drug Nanocarriers," *Particles-2010*, Lake Buena Vista, FL, May 22nd-25th, 2010.

Y. Lvov, E. Abdullayev, "Polymer composites with halloysite clay nanotubes for protective coating," 13th *International Conference on Organized Molecular Films (LB-13)*, Quebec City, Canada, July 18th-21st, 2010.

E. Abdullayev, Y. Lvov "Halloysite nanotubes for sustained release of corrosion inhibitors," *15th International Coating Science & Technology Symposium*, St. Paul, MN, Sept 12th-15th, 2010.